Multivariable PID Control with Application to Gas Turbine Engines

Thesis submitted for candidature for the degree of PhD

Seyed Saeed Tavakoli Afshari

October 2005

Department of Automatic Control and Systems Engineering

The University of Sheffield

Abstract

To meet increasing and often conflicting demands on performance, stability, fuel consumption and functionality, modern jet engines are becoming increasingly complex. Improved compressor performance is a major factor in this development process. Optimum compressor efficiency is achieved in operating regions close to flow instability. Surveying basic concepts and control methods of compressor instabilities, an overview of the fundamentals of surge and rotating stall is presented. To maximise the potential of an aero gas turbine compression system, it is proposed to use more advanced control strategies, such as multivariable control.

Multivariable control may offer the prospect of lower safety margin requirements leading to greater compressor efficiency. Alternatively, it may result in more agility in combat through improved engine responses and prolonged engine life. A multivariable control technique is proposed and tested on a Rolls-Royce three-spool high bypass ratio turbofan engine. Since elements of the 2x2 system can be represented by linear third order models, a multivariable PID controller will be sufficient provided the design requirements are not too rigorous. To have a simple and efficient design, a systematic decentralised PI (PID) control design strategy is developed. Decoupling a given 2x2 process by a stable decoupler, the elements of the resulting diagonal matrix are approximated by first (second) order plus dead time processes using the proposed model reduction techniques. Then, SISO controllers are designed for each element using the developed tuning formulae.

Any practical design method should be simple, easy to apply, flexible, generic or extendable, and applicable to complex control schemes to fulfil more demanding control requirements. It will be advantageous if the design algorithm can also directly address the design requirements, be repeatable for any control objective, constraint and category of processes, have a design parameter, and can consider any number of objectives and constraints. Formulating the PI (PID) control design problem as an optimisation problem, a non-dimensional tuning (NDT) method satisfying the above-mentioned design properties is presented. For a given first (second) order plus dead time process, the NDT method is used in conjunction with either a single-objective or a multi-objective optimisation approach to design PI (PID) controllers satisfying conflicting design requirements. In addition, considering load disturbance rejection as the primary design objective, a simple analytical PI tuning method is presented. The design problem is constrained with a specified gain or phase margin.

Compared to the corresponding conventional SISO controller, it is demonstrated that the resulting decentralised controller considerably improves the overall surge risk to the engine during the transient manoeuvres while maintaining similar thrust levels. Due to non-linearity of jet engine models, gain scheduling is necessary. Designing decentralised controllers at various operating points, the gain-scheduled controller accommodates the non-linearity in engine dynamics over the full thrust range.

Acknowledgments

This PhD is dedicated to my wife for her encouragement and support during this programme. I would like to thank my brother, Dr. Mahdi Tavakoli, for discussing some technical points of the thesis. Particular thanks also to my parents for their steady support in all stages of my studies.

I would also like to express my sincere thanks to my supervisor, Prof. Peter J. Fleming, for his invaluable help, support and encouragement throughout this research programme. Also, I am very thankful to Dr. Ian Griffin for discussing all stages of the PhD and editing drafts of my papers and dissertation. Useful discussions with my colleagues Jafar Sadeghi and Dr. Masoud Jamei are also acknowledged.

Finally, I wish to acknowledge the support of Rolls-Royce plc for partially funding this PhD programme.

Statement of Originality

Unless otherwise stated in the test, the work described in this thesis was carried out solely by the candidate. None of this work has already been accepted for any degree, nor is it concurrently submitted in candidature for any degree.

Candidate: 

Saeed Tavakoli

Supervisor: 

Peter J. Fleming

Contents

Chapter 1

Introduction

1.1. Motivation

Modern jet engines are highly complex physical processes. To design control systems for such processes, many requirements on performance, stability, economy and functionality should be taken into account. These requirements are often in competition with each other. Suitable control systems can be obtained through compromising between desirable characteristics.

In a complex process like a jet engine there are many things that must be kept under control. Jet engine control systems are required to operate the engine with due regard to performance and safety. Minimum transient behavioural characteristics are specified by contractual and legal limitations placed on engine manufacturers. Fuel costs should be minimised and restrictions on emission issues should be satisfied. Shaft overspeed and overheating should be prevented. The compressors must be operated within their surge and stall boundaries to prevent unacceptable performance loss and potential physical damage. Optimum compressor efficiency is achieved in operating regions close to flow instability and, hence, a trade-off between performance and safety is required. Circumstances other than those for which jet engines are nominally designed should also be handled. This involves consideration of issues such as engine modelling inaccuracies, manufacturing tolerances and sensor and actuator failure. Considering the non-linearity in jet engine models, changes in dynamics need to be tolerated within the control system as the engine moves through its operation envelope.

Modern jet engines are becoming more and more complex to meet the above-mentioned conflicting demands. To utilise the potential of these engines, it is essential to use more advanced control strategies, such as multivariable control, rather than conventional control.

To satisfy performance requirements and safety issues, the jet engine control configuration should have at least two outputs. One approach is to use a decoupler along with a 2x2 decentralised controller. One great advantage of this method is that it allows the use of SISO control design methods. Moreover, the number of tuning parameters in this case is significantly less than those in

the case of a full matrix controller. Furthermore, in the case of actuator or sensor failure, it is relatively easy to stabilise the loop manually, as only one loop is directly affected by the failure.

A non-linear three-spool Rolls-Royce turbofan engine is considered in this study. As the non-linear model derived from the engine physics could be reduced to linear models of the same order as the number of engine shafts, each element of the 2x2 engine model can be represented by a linear third order transfer function. As a result, a decentralised PID controller will be sufficient provided the design requirements are not too rigorous.

To balance all the conflicting requirements and provide the designer with good compromise solutions, multi-objective optimisation techniques can play an important role in control of modern jet engines. Decoupling a given 2x2 engine model, it is required to develop a multi-objective PI (PID) design technique to optimally design SISO controllers for each diagonal element. To comply with the current and future demands, the SISO design technique should be simple, flexible, generic (extendable), applicable to complex control schemes to fulfil more demanding control requirements and repeatable for any control objective, constraint and category of processes. Moreover, it is beneficial if the design algorithm can directly address the design requirements, have a design parameter to trade-off between performance and safety, and can consider any number of objectives and constraints.

1.2. Achievements

The main achievements of this research are as follows:

- Surveying basic concepts and control methods of compressor instabilities (Tavakoli, Griffin and Fleming, 2004). Here, an overview of the fundamentals of surge and rotating stall that limit the performance of gas turbine engines is presented. In addition, the major recent developments in surge and rotating stall avoidance, detection and avoidance and control techniques are reviewed (See Appendix C)
- Developing a simple non-dimensional tuning (NDT) method for designing PI (PID) controllers for first (second) order plus dead time processes (Tavakoli and Fleming, 2003; Tavakoli, Griffin and Fleming, 2005e). This flexible NDT design strategy, which directly addresses the design requirements, can be employed in either a single-objective (Tavakoli, Griffin and Fleming, 2005c) or a multi-objective approach (Tavakoli, Griffin and Fleming, 2005f) to obtain tuning formulae satisfying conflicting design requirements. It has no limitation on the number of objective functions and constraints and can be applied to any control objective, any constraint and any category of processes. Moreover, to fulfil more demanding and often conflicting control requirements, it is applicable to more complex control schemes (See Chapters 3 and 5)
- Proposing a simple and widely applicable analytical method for tuning PI controllers (Tavakoli, Griffin and Fleming, 2005b). The design problem aims to optimally reject load disturbance responses and is constrained with a specified gain or phase margin. Also, simple tuning formulae for FOPDT processes are determined (See Chapter 4)

- Proposing a simple multivariable controller for an industrial Benchmark Challenge provided by ALSTOM (Tavakoli, Griffin and Fleming, 2003). The multivariable control system was required to conform to specified performance and robustness matrices. A multivariable control design procedure using genetic algorithms based on a condition number minimisation approach was proposed for the ALSTOM gasifier problem. Minimal realization, model order reduction as well as scaling techniques were used to improve the numerical conditioning of the non-linear, highly cross-coupled and numerically ill-conditioned model of gasifier (See Appendix D)
- Developing a systematic decentralised control strategy for a given 2x2 process (Tavakoli, Griffin and Fleming, 2005a). Here, a stable decoupler is firstly introduced to decouple the process. The resulting diagonal elements are then approximated by first (second) order plus dead time processes using the proposed model reduction techniques. The decentralised controller is formed by two SISO controllers. Considering each diagonal element, the corresponding SISO controller is designed using the NDT tuning formulae (See Chapter 3 and Appendix B)
- Applying the proposed decentralized PI tuning method to a 2x2 model of a Rolls-Royce three-spool turbofan engine to improve engine safety (Tavakoli, Griffin and Fleming, 2005d). To cover the full thrust range, several linear decentralised controllers can be designed at specific operating points to form a gain-scheduled controller, which accommodates non-linearity in engine dynamics and characteristics (See Chapter 6)

1.3. Structure of dissertation

1.3.1. Chapter 2

An overview of PID control including design requirements, basic control actions, different variations and different tuning methods is presented in this chapter. In view of the number of industrial controllers which use PID control, many PID tuning methods have been derived. The chapter describes the most important of these PID design techniques together with their key characteristics.

1.3.2. Chapter 3

A simple non-dimensional tuning method, which is repeatable for any set of objective functions, constraints and processes, is proposed in this chapter. In this research, formulating the PI (PID) control design problem as an optimisation problem, it is aimed to employ the NDT method in conjunction with a multi-objective optimisation approach to obtain PI (PID) tuning rules satisfying conflicting design requirements. In this chapter, however, having chosen to consider setpoint regulation as the primary design objective, the NDT method along with a single-objective optimisation approach is used to derive good PI (PID) tuning formulae for first (second) order plus

dead time processes. Moreover, for lag dominant and integrating processes, in which load disturbances are the major issue, the tuning rules are revised.

Furthermore, a simple decentralised control strategy is developed in this chapter to obtain a decentralised PI (PID) controller for a given 2x2 process.

1.3.3. Chapter 4

Considering load disturbance rejection as the primary design objective, a simple analytical PI control design method, which can be applied to a broad range of processes, is presented in this chapter. The design problem is constrained with a specified gain or phase margin to ensure the robustness of the closed-loop system. As a large number of industrial processes can approximately be modelled by first order plus dead time models, the tuning method is then applied to this category of processes to obtain a simple set of tuning formulae.

1.3.4. Chapter 5

Using a two-degree of freedom structure in conjunction with either a single-objective or a multi-objective approach, the NDT technique is used to obtain PI tuning rules, capable of satisfying conflicting design requirements, for first order plus dead time processes.

1.3.5. Chapter 6

Compared to the conventional SISO jet engine control strategies, a more comprehensive closed-loop control approach is required to improve performance and/or safety of traditional jet engines. In this chapter, a study of multivariable jet engine control is carried out and it is shown that the multivariable controller is capable of improving engine thrust and/or efficiency. To have a simple and efficient design, the decentralised control scheme proposed in chapter 3 is applied to a 2x2 model of a Rolls-Royce three-spool turbofan engine to enhance its safety.

1.3.6. Chapter 7

This chapter summarises the research work carried out in this thesis and gives recommendation for future work.

1.3.7. Appendices

Appendix A contains an introduction to dimensional analysis, which simplifies a problem by reducing the number of its variables to the smallest number of essential parameters.

Appendix B proposes a simple method to decouple a given stable 2x2 process using a stable decoupler, when both diagonal and off-diagonal elements of the process have RHP zeros.

The compromise between performance and safety is a central issue in jet engine control. Compressor instabilities such as surge and rotating stall limit the performance and effectiveness of jet engines. To improve engine performance and efficiency through extending the stable operating range of the compressor system, advanced control strategies are employed to suppress rotating stall and surge and, therefore, to reduce the surge margin requirements. Appendix C presents an overview of the basic concepts and control techniques of these instabilities. Moreover, the major recent developments in surge and rotating stall avoidance, detection and avoidance and control techniques are surveyed.

Appendix D considers an industrial multivariable Benchmark Challenge, the ALSTOM gasifier. A number of key issues in multivariable control design are explored. The gasifier is a non-linear, highly cross-coupled and numerically ill-conditioned process. To tackle this ill-conditioned process, the numerical conditioning of the model is firstly improved using minimal realization, model reduction and scaling techniques. Then, a condition number minimisation approach is proposed to ensure that the closed-loop system is robust enough against model uncertainties.

Chapter 2

An Overview of PID Control

2.1. Introduction

Feedback is a simple but very powerful idea. Its use has often had revolutionary consequences with drastic improvements in performance (Bennett, 1979; Bennett, 1993). Applications of the feedback principle have resulted in major breakthroughs in control, communication, instrumentation, etc. Feedback control is the basic mechanism by which systems, whether mechanical, electrical, biological, etc. maintain their equilibrium. It may be defined as the use of difference signals, determined by comparing the actual values of system variables to their desired values, as a means of controlling a system. In other words, feedback control means measuring the controlled or process variable (output), comparing that measurement to the desired value (setpoint), and acting in response to the error (the difference between the setpoint and output) by adjusting the manipulated variable (input). If the process variable increases when the manipulated variable is increased, the principle of feedback can be expressed as follows:

- Increase the manipulated variable when the process variable is smaller than the setpoint
- Decrease the manipulated variable when the process variable is greater than the setpoint

This type of feedback is called negative feedback because the manipulated variable moves in the opposite direction to the process variable (Astrom and Hagglund, 1995).

In this chapter, a particular control structure, which is by far the most prevalent form of compensator used in industrial feedback control, is reviewed. This fixed-structure controller, which has three adjustable parameters, is called the PID controller. The letters P, I and D stand for Proportional, Integral and Derivative control, respectively. The PID controller has the ability to eliminate steady state errors through integral action. It can anticipate the future through derivative action.

Because of its remarkable effectiveness and simplicity of implementation, PID control is the most popular controller in process control. It is surprising how much can be achieved with such a

simple strategy. The PID controller is the "bread and butter" of automatic control. It is the first solution that should be tried when feedback is used (Astrom and Hagglund, 2001). PI (PID) control is sufficient for a large number of control problems, particularly when process dominant dynamics are of the first (second) order and the design requirements are not too rigorous (Astrom and Hagglund, 1995). It has been empirically found that PID controllers often have sufficient flexibility to yield excellent results in most industrial applications. Moreover, they have proven to be robust in the control of industrial plants (Goodwin, Graebe and Salgado, 2001).

Although significant developments have been made in control theory, according to the literature (Deshpande, 1989; Koivo and Tanttu, 1991; Ho, Lee, Xu, Zhou and Tay, 2000) more than 90% of industrial controllers are still PID, mostly PI, controllers. Bialkowski (1993) reported a typical paper mill with more than 2000 control loops, of which 97% used PI controllers. A survey of more than 11000 controllers in the refining, chemicals, and pulp and paper industries showed that 97% of the regulatory controllers were PID (Desborough and Miller, 2001).

A number of analytical and numerical methods, which are usually different in complexity, flexibility and in the amount of process knowledge used, have been proposed for tuning this controller since the 1940s (Pessen, 1954; Haalman, 1965; Lopez, Murrill and Smith, 1969; Rivera, Morari and Skogestad, 1986; Chien and Fruehauf, 1990; Shinskey, 1990; Tyreus and Luyben, 1992; Atherton, 1999; Cominos and Munro, 2002; Skogestad, 2003). In addition, most books on process control have a chapter on tuning PID controllers (McMillan, 1983; Corripio, 1990; McFarlane and Glover, 1990; Shinskey, 1996; Smith and Corripio, 1997; Marlin, 2000; Seborg, Edgar and Mellichamp, 2004).

Due to the widespread use of PID controllers, it is highly desirable to have efficient PID tuning rules. Although this controller has only three parameters it is not easy to find their optimal values without a systematic procedure (Skogestad, 2003). Nevertheless, PID control has only received moderate interest from theoreticians. Therefore, many important issues have not been well documented in the literature. However, there has been an increased interest in the last fifteen years. One reason is the emergence of automatic tuning. Another is the increased use of model predictive control that required well-tuned PID controllers at the basic level (Astrom and Hagglund, 2001). As a result, the design of PID controllers is still a challenging task for researchers and engineers.

There has been a strong resurgence in the interest towards the PID control over the last few years. As shown in Figure 2.1, many publications have appeared (Bennett, 2000).

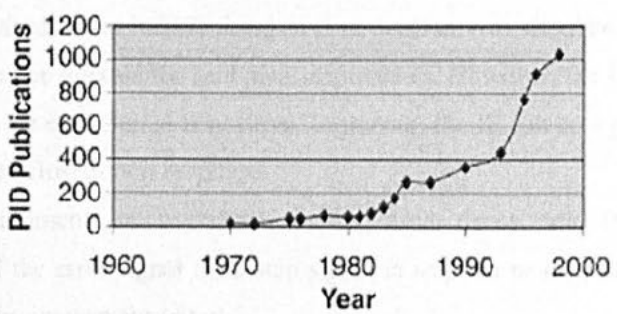

Fig. 2.1. Historical evolution of PID publications (Bennett, 2000).

The PID control has become one of the most important ways for the scientific and the industrial control users to work together (Astrom, Albertos and Quevedo, 2001).

2.2 Design requirements

In order to design a controller it is always necessary to understand what the goals of control are. Typically, the following issues should be considered for designing a PID controller:

- Setpoint regulation
- Load disturbance rejection
- Robustness to model uncertainty
- Sensitivity to measurement noise

Some of these objectives may be conflicting. Therefore, a good tuning method should consider a trade-off between the conflicting design requirements. It should also be simple, widely applicable and easy to use.

Load disturbance rejection is often the primary goal in process control, whereas setpoint regulation is typically of secondary importance. However, in some cases setpoint response may be of primary importance. An example is the motion control system (Astrom, Panagopoulos and Hagglund, 1998). Interestingly, although it has been frequently pointed out by engineers that load disturbance rejection is the primary goal, papers on PID control literature traditionally focus on setpoint regulation (Shinskey, 1990).

2.2.1. Setpoint regulation

In process control, most control loops have a constant setpoint. Due to desires to change operating conditions, the setpoint may change at certain time instances. As a result, the setpoint is typically a piece-wise constant signal. Therefore, the setpoint signal is modelled as a step function (Astrom and Hagglund, 1995). Defining the error function as the difference between the setpoint signal and output of the closed-loop system in negative feedback, standard criteria such as the integral of square error (ISE), the integral of absolute error (IAE) or the integral of time absolute error (ITAE) can be considered in assessing controller performance. The choice of ISE may be problematic, as it gives a very high weight to large errors and often leads to a poorly damped closed-loop system. The IAE is a natural choice in many cases, however, a severe drawback is that its evaluation requires significant computation of time functions or a simulation of the process (Astrom and Hagglund, 1995). Also, since the criterion is based on an infinite integral it is necessary to simulate the process for a long time. Therefore, IAE is not suitable for analytical approaches. However, the IAE is equivalent to the integral of error (IE) if the error signal is positive. Moreover, the IE can be a good approximation for the IAE for well damped closed-loop systems.

Alternatively, requirements on overshoot, settling time, decay ratio (the ratio between two consecutive maxima of the error signal for a step signal in setpoint or load disturbance) or rise time may be considered as the assessment criteria.

2.2.2. Load disturbance rejection

Load (input) disturbances are the most common and most important disturbances in process control. They are signals that drive the system away from its desired operating point. A load disturbance is typically a low frequency signal modelled as a step function added to the control signal at the process input (Astrom and Hagglund, 1995), as shown in Figure 2.2. Such a structure is called a one-degree of freedom scheme.

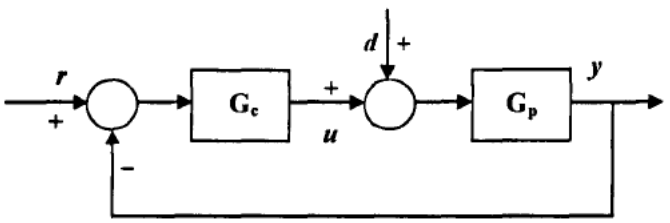

Fig. 2.2. Block diagram of one-degree of freedom feedback control system.

The output signal is given by:

$$y = \frac{G_p G_c}{1 + G_p G_c} r + \frac{G_p}{1 + G_p G_c} d, \tag{2.1}$$

where r, d and y refer to the reference, load disturbance and output signals, respectively. G_p and G_c refer to the process and controller transfer functions. In most of this thesis, the one-degree of freedom negative feedback structure shown in Figure 2.2 is used.

2.2.3. Robustness to model uncertainty

The control parameters are typically matched to the process characteristics. Since the process dynamics may change, it is important to choose the controller parameters so that the closed-loop system is as insensitive as possible to variations in process dynamics.

Linear time invariant (LTI) models approximately describe actual plant dynamics. In other words, there are differences between the actual system and the model of the system. These differences are referred to as model uncertainties.

The model uncertainty can have several different sources. It can be introduced to the system because of linearisation, change of operating conditions, unmodelled dynamics, etc. Most real processes are non-linear. If the process model is obtained via linearisation, it is accurate only in the neighbourhood of the operating point chosen for the linearisation. Moreover, the LTI model may be inaccurate if operating conditions change. In addition, fast dynamic modes are usually neglected in the model. As a result, to take the model uncertainty into account, the dynamic behaviour of a plant can be described not by a single LTI model but by a family, π, of LTI models (Morari and Zafiriou, 1989).

A control system is referred to as robust if it is insensitive to model uncertainties. Robust stability means that the system remains stable for all plants in the family, π. Robust performance means that the performance objectives are satisfied for all plants in the family, π.

Gain margin (GM), phase margin (PM) and maximum sensitivity (M_s), defined in Equation (2.2), are among the different criteria to consider sensitivity to modelling errors. Typical values of GM, PM and M_s are in the range of $30^\circ - 60^\circ$, 2-5, and 1.3-2, respectively (Astrom and Hagglund, 1995).

$$M_s = \max_{\omega} |S(j\omega)| = \max_{\omega} \left| \frac{1}{1 + G_p(j\omega)G_c(j\omega)} \right| = \|S(j\omega)\|_\infty . \tag{2.2}$$

2.2.4. Sensitivity to measurement noise

Measurement noise is generally a high frequency phenomenon. It is fed into the system through feedback and will generate control actions and control errors. Measurement noise is an important consideration in many cases, however, since its magnitude varies a lot in applications, it is difficult to give general rules about when measurement noise may be a problem. However, robust designs (small M_s) with moderate input usage are generally insensitive to measurement noise (Skogestad, 2003).

Since measurement noise does not contain any information about the status of the process, it should be filtered out (Astrom and Hagglund, 1995), especially when either the controller gain (K_c) or the derivative gain ($K_c T_d$) is large (Skogestad, 2003). This can be done through a low pass filter. Measurement noise can be modelled as an impulse function.

2.3. Basic control actions

2.3.1. Proportional action

The basic term is the proportional term, P, which causes a corrective control actuation proportional to the error signal:

$$u(t) = K_c e(t), \tag{2.3}$$

where $e(t)$, $u(t)$ and K_c are called the error signal, control signal and controller gain, respectively. No actuator constraint has been assumed in this study. Therefore, this proportional controller does not include physical limits on the controller output. Proportional control action takes immediate corrective action as soon as an error is detected. An inherent disadvantage of using only proportional control is that a steady state error (offset) occurs after a setpoint change.

2.3.2. Integral action

The integral term, I, gives a correction proportional to the integral of the error signal:

$$u(t) = \frac{K_c}{T_i} \int_0^t e(\tau)\, d\tau, \tag{2.4}$$

where T_i is called the integral time. It is widely used because it provides an important practical advantage, which is the elimination of the steady state error. In order for the process being controlled to be at steady state, $u(t)$ must be constant. Equation (2.4) implies that $u(t)$ changes with time unless the error signal is zero. Therefore, when integral action is used, $u(t)$ automatically changes until it attains the value required to make the steady state error zero. This desirable situation always occurs unless the control output saturates and thus is unable to bring the controlled value back to the setpoint. Controller saturation occurs when the setpoint or disturbance is so large that the required control effort is beyond the range of the manipulated variable.

Although the elimination of the steady state error is an important control objective, integral action is seldom used by itself because little control action takes place until the error signal has persisted for some time. Integral action is normally used in conjunction with proportional control as shown in the proportional-integral (PI) controller:

$$u(t) = K_c\left(e(t) + \frac{1}{T_i} \int_0^t e(\tau)\, d\tau\right). \tag{2.5}$$

A disadvantage of integral action is that it tends to have a destabilising effect due to increased phase lag. A limited amount of oscillation can usually be tolerated because it is often associated with a faster response. The undesirable effects of too much integral action can be avoided by proper tuning of the controller or by including derivative action, which tends to counteract the destabilising effects.

2.3.3. Derivative action

The function of derivative control action is to anticipate the future behaviour of the error signal by considering its rate of change. Derivative action is never used alone. It is always used in conjunction with proportional or proportional-integral control (Seborg, Edgar and Mellichamp, 2004). The basic structure of a proportional-derivative (PD) controller is given by:

$$u(t) = K_c\left(e(t) + T_d \frac{de(t)}{d(t)}\right), \tag{2.6}$$

where T_d is called the derivative time. Having the approximation of $e(t+T_d)$ by using the Taylor series expansion:

$$e(t+T_d) \approx e(t) + T_d \frac{de(t)}{d(t)}, \tag{2.7}$$

the control signal is proportional to the estimation of the control error at $t+T_d$:

$$u(t) = K_c e(t+T_d). \tag{2.8}$$

An ideal PD controller has the following transfer function:

$$\frac{U(s)}{E(s)} = K_c(1+T_d s). \tag{2.9}$$

It means that the derivative mode tends to stabilise the closed-loop system. It is often used to counteract the destabilising tendency of the integral mode. However, using the derivative action often leads to large control movements (Astrom and Hagglund, 1995). The derivative action also tends to improve the dynamic response of the controlled variable by decreasing the process settling time (Seborg, Edgar and Mellichamp, 2004).

If the process measurement is noisy and contains high-frequency random fluctuations, the following PD controller in which the derivative term includes a derivative filter is normally used:

$$\frac{U(s)}{E(s)} = K_c(1+\frac{T_d s}{\alpha T_d s+1}), \tag{2.10}$$

where the constant α has a value between 0.05 and 0.2, with 0.1 being a common choice.

2.4. Different variations of PID control

Many variations of PID control are used in practice. The most common forms of these variations are reviewed in this section.

2.4.1. Parallel form

The parallel form of the PID controller is given by:

$$u(t) = K_c\left(e(t) + \frac{1}{T_i}\int_0^t e(\tau)d\tau + T_d \frac{de(t)}{d(t)}\right). \tag{2.11}$$

Hence, the corresponding transfer function is:

$$\frac{U(s)}{E(s)} = K_c(1 + \frac{1}{T_i s} + T_d s). \tag{2.12}$$

The parallel form is sometimes called the ideal form. This form of PID controller has three separate elements operating in parallel on $E(s)$. Thus, it is possible to obtain pure proportional, integral or derivative action by finite values of the parameters. The integral time does not influence the derivative part and the derivative time does not influence the integral part. Therefore, this form of PID controller is called non-interacting.

As noted above, the derivative mode is usually used with a derivative filter. The parallel PID controller with a derivative filter is given by:

$$\frac{U(s)}{E(s)} = K_c(1 + \frac{1}{T_i s} + \frac{T_d s}{\alpha T_d s + 1}). \tag{2.13}$$

2.4.2. Series form

Historically, it was convenient to construct PID controllers so that PI and PD controllers operated in series:

$$\frac{U(s)}{E(s)} = K_c'(1 + \frac{1}{T_i' s})(1 + T_d' s). \tag{2.14}$$

The series form has an attractive interpretation in the frequency domain because its zeros correspond to the inverse values of the integral and derivative times (Astrom and Hagglund, 1995). In principle, it makes no difference whether the PD controller or the PI controller comes first (Seborg, Edgar and Mellichamp, 2004). This form of PID controller is called interacting as the derivative time, T_d', does influence the integral part if the PD controller comes first. It is claimed that the interacting PID controller can easier be tuned manually than the non-interacting PID controller (Astrom and Hagglund, 1995).

The interacting and non-interacting forms are different when both I and D parts of the controller are used. As a result, for the P, PI and PD controllers, these two forms are equivalent. For a PID controller, the series form can always be represented as a parallel form. The relationships between the coefficients of these two forms are given by:

$$K_c = K_c' \frac{T_i' + T_d'}{T_i'}, \tag{2.15}$$

$$T_i = T_i' + T_d', \tag{2.16}$$

$$T_d = \frac{T_i' T_d'}{T_i' + T_d'}. \tag{2.17}$$

However, it is not always possible to obtain the series form from the parallel form. If $T_i \geq 4T_d$, then the coefficients of the series form are obtained as follows:

$$K_c' = \frac{K_c}{2}\left(1 + \sqrt{1 - \frac{4T_d}{T_i}}\right), \tag{2.18}$$

$$T_i' = \frac{T_i}{2}\left(1 + \sqrt{1 - \frac{4T_d}{T_i}}\right), \tag{2.19}$$

$$T_d' = \frac{T_i}{2}\left(1 - \sqrt{1 - \frac{4T_d}{T_i}}\right). \tag{2.20}$$

This is because the parallel form is more general as it also allows for complex zeros in the controller. Therefore, the parallel form of the PID controller can be used when controlling systems with oscillatory poles, for example underdamped second order processes. Moreover, even for overdamped or critically damped processes, the parallel form may give a better performance due to its less restrictive form (Skogestad, 2003). Commercial versions of the series form of PID controller have a derivative filter:

$$\frac{U(s)}{E(s)} = K_c'\left(1 + \frac{1}{T_i' s}\right)\left(\frac{T_d' s + 1}{\alpha T_d' s + 1}\right). \tag{2.21}$$

2.4.3. Expanded form

The expanded form of PID controller is given by:

$$\frac{U(s)}{E(s)} = K_c + \frac{K_i}{s} + K_d s, \tag{2.22}$$

where K_i and K_d are called integral and derivative gains, respectively. The relationship between K_i and K_d and the parameters of the parallel form are given by:

$$K_i = \frac{K_c}{T_i}, \tag{2.23}$$

$$K_d = K_c T_d. \tag{2.24}$$

This form is often useful in analytical calculations because the parameters appear linearly. Like the parallel form, pure proportional, integral or derivative actions are obtained by finite values of the parameters.

2.4.4. Two-degree of freedom scheme

In general, a control system has many conflicting requirements. For example, if the design objectives are setpoint regulation and load disturbance rejection, the controller has to be chosen either for good setpoint regulation or good load disturbance rejection or else some compromise has to be found. If there are strict requirements on both design objectives, an acceptable compromise may not exist (Morari and Zafiriou, 1989).

There is more flexibility to cope with the conflicting design requirements by having different signal paths for the setpoint and the process output. Such a structure is called a two-degree of freedom scheme, as shown in Figure 2.3.

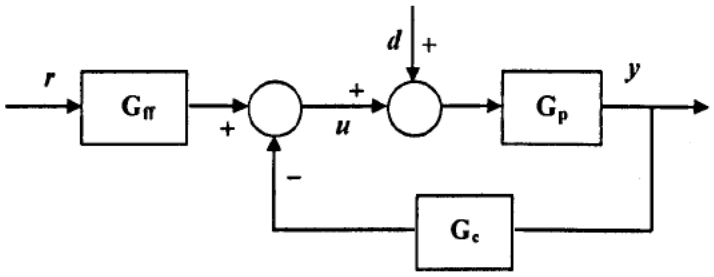

Fig. 2.3. Block diagram of two-degree of freedom feedback control system.

A PID controller of this form is given by:

$$u(t) = K_c\left(e_p(t) + \frac{1}{T_i}\int_0^t e(\tau)d\tau + T_d\frac{de_d(t)}{d(t)}\right), \tag{2.25}$$

where the error signals in proportional and derivative parts are defined in:

$$e_p(t) = br(t) - y(t), \tag{2.26}$$

$$e_d(t) = cr(t) - y(t), \tag{2.27}$$

where parameters b and c are called setpoint weights. The error signal in the integral part must be the true error signal to avoid steady state control errors (Astrom and Hagglund, 1995).

Setpoint weights have no influence on the response to disturbances, however, they have a significant influence on the response to the setpoint signal. This form of a control system is given by:

$$y = \frac{G_p G_{ff}}{1 + G_p G_c} r + \frac{G_p}{1 + G_p G_c} d, \tag{2.28}$$

where G_{ff} is:

$$G_{ff} = K_c (b + \frac{1}{T_i s} + c T_d s). \tag{2.29}$$

Therefore, a two-degree of freedom structure decouples setpoint regulation and load disturbance rejection, which are conflicting requirements.

2.5. Trial and error tuning methods

The PID controller has three adjustable parameters, K_c, T_i and T_d. An important issue is to know how the different controller parameters affect the speed of the response and the stability of the system. In addition, when using a systematic approach it may still be important to know how the different controller parameters affect the closed-loop system. This is because the systematic methods do not necessarily result in the desired control performance and subsequent fine-tuning and manual adjustments may be required.

A compromise between the requirement for speed of the response and the need for stability of the system is found by selecting the controller parameters suitably. Table 2.1 show how stability and speed change when changing the controller parameters. This table only contains rules of thumb and there are exceptions (Tan, Wang, Hang and Hagglund, 1999).

Table 2.1. Effects of PID parameters on speed and stability

Increase in	Speed	Stability
K_c	increases	reduces
T_i	reduces	increases
T_d	increases	increases

When a PID controller is manually tuned, it is usual to tune the parameters in the order P, I and D. Initially, the I and D parts are effectively disconnected by assigning a very high value to T_i and setting $T_d = 0$. Next, K_c is adjusted according to rules in Table 2.1. T_i is then reduced to a suitable value. This will result in a reduction in stability, therefore, K_c has to be reduced.

The adjustment for T_d is started when the PI controller performs satisfactorily (Tan, Wang, Hang and Hagglund, 1999). Increasing the value of T_d will normally result in an improvement in stability, which allows further increase in the value of K_c and decrease in T_i.

This table shows that increasing the derivative part results in both faster responses and more stable systems. This rule is only true up to a certain limit and if the feedback signal is sufficiently free of noise. The noise is amplified when T_d is increased, therefore, the upper limit of magnitude of T_d is often set by noise. If the level of noise is too high, PI controllers may be recommended even at the cost of poorer control performances.

It is well-known that fast responses are usually accompanied by poor stability and oscillations, therefore, a step change in the setpoint may result in a severe overshoot. On the other hand, very stable systems without overshoot are usually achieved at the expense of a more sluggish response to setpoint change and load disturbance signals. As a result, controllers that are tuned to give fast responses are usually more sensitive to variations in the process than controllers that are more conservative in their settings (Tan, Wang, Hang and Hagglund, 1999). Therefore, a compromise between the desired speed of the response and the desired stability of the system is necessary.

The most common criterion behind the principles of many tuning methods is to adjust the controller parameters so that the system response has a decay ratio of 25%. There is not a direct mathematical justification for such a choice. However, this is a good tuning criterion if the primary objective is load disturbance rejection. On the other hand, these methods often have problems with setpoint regulation.

2.6. Traditional tuning methods

2.6.1. Ziegler-Nichols methods

Ziegler and Nichols presented two classical methods for determining PID parameters. These methods are still widely used either in the original or in the revised form (Astrom and Hagglund, 1995).

2.6.1.1. Frequency response method

In the Ziegler-Nichols frequency response method (Ziegler and Nichols, 1942), the key issue is to determine the point where the Nyquist curve of the loop transfer function intersects the negative real axis. First the PID controller is connected to the process to form the closed-loop system. Then, integral and derivative terms of the controller are disabled and the proportional gain is gradually increased until a continuous oscillation occurs at gain K_u. Considering K_u and its related oscillating period, T_u, the PID parameters can be calculated from the Ziegler-Nichols tuning formulae. K_u and T_u are called ultimate gain and ultimate period, respectively.

The Ziegler-Nichols tuning rules were originally designed to give closed-loop systems that are able to reject load disturbance signals well. A decay ratio of 25% that is equivalent to a damping

factor of 0.216 was the criterion. The tuning formulae are simple and need only a little knowledge about the process.

2.6.1.2. Step response method

The Ziegler-Nichols step response method (Ziegler and Nichols, 1942) is based on the step response of the open-loop process. The main design objective is to reject load disturbance signals. Again, the design method tries to provide a decay ratio of 25% for the closed-loop step response. First, the unit step response of the process is experimentally determined. It is assumed that the step response is monotonic. Therefore, the process is identified by a first order plus dead time (FOPDT) model:

$$G(s) = \frac{K_p e^{-\tau_d s}}{Ts + 1}. \tag{2.30}$$

Then, control parameters are determined from the model parameters using the Ziegler-Nichols tuning formulae. According to these tuning formulae, the controller gain is inversely proportional to the static gain of the process and the ratio of dead time to time constant (normalised dead time). Therefore, if the process has a high gain, the controller should compensate for this by having a low gain, and vice versa. If the normalised dead time in the process is long, the process is difficult to control and a relatively low controller gain should be used. Both integral and derivative times are proportional to the dead time of the process. This is also sensible, because the time parameters of the controller have to lie in the same range as the process time scale (Tan, Wang, Hang and Hagglund, 1999). Because only a step experiment is required, the main advantage of the Ziegler-Nichols time response method is its simplicity. A common disadvantage of the Ziegler-Nichols methods is that, according to the reports (Astrom and Hagglund, 1995; Friedland, 1996), the resulting closed-loop system is often more oscillatory than desirable.

2.6.2. Cohen-Coon method

The Cohen-Coon method (Cohen and Coon, 1953) is based on FOPDT processes and is very similar to the Ziegler-Nichols step response method. Again, the primary design objective is to reject load disturbance signals. The design method attempts to provide a decay ratio of 25% for dominant closed-loop poles and minimise integral of error (IE), however, the design method gives closed-loop systems with poor damping and high sensitivity (Astrom and Hagglund, 1995).

Both Ziegler-Nichols and Cohen-Coon methods are quite similar when the normalised dead time is small. However, the Cohen-Coon formulae are not as well-known as the Ziegler-Nichols rules. One reason is that they are more demanding in calculation.

It is well-known that the derivative part should not be used for long dead time processes (Tan, Wang, Hang and Hagglund, 1999). When the normalised dead time is high, the derivative part of the Cohen-Coon controllers tends towards zero. This is why the Cohen-Coon controllers perform better than the Ziegler-Nichols ones for such processes.

2.7. Modern tuning techniques

2.7.1. Analytical tuning methods

Analytical tuning methods attempt to directly obtain the controller parameters from the specifications. Specifications, which are normally conflicting, can be expressed in many different ways, such as features of time response for typical inputs or features of frequency responses.

Let $G_p(s)$ and $G_c(s)$ be the transfer functions of the process and controller. The controller can be calculated from:

$$G_c(s) = \frac{1}{G_p(s)} \frac{M(s)}{1 - M(s)}, \tag{2.31}$$

where $M(s)$ is the desired closed-loop transfer function. The key point is to find a reasonable $M(s)$ based on engineering specifications of the system. The λ-tuning (direct synthesis), Haalman method and internal model control (IMC) are among popular analytical tuning methods.

The analytical tuning methods give controllers that cancel poles and zeros in the loop transfer function. It results in a lack of observability and controllability (Shinskey, 1991; Morari and Lee, 1991). Having uncontrollable modes in the closed-loop system may lead to poor performance if the modes are excited. As a result, these methods cannot be applied to processes with poorly damped poles and zeros. In particular, responses to load disturbance signals will be very sluggish for processes with dominating time constants (Astrom and Hagglund, 1995).

2.7.2. Pole placement design techniques

Pole placement is a straightforward design method much used in control engineering. It simply attempts to obtain controllers that give desired closed-loop poles. The advantage of this method is that the closed-loop poles are directly specified. One difficulty with this method is that because all the closed-loop poles are assigned, complex processes lead to complex controllers. The so-called dominant pole placement design method tries to assign only a few poles. As a result, it is possible to design simple controllers for complex processes. The Cohen-Coon method is an early example of dominant pole placement design methods. Some other examples can be found in Person (1992); Person and Astrom (1992); Person and Astrom (1993).

2.7.3. Gain and phase margin design methods

Gain and phase margins are classical control loop specifications associated with the frequency response technique, reflecting the performance and stability of the system and are widely used in controller design procedures (Tan, Wang, Hang and Hagglund, 1999). On the one hand, gain and phase margins are measures of stability robustness and, therefore, should be specified according to the uncertainties of the process. On the other hand, they are also related to the performance of the

closed-loop system and, hence, should be specified to give a good performance (Ho, Lim, Hang and Ni, 1999).

Designing PI (PID) controllers to meet gain and phase margin specification is a well-known design technique. According to reports in Ho, Hang and Zhou (1995); Ho, Gan, Tay and Ang (1996), many of tuning formulae in the PI (PID) control literature give gain and phase margins less than 1.5 and 30°, which are outside the recommended ranges. In order to meet desired gain and phase margins for first and second order plus dead time processes (SOPDT), simple analytical formulae to design the PID controllers were presented in Ho, Hang and Cao (1995). In addition, Ho, Lim and Xu (1998) introduced PID tuning formulae satisfying user-specified gain and phase margins and minimising the ISE performance index.

However, these formulae give the relations between controller parameters and specifications after some approximations. A simple and straightforward design method based on a graphical approach which can simultaneously achieve exact gain and phase margins for a general linear plant without making any structural assumptions was presented in Wang, Fung and Zhang (1999). It is based on utilisation of the frequency response of the process. Using the critical point information and the specified gain margin, the proportional gain of the controller is determined. The phase margin is then used for the calculation of the integral and derivative times.

2.7.4. Optimisation methods

Many PID design techniques are based on optimisation approaches. In these methods, the control problem is formulated as an objective function to be optimised subject to satisfying constraints. The advantage of this approach is that it may simultaneously capture different aspects of the design problem. As an initial study on this topic, minimising certain integral error criteria such as IE, IAE, ISE or ITAE was suggested in Graham and Lathrop (1953) to synthesize optimum transient responses. Recently, several PID tuning rules based on minimising integral error criteria have been presented (Shinskey, 1996; Astrom, Panagopoulos and Hagglund, 1998; Panagopoulos, Astrom and Hagglund, 2002). As a recent research work, minimising the maximum sensitivity subject to satisfying a specified damping ratio was proposed in Toscano (2005) to achieve good transient response, good stability margin, good robustness in the face of model uncertainties and good rejection of load disturbances. Because the design requirements are usually conflicting, utilisation of multi-objective optimisation is a promising idea to find the best compromise controller.

2.7.5. Auto-tuning methods

Relay auto-tuning, proposed by Astrom and Hagglund (1984), is an alternative to the Ziegler-Nichols frequency response method. In this method, a simple experimental test is used to determine K_u and T_u. For this test, the PID controller is temporarily replaced by an on-off controller (or relay). After the control loop is closed, the process output exhibits a sustained oscillation. Considering the amplitude and frequency of this signal, K_u and T_u are obtained.

With an ordinary relay, a small amount of noise can switch the relay randomly. To avoid frequent switching caused by measurement noise, the operation of the relay auto-tuner includes a dead band.

Compared to the Ziegler-Nichols frequency response method, the relay auto-tuning method has several important advantages (Seborg, Edgar and Mellichamp, 2004), as follows:

- Only a single experimental test is required instead of a trial and error procedure
- The amplitude of the process output can be restricted by adjusting relay amplitude
- The process is not forced to a stability limit
- The experimental test is easily automated using commercial products

The relay auto-tuning method also has a disadvantage. For slow processes, it may not be acceptable to subject the process to the two to four cycles of oscillation required to complete the test.

2.8. PID control of MIMO systems

Generally, most industrial processes are multivariable systems. When the interactions in different channels of a process are negligible, a diagonal PID controller is often adequate (Palmor, Halevi and Krasney, 1995). For such processes, a simple and practical multi-loop design method called the biggest log modulus tuning (BLT) method was proposed in Luyben (1986).

However, when interactions are significant, the multi loop PID controller design method often fails to give acceptable responses. In order to obtain a good response, one approach is to develop a full matrix PID controller, but this method has two important deficiencies. First, there are a large number of parameters to be tuned. Assuming a square system, the number of tuning parameters for a full matrix PID controller is $3n^2$, where n is the number of inputs or outputs. Second, cross coupling of the process channels make it difficult to design each loop independently. In other words, adjusting controller parameters of one loop affects the performance of another, sometimes to the extent of destabilizing the entire system. As a result, many industrial multi-loop controllers are tuned loosely to ensure stability. This causes inefficient operation and higher energy costs (Wang, Huang and Guo, 2000).

Another approach is to use a decoupler plus decentralised PID controller. Decentralised PID control is one of the most common control schemes for interacting MIMO plants in process control. The main reason for this is its relatively simple structure, which is easy to understand and to implement. The number of tuning parameters in this case is $3n$, which is significantly less than those in the case of the full matrix PID. Moreover, in the case of actuator or sensor failure, it is relatively easy to stabilize the loop manually, because only one loop is directly affected by the failure (Palmor, Halevi and Krasney, 1995).

One of the most prevalent categories of multivariable systems is the class of two-input two-output (TITO) systems. A comprehensive discussion about decoupling methods of these processes is found in Shinskey (1996). The design of decentralised PID controllers for TITO processes has attracted the attention of a number of academic and industrial researchers. This attention is mainly due to the simplicity of this design technique and the large number of TITO processes in industry.

2.9. Motivation for new tuning rules

Tuning is a trade-off between performance and robustness. Good tuning rules should be simple, easy to use, widely applicable and easy to memorise. There are many issues that have to be taken into account when designing a controller. A reasonable design method should consider conflicting requirements in terms of responses to load disturbance, setpoint and measurement noise as well as robustness to model uncertainties.

2.9.1. Characteristics of good tuning methods

A good tuning technique should be simple, flexible and either generic or extendable. It should be easy to understand, easy to apply and widely applicable. The algorithm should be repeatable for any control objective such as minimisation of rise time, any constraint such as an upper limit on maximum overshoot and any category of processes such as SOPDT processes. It is advantageous if the design method can directly address the design requirements. It is desirable to have a design parameter to change the properties of the closed-loop system and, therefore, the trade-off between performance and robustness. Ideally, a good tuning method should be able to consider any number of objectives and constraints. In order to fulfil more demanding control requirements, the design technique should be applicable to complex control schemes such as double two-degree of freedom structures. It is beneficial if the design procedure can be applied to other types of controller such as lead-lag.

Since the 1940s, many different types of PID tuning rules have been proposed in the literature. A drawback of many of them is that such rules either are not simple or do not consider all the control requirements in a manner in which the designer can achieve the desired trade-off. As a result, obtaining simple tuning rules which provide good compromise solutions is still a compelling task for researchers.

2.9.2. Analysis of some prevalent tuning rules

The ZN rules, which are simple and easy to use, have little emphasis on setpoint response, measurement noise and sensitivity to process variations. Therefore, they do not give good compromise solutions. In contrast, the design method proposed by Astrom, Panagopoulos and Hagglund (1998), called APH in this thesis, performs well in coping with conflicting design requirements. However, it is not easy to obtain the APH controller parameters.

The IMC method results in simple tuning rules. IMC controllers give good responses to setpoint and output disturbance signals. However, since the design method inherently implies that poles and zeros of the plant are cancelled, the response to load disturbance may be poor for lag dominant processes. Skogestad (2003) proposed a tuning method, called SIMC (Skogestad internal model control), to overcome the latter problem.

A common problem with the IMC and APH methods is that they do not address objective functions directly. For example, if the control objective is to have a specified maximum overshoot,

limits on PO have to be transformed into limits on the SIMC's design parameter, τ_c. This is a drawback because the transformation procedure becomes iterative, as shown in Figure 2.4.

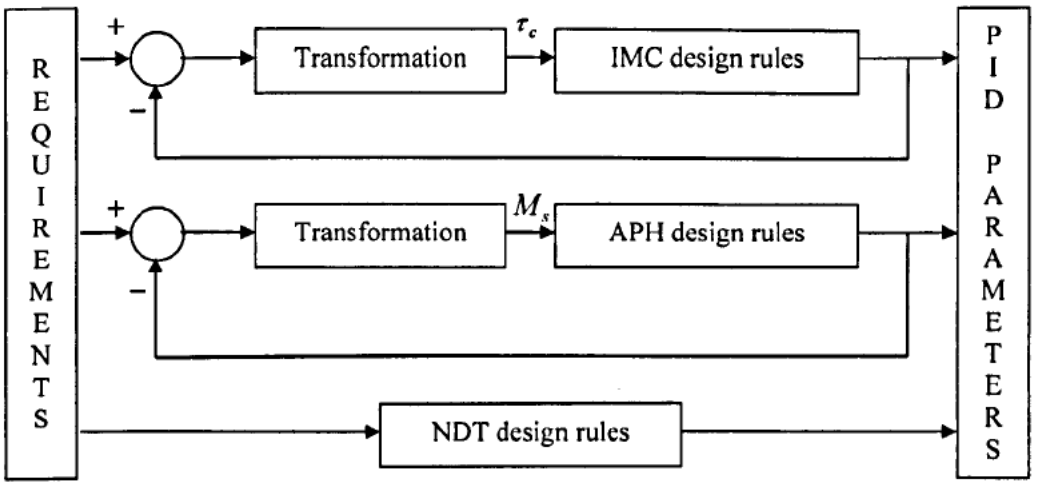

Fig. 2.4. Design diagram of the IMC, APH and NDT tuning methods.

It is the intention of this work to develop a method that retains the advantages of currently established techniques whilst avoiding iteration for a given design problem. In Chapter 3, a non-dimensional tuning (NDT) method is proposed in order to achieve this goal. A comparison of properties of some tuning methods is shown in Table 2.2.

Table 2.2. Comparison of properties of some tuning methods

Property	ZN	SIMC	APH	NDT
Simple	yes	yes	no	yes
Generic or extendable	yes	yes	yes	yes
Address any control aim/objective/constraint	no	no	no	yes
Limitation on number of objectives/constraints	yes	yes	yes	no
Direct objective satisfaction	no	no	no	yes
Trade-off adjustment parameter	no	yes	yes	yes

2.10. Summary

In this chapter, the PID controller, a particular control structure that has become predominantly used in industrial control, is reviewed. A PID controller is sufficient when the dynamics of the process are simple. It has been empirically found that PID controllers often have sufficient flexibility to yield excellent results in many applications.

In view of the large number of controllers used in industry, there is a need for simple, flexible and extendable PID tuning methods. Considering setpoint regulation as the primary design objective, an NDT tuning method for designing PI (PID) controllers for FOPDT (SOPDT) processes is proposed in Chapter 3. This approach is then extended to design a decentralised controller for a given TITO process.

Chapter 3

Non-Dimensional PID Tuning for Setpoint Regulation

3.1. Design of SISO PI controllers

3.1.1. Introduction

Despite the continual advances in control theory, PID control is still the most commonly used algorithm in the process control industry (Liu and Daley, 1999). Traditionally, PID controllers have been tuned empirically, e.g., using the first method of Ziegler and Nichols referred to as continuous cycling method (Ziegler and Nichols, 1942). This method has traditionally been widely known as a fairly accurate heuristic method of determining good settings for PID controllers for a wide range of common industrial process (Hang, Astrom and Ho, 1991). It also has the advantage of requiring very little information about the process, however, it does require knowledge about the ultimate data obtained by destabilising the system under proportional feedback. Moreover, the method inherently leads to an oscillatory response in the face of a change in the setpoint (Friedland, 1996; Liu and Daley, 2001).

It is a common and well-accepted practice to approximate high-order processes by low-order plus dead time models. A large number of industrial plants can approximately be modelled by a FOPDT transfer function:

$$G(s) = \frac{K_p e^{-\tau_d s}}{Ts + 1}. \tag{3.1}$$

Although a FOPDT model does not capture all the features of a high-order process, it often reasonably describes the process gain, dominant time constant and effective dead time of such a process (Dougherty and Cooper, 2003).

In order to design PI controllers for this important category of industrial plants, various methods have been suggested over the past sixty years. The second method of Ziegler and Nichols known as process reaction curve method (Ziegler and Nichols, 1942) and that of Cohen and Coon (Cohen and Coon, 1953) are the most prominent methods mentioned in most control textbooks for control of such processes. Similar to the Ziegler and Nichols methods, the Cohen and Coon technique sometimes brings about oscillatory responses to setpoint changes.

In general, an efficient design method should satisfy the design specifications and be robust in the face of model uncertainties. In this chapter, a new non-dimensional tuning method for FOPDT (SOPDT) processes is proposed. In this method, the control problem is formulated as an optimisation problem. First, performance requirements are introduced in terms of a set of objective functions. Second, robustness issues are taken into account through defining a set of constraints. Finally, PI (PID) tuning formulae are determined using the proposed non-dimensional tuning method.

3.1.2. PI control problem formulation

Generally, a PI controller has the following transfer function:

$$K(s) = K_c\,(1+\frac{1}{T_i s}). \tag{3.2}$$

In order to obtain optimal PI tuning formulae for a FOPDT process, PI parameters can be defined based on the process parameters:

$$K_c = f_1(K_p, \tau_d, T), \tag{3.3}$$

$$T_i = f_2(K_p, \tau_d, T). \tag{3.4}$$

Functions f_1 and f_2 should be determined such that a set of performance criteria are optimised. The optimisation problem may also include constraints. The problem is that it is very difficult to determine these functions because each controller parameter is a function of three process parameters. In order to overcome this difficulty, the procedure for determining f_1 and f_2 is significantly simplified using dimensional analysis, see Appendix A.

The unit of both dead time (τ_d) and time constant (T) in Equation (3.1) is second. The unit of process gain (K_p) depends on the nature of the system. Because process gain along with either dead time or time constant covers all the units in Equations (3.3) and (3.4), m is equal to 2. Therefore, there is only one dimensionless number in the process, namely $\frac{\tau_d}{T}$, which is named dimensionless

dead time. Considering the PI controller in Equation (3.2), the unit of integral time (T_i) is second. The unit of controller gain is the inverse of unit of process gain. As a result, other dimensionless numbers for the combined process and controller are dimensionless gain (K_pK_c) and dimensionless integral time ($\frac{T_i}{\tau_d}$ or $\frac{T_i}{T}$). Based on Buckingham's pi-theorem, these dimensionless numbers are functions of the dimensionless number in the process. Therefore, PI parameters are obtained through determining K_pK_c and $\frac{T_i}{\tau_d}$ (or $\frac{T_i}{T}$) from $\frac{\tau_d}{T}$ as follows:

$$K_pK_c = g_1(\frac{\tau_d}{T}), \tag{3.5}$$

$$\frac{T_i}{\tau_d} = g_2(\frac{\tau_d}{T}). \tag{3.6}$$

Clearly, g_1 and g_2 in Equations (3.5) and (3.6) can be determined much more easily than f_1 and f_2 in Equations (3.3) and (3.4) as there are fewer variables.

GM and PM are typical control loop specifications associated with the frequency response techniques. Not only do they serve as important indicators of system robustness (Ho, Hang and Cao, 1995), they also reflect on the performance and stability of the system and therefore are widely used for controller design (Ho, Gan, Tay and Ang, 1996). Considering the role of GM and PM, a new set of PI tuning formulae for first order processes with dead time/long dead time was presented in Tavakoli and Fleming (2003).

Optimal PI tuning formulae can be derived by determining optimal g_1 and g_2 satisfying a given set of requirements. The optimisation problem is defined as follows:

$$\min f(x)$$
$$subject\ to\ g(x) \geq C$$

where vector x is equal to $[K_c, T_i]$ and C is a pre-defined value. The objective function chosen here is the IAE criterion to the setpoint signal. The constraints are chosen as $GM \geq 3$ and $PM \geq 60°$ to ensure that the resulting system has the adequate robustness. A penalty value is added to the objective function if a given x could not satisfy the constraints.

3.1.3. PI control design procedure and tuning formulae

The following procedure is proposed for generating PI tuning formulae using dimensional analysis.

Step 1. The values of $\frac{\tau_d}{T}$ are selected.

Step 2. For each value of $\frac{\tau_d}{T}$, controller parameters that minimise the objective function for a FOPDT process are determined using a numerical optimisation technique such as genetic algorithms (GAs) (Goldberg, 1989; Fleming and Purshouse, 2002).

Step 3. Optimal values of K_pK_c and $\frac{T_i}{\tau_d}$ versus $\frac{\tau_d}{T}$ are drawn, respectively.

Step 4. g_1 and g_2 are determined using curve-fitting techniques.

In order to take FOPDT processes with small, medium and fairly long dead time into account, the values of dimensionless dead time are considered from 0.1 to 2. Optimal values of the dimensionless gain and dimensionless integral time resulting from step 2 are shown in Table 3.1.

Table 3.1. Optimal PI parameters for a FOPDT model

$\frac{\tau_d}{T}$	K_pK_c	$\frac{T_i}{\tau_d}$
0.1	4.8902	10.022
0.2	2.5627	5.3250
0.3	1.7361	3.5403
0.4	1.2983	2.6305
0.5	1.0517	2.1332
0.6	0.8879	1.8127
0.7	0.7653	1.5560
0.8	0.6797	1.3954
0.9	0.6063	1.2351
1.0	0.5557	1.1450
1.1	0.5098	1.0429
1.2	0.4744	0.9711
1.3	0.4400	0.8946
1.4	0.4164	0.8475
1.5	0.3918	0.7931
1.6	0.3756	0.7626
1.7	0.3557	0.7177
1.8	0.3405	0.6857
1.9	0.3240	0.6479
2.0	0.3157	0.6327

Figure 3.1 shows optimal values of dimensionless gain across the selected values of dimensionless dead time. It can be seen from this figure that dimensionless gain is a function of dimensionless dead time as shown in Equation (3.7).

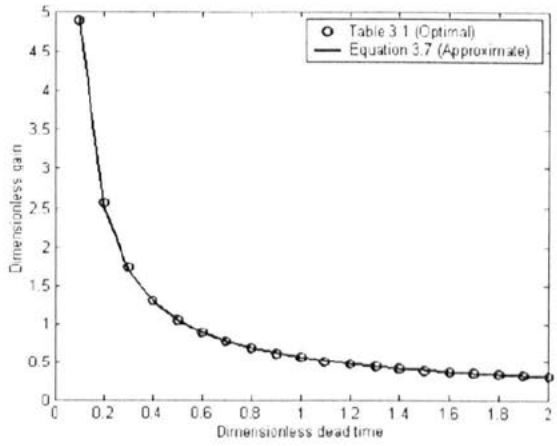

Fig. 3.1. Optimal values of dimensionless gain and values of dimensionless gain given by Equation (3.7) versus dimensionless dead time.

$$K_p K_c = A + \frac{B}{\frac{\tau_d}{T}}. \tag{3.7}$$

Using the method of least-squares, A and B are determined for the best match with Table 3.1. The optimal values of A and B are 0.0754 and 0.4856, respectively. For these values, Figure 3.1 also shows values of $K_p K_c$ given by Equation (3.7), which are very close to optimal values of $K_p K_c$. Similarly, values of $\frac{T_i}{\tau_d}$ are determined from the values of $\frac{\tau_d}{T}$, using Equation (3.8):

$$\frac{T_i}{\tau_d} = 0.1438 + \frac{0.9982}{\frac{\tau_d}{T}}. \tag{3.8}$$

After simplification, the proposed non-dimensional tuning (NDT) method results in the PI tuning formulae shown in:

$$K_c K_p = \frac{T}{2\tau_d} + \frac{1}{14}, \tag{3.9}$$

$$T_i = T + \frac{\tau_d}{7}. \tag{3.10}$$

It is worth mentioning that this design procedure can be used to derive PI tuning formulae for any objective function such as the fastest rise time, any constraint such as an upper limit on overshoot and any control aim such as input regulation or load disturbance rejection.

3.1.4. Simulation results

In this section, the performance of the NDT-PI controller is compared with that of some well-known traditional or recent techniques. For simplicity, the abbreviations shown in Table 3.2 are used for different techniques.

Table 3.2. Different design methods and abbreviations

Method	Abbreviation
Cohen-Coon	CC
Hagglund	Hag
Lee-Edgar	LE
Refined Ziegler-Nichols	RZN
Skogestad internal model control	SIMC
First Ziegler-Nichols	ZN1
Second Ziegler-Nichols	ZN2

Percentage overshoot and settling time (2%) are abbreviated as PO and T_s, respectively. Comparison results of the performance of different design methods applied to simulation examples are summarised in Table 3.5.

Example 3.1.

As a simple example, consider the FOPDT process:

$$G_1(s) = \frac{e^{-0.5s}}{s+1}.$$

Using a one-degree of freedom structure, closed-loop step responses, the responses to a unit step in the setpoint input applied at $t = 0$ and a unit step in the load disturbance input applied at $t = 10$, resulting from the selected design methods are shown in Figure 3.2.

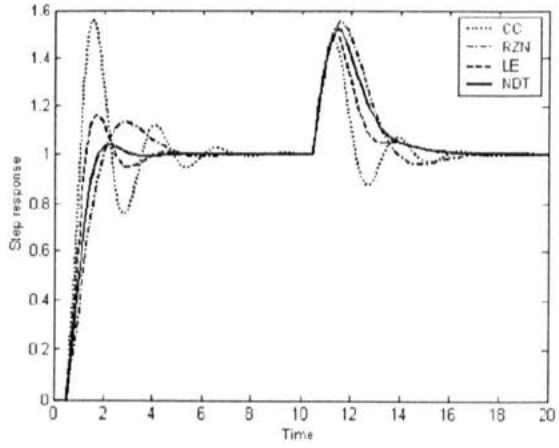

Fig. 3.2. Closed-loop step responses resulting from applying the CC, RZN, LE and NDT methods to $G_1(s)$.

The response given by the CC method has the biggest PO, the longest T_s and the least GM and PM but the fastest load disturbance response. The responses resulting from the ZN1, ZN2 are acceptable but inferior to those given by the RZN (Hang, Astrom and Ho, 1991), LE (Lee and Edgar, 2002), SIMC (Skogestad, 2003) and NDT techniques. The response resulting from the NDT technique has the least PO, the shortest T_s and gives the pre-defined minimum amounts of GM and PM as well as a fairly satisfactory load disturbance response.

The results conform to expectations, as the main design objective of the CC method is to reject load disturbances whereas the NDT technique is to regulate setpoint signals subject to satisfying constraints on gain and phase margins. The results of comparison can be seen in Table 3.5.

In order to investigate the robustness, model parameters are deviated by as much as 20% of their nominal values to represent uncertainties in the model. The different controllers are applied to the perturbed model and the results of the comparison are shown in Table 3.3. In the first column of this table, for example, τ_d and T have no changes, while K_p has a reduction of 20%. It can be seen from the last column of the table that the worst case is related to an increase of 20% in K_p and τ_d and a decrease of 20% in T, simultaneously. For this case, the closed-loop system resulting from the CC controller is unstable, whereas the ZN1, ZN2 and LE methods result in highly oscillatory and slow responses. The remaining techniques perform satisfactorily. For any set of process parameters the best criteria are shown in bold.

Table 3.3. Comparison of the performance of different methods of controlling perturbed $G_1(s)$

Altered values		K_p 0.8	τ_d 0.5	T 1	K_p 1.2	τ_d 0.5	T 1	K_p 1	τ_d 0.4	T 1	K_p 1	τ_d 0.6	T 1	K_p 1	τ_d 0.5	T 0.8	K_p 1	τ_d 0.5	T 1.2	K_p 1.2	τ_d 0.6	T 0.8
CC	*PO*	36.18			75			34.91			76.65			64.44			49.6					
	T_s	4.98			10.9			3.91			13.25			8.39			6.26			Unstable		
	GM	1.98			1.32			2.01			1.3			1.36			1.8					
	PM	39.3			19.19			40.44			18.06			24.24			31.57					
ZN1	*PO*	2.79			34.27			5.08			31.88			25.51			13.8			62.16		
	T_s	4.49			5.22			4.1			6.14			5.08			3.82			16.25		
	GM	2.5			1.67			2.46			1.6			1.7			2.3			1.21		
	PM	65.09			42.34			62.65			44.64			49.04			55.58			20.83		
ZN2	*PO*	4.95			37.99			7.39			34.6			29.04			15.74			68.38		
	T_s	4.54			5.17			4.38			6.12			5.01			3.75			19.57		
	GM	2.39			1.59			2.35			1.62			1.62			2.2			1.16		
	PM	63.85			39.64			61.11			42.13			45.91			54.29			16.25		
RZN	*PO*	7.85			18.47			8.13			19.34			8.67			16.35			26.37		
	T_s	5.48			4			4.71			6.3			3.77			5.23			**4.92**		
	GM	**4.69**			**3.13**			**4.85**			**3.02**			**3.27**			**4.22**			**2.24**		
	PM	58.64			48.66			58.66			48.1			57.2			50.25			44.91		
LE	*PO*	3.28			29.26			4.23			28.38			20.47			13.26			54.04		
	T_s	3.78			4.37			3.2			5.21			**3.35**			**2.96**			9.23		
	GM	2.83			1.89			2.81			1.9			1.93			2.6			1.37		
	PM	62.98			45.49			62.2			46.36			53.05			54.1			29.77		
SIMC	*PO*	**0.13**			**11.69**			**0.11**			11.82			**2.47**			7.13			**25.61**		
	T_s	**2.72**			**2.86**			**2.17**			**3.46**			3.84			4.47			4.99		
	GM	3.96			2.64			3.96			2.64			2.71			3.62			1.91		
	PM	67.08			55.63			67.08			55.63			64.35			58.63			**49.11**		
NDT	*PO*	0			12.1			0			**11.77**			3.21			**5.83**			26.92		
	T_s	3.04			3.67			2.36			4.27			3.91			4.01			4.94		
	GM	3.76			2.51			3.75			2.52			2.57			3.45			1.81		
	PM	**68.36**			**56.0**			**68.19**			**56.31**			**64.78**			**59.79**			48.28		

Considering this example, another test is to determine the ultimate values of K_p, τ_d and T, for which the closed-loop system becomes unstable. The ultimate amount of K_p for any design method is equal to the nominal value of K_p times the value of GM for that technique. The ultimate values of τ_d and T can be seen in Table 3.4.

Table 3.4. Comparison of the ultimate values of τ_d and T as well as the ultimate simultaneous changes in $G_1(s)$

	CC	ZN1	ZN2	RZN	LE	SIMC	NDT
Max τ_d	0.763	1.053	1.105	1.517	1.194	1.582	1.559
Min T	0.477	0.377	0.344	0	0.252	0.028	0.08
Ultimate Changes	17.8%	26.2%	28.3%	59.5%	33.7%	49.8%	47.2%

Considering simultaneous changes in the model parameters, Table 3.4 also shows the percentage of ultimate increase in K_p and τ_d and decrease in T that can be tolerated by the closed-loop system before becoming unstable. Obviously, the RZN design method shows the highest degree of performance robustness, while the SIMC and NDT techniques are satisfactorily robust against model uncertainties. This example clearly shows that good load disturbance rejection and good robustness requirements are conflicting objectives.

Example 3.2.

Consider the third order model with a right half plane (RHP) zero:

$$G_2(s) = \frac{(-s+1)e^{-s}}{(6s+1)(2s+1)^2}.$$

It is well-known that RHP zeros contribute additional phase lag to the system and, therefore, limit the achievable control performance (Skogestad and Postlethwaite, 1996). In order to obtain PI parameters suggested by the CC, ZN2, SIMC and NDT techniques for this example, $G_2(s)$ is approximated by the following FOPDT model, using the half rule approach (Skogestad, 2003):

$$\hat{G}_2(s) = \frac{e^{-5s}}{7s+1}.$$

In order to determine the PI parameters suggested by the ZN1 and RZN methods, first K_u and ω_u are determined from Equations (3.11) and (3.12).

$$K_u = \frac{(\sqrt{36\omega_u^2+1})(4\omega_u^2+1)}{\sqrt{\omega_u^2+1}}. \tag{3.11}$$

$$tg^{-1}(\omega_u) + \omega_u + tg^{-1}(6\omega_u) + 2tg^{-1}(2\omega_u) = \pi. \tag{3.12}$$

The response of the CC method to a setpoint change is again the poorest, whereas the performance of the RZN, SIMC and NDT techniques are satisfactory. The response given by the ZN2 method shows the least PO and highest PM, however, it has the biggest undershoot and a fairly long T_s. Comparing the responses given by the RZN, SIMC and NDT techniques, the latter has the least PO. As expected, the best load disturbance response in terms of the least peak and fastest response is given by the CC. However, the IAE criterion to a unit step load disturbance is almost the same for all the methods. The selected closed-loop step responses are shown in Figure 3.3. Also, the results of comparison can be seen in Table 3.5.

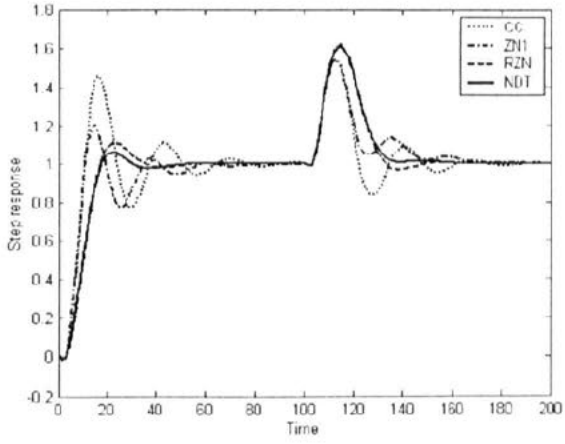

Fig. 3.3. Closed-loop step responses resulting from applying the CC, ZN1, RZN and NDT methods to $G_2(s)$.

Example 3.3.

Consider the process with long dead time:

$$G_3(s) = \frac{e^{-10s}}{s+1}.$$

It is generally believed that control of systems with long dead time is difficult and the control performance obtained by a PI controller is seriously limited (Astrom and Hagglund, 1995). Except for the very sluggish responses given by the ZN1 and ZN2 methods, good setpoint and load disturbance responses are given by other methods. Step responses given by the CC, RZN, Hag (Hagglund, 1996) and NDT methods are shown in Figure 3.4. Among these methods, the last controller gives the highest degree of robustness but the poorest response to the setpoint and load disturbance. In contrast, the RZN controller shows a very good performance but the poorest robustness. Again, this conforms to expectations, as tuning is a trade-off between the performance and robustness.

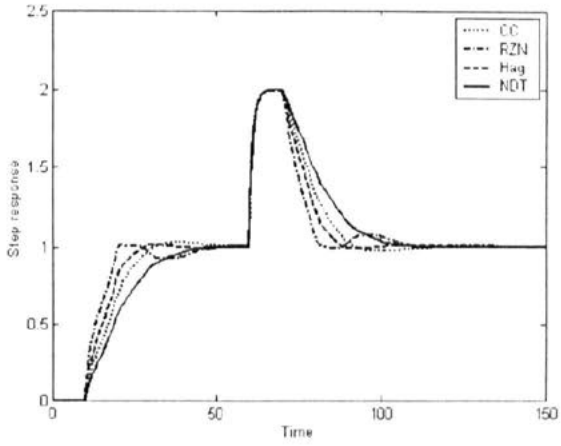

Fig. 3.4. Closed-loop step responses resulting from applying the CC, RZN, Hag and NDT methods to $G_3(s)$.

A challenging perturbation of $G_3(s)$ is given by:

$$\hat{G}_3(s) = \frac{1.2e^{-12s}}{0.8s+1}.$$

The controller parameters resulting from the different design methods are applied to $\hat{G}_3(s)$ and the results of comparison are shown in Table 3.5.

As shown in Figure 3.5, the closed-loop step responses resulting from the CC, Hag, SIMC and NDT methods are satisfactory. Again, the ZN1 and ZN2 methods result in very slow responses. In addition, the response resulting from the RZN controller is too oscillatory. However, the best step response in terms of the least PO, the shortest T_s, the highest GM and the highest PM is given by the NDT controller.

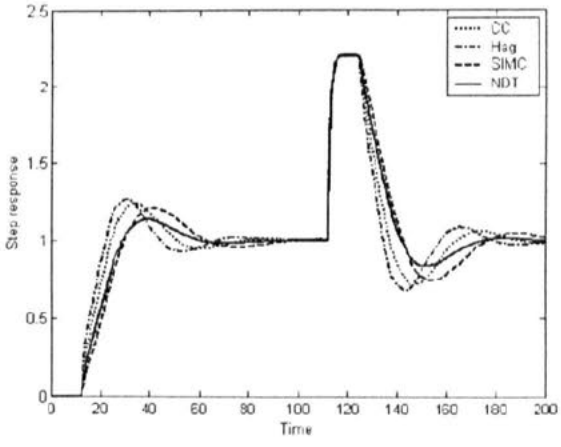

Fig. 3.5. Closed-loop step responses resulting from applying the CC, Hag, SIMC and NDT methods to $\hat{G}_3(s)$.

Table 3.5. Comparison of the performances of different methods of controlling $G_1(s)$, $G_2(s)$, $G_3(s)$ or $\hat{G}_3(s)$

Process	method	K_c	T_i	PO	T_s	GM	PM
$G_1(s)$	CC	1.88	0.83	55.3	6.9	1.58	29.08
	ZN1	1.71	1.45	18.36	3.54	2	53.6
	ZN2	1.8	1.5	21.28	5.24	1.91	51.61
	RZN	0.73	0.69	13.03	4.58	**3.73**	53.19
	LE	1.45	1.16	15.68	3.68	2.27	54.3
	SIMC	1	1	4.53	3.1	3.17	61.35
	NDT	1.07	1.07	**3.45**	**2.62**	3.01	**62.25**
$G_2(s)$	CC	1.34	6.9	46.08	73.4	1.72	31.25
	ZN1	1.59	14.47	20.44	54.7	1.89	48.83
	ZN2	1.26	15	**3.17**	61.8	2.4	**67.19**
	RZN	0.71	6.6	11.19	33.1	3.18	56.35
	SIMC	0.7	7	7.5	**32.08**	**3.34**	59.61
	NDT	0.77	7.71	6.3	40.27	3.19	61.11
$G_3(s)$	CC	0.17	2.87	3.38	45	2.83	61.42
	ZN1	0.47	18.66	**0**	182	2.18	**100.01**
	ZN2	0.09	30	**0**	1362	11.5	93.27
	RZN	0.38	5.61	1.99	45.2	2.13	66.07
	Hag	0.25	3.9	1.34	**25.7**	2.58	62.83
	SIMC	0.05	1	4.09	60.81	3.17	61.35
	NDT	0.12	2.43	0.33	40.02	**3.4**	65.26
$\hat{G}_3(s)$	CC	0.17	2.87	24.32	71.87	2.04	48.64
	ZN1	0.47	18.66	**0**	152.9	1.76	**97.49**
	ZN2	0.09	30	**0**	1138	**9.36**	93.54
	RZN	0.38	5.61	37.8	84.44	1.63	50.41
	Hag	0.25	3.9	27.05	76.95	1.87	48.48
	SIMC	0.05	1	21.38	87.8	2.23	49.41
	NDT	0.12	2.43	13.64	**56.65**	2.43	54.42

When controlling $\hat{G}_3(s)$, PO for the NDT method is 13.64%, whereas it is 0.33% when controlling $G_3(s)$. As a result, an increase of 13.31% in PO is shown. Table 3.6 shows the comparison of changes in PO, T_s, GM and PM when the CC, RZN, Hag, SIMC and NDT controllers are applied to $G_3(s)$ and $\hat{G}_3(s)$. It clearly shows that the NDT method gives the highest degree of performance robustness.

Table 3.6. Comparison of changes in PO, T_s, GM and PM resulting from applying different methods to $G_3(s)$ and $\hat{G}_3(s)$

	ΔPO	ΔT_s	ΔGM	ΔPM
CC	20.94	26.87	0.79	12.78
RZN	35.81	39.24	**0.5**	15.66
Hag	25.71	51.25	0.71	14.35
SIMC	17.29	26.99	0.94	11.94
NDT	**13.31**	**16.63**	0.97	**10.84**

3.1.5. Comments on the NDT-PI tuning formulae

The tuning formulae in Equations (3.9) and (3.10) are slightly different from the settings proposed by the IMC method (Chien and Fruehauf, 1990). These settings are believed to be robust and result in very good responses to setpoint and disturbances entering directly at the output of the process (Skogestad, 2003). However, since the IMC technique inherently implies a pole-zero cancellation, the responses to load disturbance signals may be poor if the ratio of time delay to time constant is small, e.g. less than 0.1, (Astrom and Hagglund, 1995; Skogestad, 2003). These processes are referred to as lag dominant processes.

In order to derive the tuning formulae capable of coping with both setpoint regulation and load disturbance rejection, one can apply unit step signals to setpoint and load disturbance inputs independently. The objective function, $f(x)$, is formed as shown below:

$$f(x) = f_1(x) + f_2(x), \tag{3.13}$$

where $f_1(x)$ and $f_2(x)$ are the IAE criterion to setpoint and the IAE criterion to load disturbance signals, respectively. Considering this aggregated objective function and the previous robustness constraints, the optimisation problem was solved. However, the resulting tuning formulae were found to be very similar to the settings in Equations (3.9) and (3.10). This outcome is illustrated in Example 3.4.

Example 3.4.

Consider the lag dominant process:

$$G_4(s) = \frac{e^{-s}}{30s+1}.$$

Therefore, a sluggish load disturbance response is expected if the NDT formulae are used. Closed-loop step responses resulting from the NDT, SIMC and CC methods are shown in Figure 3.6.

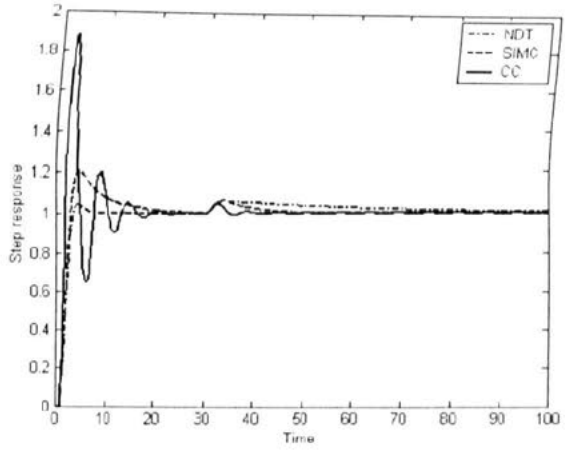

Fig. 3.6. Closed-loop step responses resulting from applying the NDT, SIMC and CC methods to $G_4(s)$.

The CC controller rejects the load disturbances very well but shows a very oscillatory setpoint response. The controller given by the SIMC method gives a good load disturbance response while the best response to setpoint is given by the NDT controller. Values of the aggregated criterion given in Equation (3.13) are 3.97 and 3.39 for the SIMC and NDT controllers, respectively. Also, phase margins are 50.61° for the SIMC and 61.24° for the NDT controllers.

It may seem that the NDT method is superior to SIMC as it gives a higher degree of robustness and a lower value for the aggregated objective function, however, if the objective function is given by Equation (3.14), i.e. more importance on load disturbance rejection, the situation may differ and the SIMC method may result in a better controller.

$$f(x) = f_1(x) + nf_2(x), \quad n > 1 \tag{3.14}$$

As a result, Equation (3.10) needs to be revised for lag dominant processes.

3.1.6. NDT-PI tuning formulae for integrating processes

If the time constant, T, becomes too large a FOPDT process is converted to an integrating process with dead time, as shown below:

$$G(s) = \lim_{T\to\infty} \frac{K_p e^{-\tau_d s}}{Ts+1} = \frac{K'_p e^{-\tau_d s}}{s}, \tag{3.15}$$

where K'_p is given by:

$$K'_p = \frac{K_p}{T}. \tag{3.16}$$

Therefore, optimal PI parameters for an integrating process should be determined by using optimal PI parameters for a FOPDT process with a very large time constant. However, use of Equations (3.9) and (3.10) with a very large time constant leads to a very large integral time, T_i, which is obviously unacceptable and needs revising.

3.1.7. Modification of integral time for lag dominant processes

The value of integral time should be revised for lag dominant and integrating processes. To this end, obtaining NDT-PI tuning formulae resulting in optimisation of both $f_1(x)$ and $f_2(x)$ by using multi-objective optimisation is a straightforward solution. Alternatively, a simple and promising idea for modifying the integral time is to consider load disturbance rejection instead of setpoint regulation for lag dominant processes. Because good load disturbance rejection and good robustness are conflicting requirements, the modification of integral time is expected to lead to a better load disturbance rejection but at the cost of sacrificing robustness and setpoint responses. GM remains unchanged, as there is no change in the value of K_c. PM will be decreased due to a reduction in T_i. Considering the IAE criterion to a step load disturbance, Table 3.7 shows the optimal values of the integral time for lag dominant processes. It clearly shows that PM is sacrificed to improve load disturbance response.

Table 3.7. Optimal values of T_i for lag dominant process

$\frac{\tau_d}{T}$	T_i	GM	PM	TV
0.1	0.927	3.109	60.005	1.116
0.05	0.491	3.069	55.029	1.271
0.02	0.202	3.044	52.004	1.399
0.01	0.112	3.048	52.011	1.482

The last column of the table shows the values of total variations (TV) of control signal, which is defined as follows:

$$TV = \sum_{i=1}^{\infty} \left| u_{i+1} - u_i \right|, \tag{3.17}$$

where $u(t)$ is the control signal. TV, which is a good measure of "smoothness" of the control signal and also an indication of the usage of the control signal, should be as small as possible. Table 3.7 also shows that good load disturbance rejection and small TV are conflicting objectives.

Using curve-fitting techniques, optimal values of the integral time can be determined from:

$$T_i = 9.0787\tau_d + 0.0242. \tag{3.18}$$

Hence, for lag dominant processes, $\frac{\tau_d}{T} \leq \frac{1}{9}$, the integral time is revised as follows:

$$T_i = 9\tau_d. \tag{3.19}$$

Therefore, the NDT-PI tuning formulae capable of coping with FOPDT, lag dominant and integrating processes are given by:

$$K_c K_p = \frac{T}{2\tau_d} + \frac{1}{14}, \tag{3.20}$$

$$\frac{T_i}{T} = \min(1 + \frac{1}{7}\frac{\tau_d}{T}, 9\frac{\tau_d}{T}). \tag{3.21}$$

Applying Equations (3.20) and (3.21) to $G_4(s)$, Figure (3.7) shows the closed-loop step responses given by the NDT and SIMC controllers.

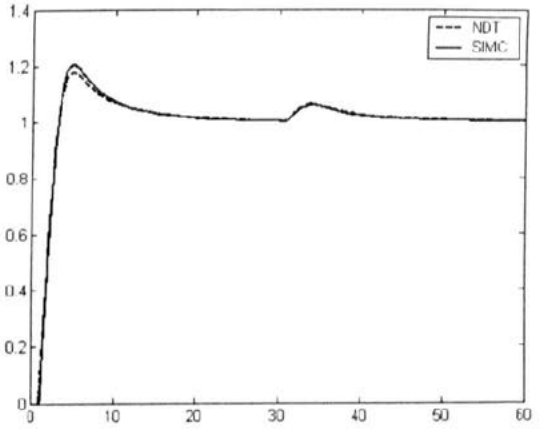

Fig. 3.7. Closed-loop step responses resulting from applying the NDT formulae in Equations (3.20) and (3.21) and SIMC to $G_4(s)$.

The NDT-PI tuning formulae for the integrating process shown in Equation (3.15) are given by:

$$K_c K_p' = \frac{1}{2\tau_d}, \tag{3.22}$$

$$T_i = 9\tau_d. \tag{3.23}$$

3.2. Design of SISO PID controllers

3.2.1. Introduction

Although a large number of industrial process can be modelled fairly accurately using a FOPDT transfer function, if the process has an oscillatory step response, the FOPDT transfer function cannot model the plant efficiently. A more accurate model of the plant can be obtained using the SOPDT model:

$$G(s)=\frac{K_p\omega_n^2 e^{-\tau_d s}}{s^2+2\xi\omega_n s+\omega_n^2},\quad 0<\xi<1 \tag{3.24}$$

3.2.2. PID control problem formulation

A parallel PID controller is given by:

$$K(s)=K_c\,(1+\frac{1}{T_i s}+T_d s). \tag{3.25}$$

In order to obtain optimal PID tuning formulae for a SOPDT model, the PID parameters can be defined based on the model parameters:

$$K_c=f_1(K_p,\ \omega_n,\ \tau_d,\ \xi), \tag{3.26}$$

$$T_i=f_2(K_p,\ \omega_n,\ \tau_d,\ \xi), \tag{3.27}$$

$$T_d=f_3(K_p,\ \omega_n,\ \tau_d,\ \xi). \tag{3.28}$$

Dimensional analysis can be used to simplify Equations (3.26)-(3.28). Considering the process model in Equation (3.24), unit of natural frequency (ω_n) is $\frac{rad}{\sec}$ while damping ratio (ξ) is a dimensionless number. As the process gain and either dead time or natural frequency includes all the units in Equations (3.26)-(3.28), m is equal to 2. As a result, there are two dimensionless numbers in the model, which are damping ratio and dimensionless dead time ($\omega_n\tau_d$). Dimensionless gain, dimensionless integral time ($\frac{T_i}{\tau_d}$ or $T_i\omega_n$) as well as dimensionless derivative time ($\frac{T_d}{\tau_d}$ or $T_d\omega_n$) are other dimensionless numbers for the combined model and controller. Therefore, the simplified relationships among dimensionless numbers in the controller and model are given by:

$$K_p K_c = g_1(\xi, \omega_n \tau_d), \tag{3.29}$$

$$\frac{T_i}{\tau_d} = g_2(\xi, \omega_n \tau_d), \tag{3.30}$$

$$\frac{T_d}{\tau_d} = g_3(\xi, \omega_n \tau_d), \tag{3.31}$$

Obviously, g_1, g_2 and g_3 in Equations (3.29)-(3.31) can be determined much more easily than f_1, f_2 and f_3 in Equations (3.26)-(3.28). However, it is still a challenging task to determine these functions, because $K_p K_c$, $\frac{T_i}{\tau_d}$ and $\frac{T_d}{\tau_d}$ are functions of two dimensionless numbers, namely ξ and $\omega_n \tau_d$. It is worth noting that radian is considered dimensionless.

3.2.3. PID control design procedure and tuning formulae

The following procedure is proposed for generating PID tuning formulae.

Step 1. The values of $\omega_n \tau_d$ are selected.

Step 2. A set of n values for which ξ varies from 0 to 1 is selected.

Step 3. For $\xi = \xi_1$ (ξ_1 is a pre-defined value) and for any value of $\omega_n \tau_d$, controller parameters that minimise the chosen objective function for the SOPDT model are determined.

Step 4. The optimal values of $K_p K_c$, $\frac{T_i}{\tau_d}$ and $\frac{T_d}{\tau_d}$ versus $\omega_n \tau_d$ are drawn.

Step 5. Using curve-fitting techniques, $g_1(\omega_n \tau_d)\big|_{\xi=\xi_1}$, $g_2(\omega_n \tau_d)\big|_{\xi=\xi_1}$ and $g_3(\omega_n \tau_d)\big|_{\xi=\xi_1}$ are determined.

Step 6. Steps 3-5 are repeated for $\xi = \xi_2$, $\xi = \xi_3$, ..., $\xi = \xi_n$.

Step 7. g_1, g_2 and g_3 are determined using curve-fitting methods.

Considering dimensionless dead time from 0.1 to 2 and for any value of ξ, dimensionless gain is a function of dimensionless dead time:

$$K_p K_c = A(\xi) + \frac{B(\xi)}{\tau_d \omega_n}. \tag{3.32}$$

Table 3.8 shows the optimal values of $A(\xi)$ and $B(\xi)$ for different values of ξ.

Table 3.8. Optimal values of $A(\xi)$ and $B(\xi)$ in Equation (3.32) versus ξ

ξ	$A(\xi)$	$B(\xi)$
0.1	0.008	0.097
0.2	0.018	0.181
0.3	0.026	0.286
0.4	0.031	0.386
0.5	0.041	0.482
0.6	0.046	0.578
0.7	0.057	0.677
0.8	0.068	0.771
0.9	0.075	0.867
1	0.086	0.966

Using curve-fitting methods, the optimal values of $A(\xi)$ and $B(\xi)$ are given by:

$$A(\xi) = 0.0802\xi, \tag{3.33}$$

$$B(\xi) = 0.9636\xi. \tag{3.34}$$

As a result, the value of dimensionless gain is as follows:

$$K_p K_c = 0.0802\xi + \frac{0.9636\xi}{\tau_d \omega_n}. \tag{3.35}$$

Similarly, the values of $\frac{T_i}{\tau_d}$ and $T_d\omega_n$ can be obtained using:

$$\frac{T_i}{\tau_d} = 0.101\xi + \frac{1.9778\xi}{\tau_d \omega_n}, \tag{3.36}$$

$$T_d\omega_n = 0.0267 + \frac{0.4958}{\xi}. \tag{3.37}$$

Finally, the simplified NDT formulae for PID controllers are given by:

$$K_c = \frac{\xi}{K_p \tau_d \omega_n}, \tag{3.38}$$

$$T_i = \frac{2\xi}{\omega_n}, \tag{3.39}$$

$$T_d = \frac{1}{2\xi\omega_n}. \tag{3.40}$$

3.2.4. Simulation results

In this section, the performance of the NDT-PID controller is compared with that of some other techniques. For simplicity, the Shen-Yu (Shen and Yu, 1994), Semino-Scali (Semino and Scali, 1998) and Ho-Hang-Cao (Ho, Hang and Cao, 1995) methods are abbreviated as shown in Table 3.9.

Table 3.9. Different design methods and abbreviations

Method	Abbreviation
Ho-Hang-Cao	HHC
Semino-Scali	SS
Shen-Yu	SY

Comparison results of the performance of different design methods applied to simulation examples are shown in Table 3.11.

Example 3.5.

In order to investigate the ability of the NDT-PID formulae to deal with oscillatory or fairly oscillatory systems, the following process is considered:

$$G_5(s) = \frac{e^{-s}}{s^2 + 2\xi s + 1}.$$

For $\xi = 0$, the open-loop step response of the system is oscillatory, and remains fairly oscillatory for small values of ξ. Figure 3.8 shows the open and closed-loop step responses for $\xi = 10^{-6}$. PO, T_s, GM and PM for the closed-loop system are 4.09%, 6.1 sec, 3.17 and 61.35°, respectively. This example shows that the NDT-PID controller results in a very good setpoint response for such an oscillatory process.

Example 3.6.

Consider the underdamped SOPDT process:

$$G_6(s) = \frac{2.1e^{-0.2s}}{36s^2 + 6s + 1}.$$

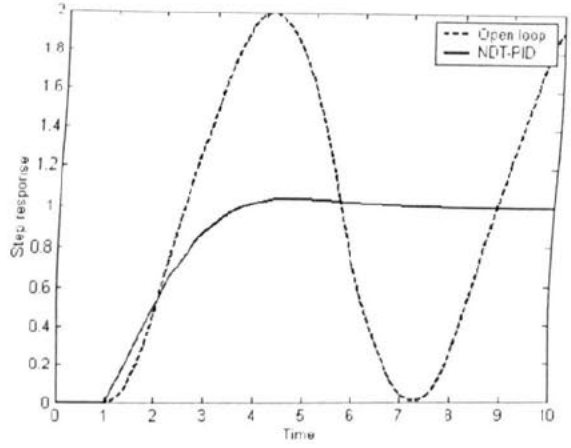

Fig. 3.8. Open-loop and closed-loop step responses resulting from the NDT-PID formulae for $G_5(s)$.

The SY, ZN1, SS and NDT methods are applied to design a PID controller for $G_6(s)$. The SY controller gives a too oscillatory response as the given PM by this method is as small as 5.37°. Figure 3.9 shows the step responses given by the ZN1, SS and NDT methods. The ZN1 controller provides a good load disturbance rejection but a too oscillatory setpoint response. Moreover, it gives a low degree of robustness, a small GM of 0.25 and an insufficient PM of 17.26. The SS method results in having a huge peak in load disturbance response. The reason for such behaviour is that load disturbance rejection and robustness are conflicting requirements and the SS controller gives a GM of 6.61, which is too much.

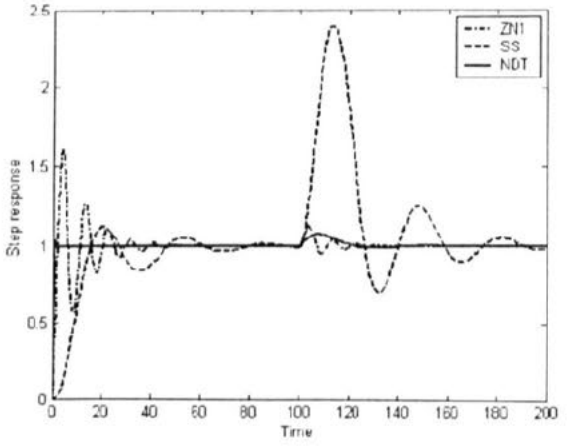

Fig. 3.9. Closed-loop step responses resulting from applying the ZN1, SS and NDT methods to $G_6(s)$.

As a result, the SY, ZN1 and SS methods suffer from improper tuning and, therefore, are unable to give a good compromise solution for $G_6(s)$. Clearly, the NDT controller results in a good compromise solution as it gives an excellent setpoint response, a good ability of load disturbance rejection and a good degree of robustness. The results of comparison are shown in Table 3.11.

Example 3.7.

Consider the 7th order process with a RHP zero:

$$G_7(s) = \frac{(-0.3s+1)(0.08s+1)}{(2s+1)(s+1)(0.4s+1)(0.2s+1)(0.05s+1)^3}.$$

Using the half rule technique, the first and second order approximate models for $G_7(s)$ are given by $\hat{G}_{71}(s)$ and $\hat{G}_{72}(s)$, respectively:

$$\hat{G}_{71}(s) = \frac{e^{-1.47s}}{2.5s+1},$$
$$\hat{G}_{72}(s) = \frac{e^{-0.77s}}{2.4s^2+3.2s+1}.$$

The second order approximate model is not an underdamped or critically damped system. As shown in Table 3.11, the lowest degree of robustness is given by CC and ZN1. Comparing the CC, ZN1 and ZN2 techniques, the latter is superior as it gives a better setpoint response and degree of robustness but a little bit worse load disturbance response. The ZN2 and NDT-PID controllers present almost similar responses. The SIMC-PI and NDT-PI controllers lead to slow responses, however, they show the highest degree of robustness. The closed-loop step responses given by ZN1, NDT-PI and NDT-PID are shown in Figure 3.10.

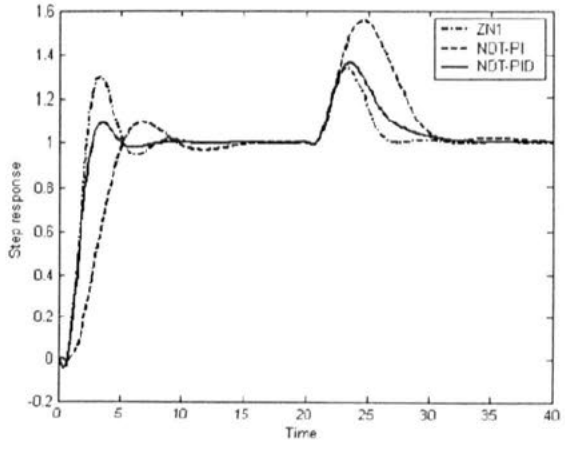

Fig. 3.10. Closed-loop step responses given by applying the ZN1, NDT-PI and NDT-PID methods to $G_7(s)$.

3.2.5. Comments on the NDT-PID tuning formulae

After some approximations and simplifications, the proposed NDT-PID tuning formulae are identical to the IMC settings. Interestingly, the only similarity of these two approaches is that they lead to the same degree of robustness. Again, despite good robustness and very good responses to setpoint and output disturbances, the response to load disturbances may be poor if the cancelled poles are slow in

comparison with the dominant poles (Astrom and Hagglund, 1995). Considering an aggregated objective function, the optimisation problem for unit step signals in setpoint and load disturbance inputs is solved. Using curve-fitting techniques and after some approximations, results are as follows:

$$K_c K_p = (\frac{4}{3}\xi - \frac{1}{12})(\tau_d \omega_n)^{-(0.75+\frac{1}{12\xi})}, \tag{3.41}$$

$$\frac{T_i}{\tau_d} = -\frac{0.01}{\xi} + (1.9\xi + \frac{1}{7})(\tau_d \omega_n)^{-(0.9+\frac{1}{30\xi})}, \tag{3.42}$$

$$T_d \omega_n = \frac{\xi}{40} + \frac{0.4}{\xi}(1 + \frac{0.1}{\xi})(\tau_d \omega_n)^{3.5(\xi-\frac{2}{3})(\xi-0.45)}. \tag{3.43}$$

These tuning formulae are referred to as aggregated non-dimensional tuning (ANDT) formulae.

Example 3.8.

Consider the overdamped process:

$$G_8(s) = \frac{2e^{-s}}{s^2 + 3s + 2}.$$

Figure 3.11 shows that HHC gives the poorest response. The lowest degree of robustness is given by ZN1. Although the NDT formulae are for underdamped and critically damped systems, the NDT controller shows a satisfactory load disturbance rejection because the cancelled poles are not slow. Compared to NDT, a better load disturbance rejection is given by ANDT but at the cost of inferior setpoint response and robustness.

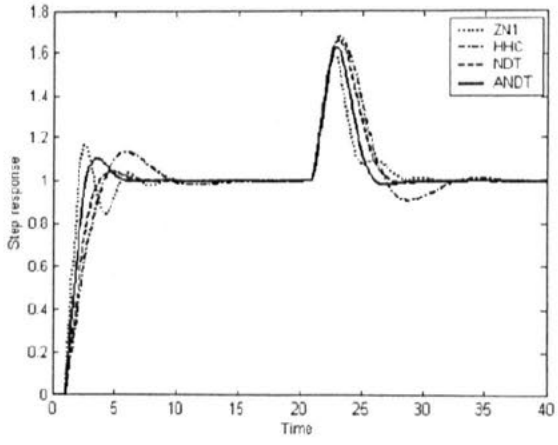

Fig. 3.11. Closed-loop step responses resulting from applying the ZN1, HHC, NDT and ANDT methods to $G_8(s)$.

In order to investigate the robust performance of the worst perturbed models, K_p and τ_d are increased as much as 20%. Then, applying a reduction of 20% in ξ and ω_n, for example, results in the perturbed model given by:

$$\hat{G}_8(s) = \frac{1.536e^{-1.2s}}{s^2 + 1.92s + 1.28}.$$

To produce three more perturbed models of $G_8(s)$, a 20% increase in ξ and a 20% decrease in ω_n, a 20% decrease in ξ and a 20% increase in ω_n, and a 20% increase in both of them are considered. The results of the comparison are summarised in Table 3.10. It shows that all the methods are satisfactorily robust against the perturbations except ZN1.

Table 3.10. Comparison of the performance of different methods of controlling perturbed $G_8(s)$

		$\xi = 0.85$ $\omega_n = 1.13$	$\xi = 1.27$ $\omega_n = 1.13$	$\xi = 0.85$ $\omega_n = 1.7$	$\xi = 1.27$ $\omega_n = 1.7$
ZN1	*PO*	60.73	31.5	Unstable	47.73
	T_s	29.25	**7.2**		14.22
	GM	1.25	1.91		1.37
	PM	23.74	**44.63**		46.7
HHC	*PO*	34.67	37.08	15.92	23.03
	T_s	16	20.67	**6.49**	12.57
	GM	**2.33**	3.29	2.44	3.53
	PM	37.1	33.73	50.65	44.18
NDT	*PO*	**33.57**	**27.46**	26.24	**16.29**
	T_s	**15.19**	13.16	10.94	**6.31**
	GM	1.86	2.79	1.68	2.43
	PM	**42.06**	41.81	**54.79**	**51.7**
ANDT	*PO*	50.56	35.59	52.28	29.39
	T_s	19.31	14.31	21.73	7.03
	GM	1.53	2.35	1.3	1.92
	PM	30.83	36.67	38.06	45.62

Example 3.9.

Consider the SOPDT process with slow poles:

$$G_9(s) = \frac{8e^{-0.25s}}{25s^2 + s + 1}.$$

To obtain PID parameters suggested by the CC method $G_9(s)$ is approximated by a FOPDT model. Using the model reduction method in section 3.3.3.1, the approximate model is given by:

$$\hat{G}_9(s) = \frac{8e^{-4.09s}}{8.68s + 1}.$$

Figure 3.12 shows the closed-loop step responses. The expectation is to achieve good load disturbance rejection by using the CC and ZN1 methods, however, they show excessively oscillatory responses to both load disturbance and setpoint signals. On the other hand, CC and ZN1 give too much GM. Therefore, due to bad tuning there is not a good balance between performance and robustness. The NDT controller has a good response to setpoint change, however, it cannot reject load disturbance signals well due to slow cancelled poles. Figure 3.12 shows that the ANDT controller performs extremely well in regulating the setpoint and rejecting the load disturbance signal.

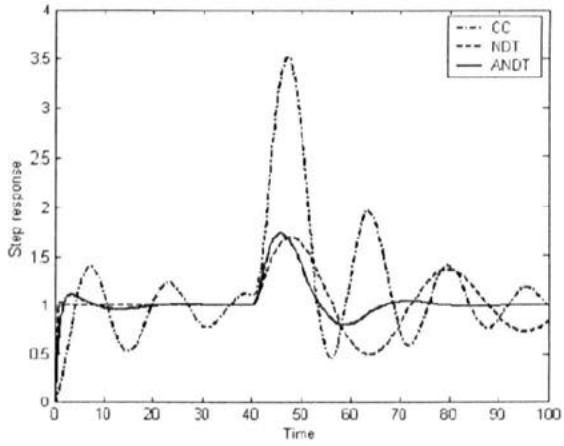

Fig. 3.12. Closed-loop step responses resulting from applying the CC, NDT and ANDT methods to $G_9(s)$.

As a result, if the objective function is given by Equation (3.13), ANDT formulae can be used to overcome the problem of slow responses to load disturbance signals. However, for the objective function in Equation (3.14) it is suggested to use multi-objective optimisation or to consider load disturbance rejection instead of setpoint regulation when the cancelled poles are slow in comparison with the closed-loop poles.

Table 3.11. Comparison of the performances of different methods of controlling $G_6(s)$, $G_7(s)$, $G_8(s)$ or $G_9(s)$

Process	method	K_c	T_i	T_d	PO	T_s	GM	PM
$G_6(s)$	ZN1	8.57	3.4	0.85	62.23	37.26	0.25	17.26
	SY	4.61	14	-	76.17	163.8	1.83	5.37
	SS	0.28	5.6	-	12.16	74.5	**6.61**	51.98
	NDT	7.14	6	6	**4.25**	**1.23**	3.17	**61.35**
$G_7(s)$	CC	2.52	2.95	0.48	34.31	10.96	2.29	37.33
	ZN1	2.57	2.65	0.66	29.71	7.39	2.39	42.18
	ZN2	2.04	2.94	0.74	11.43	**5.45**	2.97	55.67
	SIMC-PI	0.85	2.5	-	9.87	13.57	**3.37**	57.82
	NDT-PI	0.92	2.71	-	9.22	13.53	3.24	**58.79**
	NDT-PID	2.08	3.2	0.75	**8.99**	6.34	2.9	57.99
$G_8(s)$	ZN1	1.37	2.08	0.52	16.48	8.17	1.78	**62.88**
	HHC	0.52	1	0.5	13.61	9.07	**4.72**	53.05
	NDT	0.75	1.5	0.33	**4.07**	6.07	3.17	61.35
	ANDT	1	1.55	0.41	10.46	**5.16**	2.5	56.38
$G_9(s)$	CC	0.38	8.49	1.37	41.41	80.07	34.4	16.64
	ZN1	0.3	7.04	1.76	35.66	80.2	**35.17**	18.56
	NDT	0.25	1	25	**4.06**	**1.52**	3.17	61.35
	ANDT	0.72	3.32	5.01	11.47	18.23	5.41	**65.28**

3.3. Design of MIMO PI (PID) controllers

3.3.1. Introduction

Generally, most industrial processes are multivariable systems. When the interactions in different channels of the process are negligible, a diagonal PID controller is typically adequate. To cope with such processes, Luyben (1986) proposed a simple and practical multi-loop design method called the biggest log modulus tuning method. Nevertheless, the multi-loop PID controller design method often fails to give acceptable responses when interactions are significant. In order to obtain a good response, one approach is to develop a full matrix PID controller, but this method has two important deficiencies. First, cross coupling of the process channels makes it difficult to design each loop independently. In other words, adjusting controller parameters of one loop affects the performance of another, sometimes to the extent of destabilizing the entire system. To ensure stability, many industrial multi-loop controllers are tuned loosely, which causes inefficient operation and higher energy costs. Second, for a full matrix PID controller, $3np$ parameters should be tuned where n is the number of inputs and p is the number of outputs.

Another approach for square systems is to use a decoupler plus a decentralised PID controller. One great advantage of this method is that it allows the use of single-input single-output (SISO) controller design methods. Moreover, the number of tuning parameters in this case is $3n$, which is significantly less than those in the case of the full matrix PID. Furthermore, in the case of actuator or sensor failure, it is relatively easy to stabilise the loop manually, as only one loop is directly affected by the failure (Palmor, Halevi and Krasney, 1995).

TITO systems are one of the most prevalent categories of multivariable systems. Gawthrop (1987) developed a TITO auto-tuner by using a feed-forward design. Using a multi-loop relay auto tuner, an automatic tuning strategy for decentralised PID control for TITO plants was proposed in Palmor, Halevi and Krasney (1995). Ho, Lee, Xu, Zhou and Tay (2000) suggested a method to auto-tune a decoupling controller for TITO processes. Gilbert, Yousef, Natarajan and Deighton (2002) demonstrated a method of tuning PI controllers with one-way decoupling for TITO processes using a finite number of frequency response data.

In this section, a decentralised PI (PID) tuning method for TITO processes is presented. First the process is decoupled through a decoupler matrix. Next, a first (second) order plus dead time model is determined for each element of the decoupled process. Then, a decentralised PI (PID) controller is obtained using the NDT formulae.

3.3.2. Decoupling

Let the TITO process be:

$$G(s)=\begin{bmatrix} g_{11}(s)e^{-\tau_{11}s} & g_{12}(s)e^{-\tau_{12}s} \\ g_{21}(s)e^{-\tau_{21}s} & g_{22}(s)e^{-\tau_{22}s} \end{bmatrix}. \tag{3.44}$$

It is assumed that either diagonal or off-diagonal elements of $G(s)$ have no RHP poles. Considering the following cases $G(s)$ is decoupled through a decoupler matrix.

Case 1. It is supposed that off-diagonal elements of $G(s)$ have no RHP poles. Another assumption is that diagonal elements of $G(s)$ have no RHP zeros. Considering the decoupler suggested by Wang, Huang and Guo (2000):

$$D(s)=\begin{bmatrix} v_1(s) & d_{12}(s)v_2(s) \\ d_{21}(s)v_1(s) & v_2(s) \end{bmatrix}, \tag{3.45}$$

where $v_1(s)$, $v_2(s)$, $d_{12}(s)$ and $d_{21}(s)$ are shown in Equation (3.46), $Q(s)$ in Equation (3.47) is a diagonal matrix. $Q(s)$ is to be controlled through a decentralised PI (PID) controller. In other words, $q_1(s)$ and $q_2(s)$, which are two SISO plants, are controlled through $k_1(s)$ and $k_2(s)$ respectively.

$$
\begin{aligned}
v_1(s) &= \begin{cases} 1 & \tau_{21} \geq \tau_{22} \\ e^{(\tau_{21}-\tau_{22})s} & \tau_{21} < \tau_{22} \end{cases}, \\
v_2(s) &= \begin{cases} 1 & \tau_{12} \geq \tau_{11} \\ e^{(\tau_{12}-\tau_{11})s} & \tau_{12} < \tau_{11} \end{cases}, \\
d_{12}(s) &= -\frac{g_{12}(s)}{g_{11}(s)} e^{-(\tau_{12}-\tau_{11})s}, \\
d_{21}(s) &= -\frac{g_{21}(s)}{g_{22}(s)} e^{-(\tau_{21}-\tau_{22})s}.
\end{aligned} \tag{3.46}
$$

$$
Q(s) = G(s)D(s) = diag\{q_1(s), q_2(s)\}. \tag{3.47}
$$

It is worth noting that interactions are zero unless additional large poles are added to the decoupler to make it proper.

Case 2. If there are no RHP poles in diagonal and no RHP zeros in off-diagonal elements of $G(s)$, the following decoupler can be used:

$$
\begin{aligned}
D(s) &= \begin{bmatrix} d_{11}(s)v_3(s) & v_3(s) \\ v_4(s) & d_{22}(s)v_4(s) \end{bmatrix}, \\
v_3(s) &= \begin{cases} 1 & \tau_{22} \geq \tau_{21} \\ e^{(\tau_{22}-\tau_{21})s} & \tau_{22} < \tau_{21} \end{cases}, \\
v_4(s) &= \begin{cases} 1 & \tau_{11} \geq \tau_{12} \\ e^{(\tau_{11}-\tau_{12})s} & \tau_{11} < \tau_{12} \end{cases}, \\
d_{11}(s) &= -\frac{g_{22}(s)}{g_{21}(s)} e^{-(\tau_{22}-\tau_{21})s}, \\
d_{22}(s) &= -\frac{g_{11}(s)}{g_{12}(s)} e^{-(\tau_{11}-\tau_{12})s}.
\end{aligned} \tag{3.48}
$$

Case 3. Assuming a stable $G(s)$, if both diagonal and off-diagonal elements of $G(s)$ have RHP zeros, a stable decoupler cannot be obtained using decouplers in Equations (3.45) or (3.48). In appendix B, a simple method is suggested to decouple such TITO processes using stable decouplers.

3.3.3. Model reduction

In this section a FOPDT (SOPDT) process is determined for each element of the decoupled process.

3.3.3.1. FOPDT approximate model

Approximation of high-order processes by low-order plus dead time models is a common practice. In order to find an approximate FOPDT model for $h(s)$, which is an element of $H(s)$, three unknown parameters in Equation (3.49), namely k_p, τ_d and T, should be determined:

$$l(s)=\frac{k_p e^{-\tau_d s}}{Ts+1}. \tag{3.49}$$

Fitting Nyquist plots of high-order and low-order models at particular points was successfully used in Wang, Lee, Fung, Bi and Zhang (1999). In this research work, Equation (3.50) is suggested to calculate the values of k_p, τ_d and T. This equation indicates that the steady state gain and gain margin are the same for the high-order process and FOPDT model:

$$\begin{aligned} &l(0)=h(0),\\ &|l(j\omega_c)|=|h(j\omega_c)|,\\ &\angle\{l(j\omega_c)\}=\angle\{h(j\omega_c)\}, \end{aligned} \tag{3.50}$$

where the cross over frequency, ω_c, of the original system is determined using:

$$\angle h(j\omega_c)=\pi. \tag{3.51}$$

As a result, the parameters of the FOPDT model can be calculated using:

$$\begin{aligned} k_p &= h(0),\\ T &= \frac{\sqrt{(\frac{h(0)}{|h(j\omega_c)|})^2-1}}{\omega_c},\\ \tau_d &= \frac{\pi-\tan^{-1}(T\omega_c)}{\omega_c}. \end{aligned} \tag{3.52}$$

3.3.3.2. SOPDT approximate model

When a process has an oscillatory step response, a FOPDT model cannot model it well. In this case, a more accurate model of the process can be obtained using the SOPDT model:

$$\tilde{l}(s)=\frac{K_p\omega_n^2 e^{-\tau_d s}}{s^2+2\xi\omega_n s+\omega_n^2}, \quad 0<\xi\le 1. \tag{3.53}$$

Four unknown parameters in Equation (3.53) should be determined to find an approximate SOPDT model for each element of Q(s). To do so, Equation (3.54) was suggested by Wang, Lee, Fung, Bi and Zhang (1999):

$$\begin{aligned} &\tilde{l}(j\omega_b)=h(j\omega_b),\\ &\tilde{l}(j\omega_c)=h(j\omega_c), \end{aligned} \tag{3.54}$$

where ω_b is determined using:

$$\angle h(j\omega_b) = -\frac{\pi}{2}. \tag{3.55}$$

$h(j\omega_b)$ and $h(j\omega_c)$ can be written as:

$$\begin{aligned} h(j\omega_b) &= |h(j\omega_b)|e^{-j\frac{\pi}{2}} = -j|h(j\omega_b)|, \\ h(j\omega_c) &= |h(j\omega_c)|e^{-j\pi} = -|h(j\omega_c)|. \end{aligned} \tag{3.56}$$

Inserting Equation (3.56) into Equation (3.54) results in:

$$K_p\omega_n \cos(\omega_b\tau_d) = 2\xi\omega_b|h(j\omega_b)|, \tag{3.57}$$

$$K_p\omega_n^2 \sin(\omega_b\tau_d) = (\omega_n^2 - \omega_b^2)|h(j\omega_b)|, \tag{3.58}$$

$$K_p\omega_n^2 \cos(\omega_c\tau_d) = -(\omega_n^2 - \omega_c^2)|h(j\omega_c)|, \tag{3.59}$$

$$K_p\omega_n \sin(\omega_c\tau_d) = 2\xi\omega_c|h(j\omega_c)|. \tag{3.60}$$

In order to simplify these equations, Equations (3.57) and (3.60) are merged to form:

$$\frac{\cos(\omega_b\tau_d)}{\sin(\omega_c\tau_d)} = \frac{\omega_b|h(j\omega_b)|}{\omega_c|h(j\omega_c)|}. \tag{3.61}$$

Using an iterative technique such as the Newton-Raphson, τ_d is determined from Equation (3.61). Merging Equations (3.58) and (3.59), results in:

$$\frac{\omega_n^2 - \omega_b^2}{\omega_n^2 - \omega_c^2} = -\frac{\sin(\omega_b\tau_d)|h(j\omega_c)|}{\cos(\omega_c\tau_d)|h(j\omega_b)|}. \tag{3.62}$$

Equation (3.62) gives the value of ω_n. Then, K_p and ξ are determined from Equations (3.58) and (3.57), respectively.

3.3.4. Simulation results

In order to evaluate the performance of the proposed decentralised tuning method, it is applied to four processes and the results are compared with those of some prevalent techniques.

Example 3.10.

The Wood-Berry binary distillation column plant (Wood and Berry, 1973) is a multivariable system that has been studied extensively. The process has the following transfer matrix:

$$G_{10}(s)=\begin{bmatrix}\dfrac{12.8e^{-s}}{16.7s+1} & \dfrac{-18.9e^{-3s}}{21.0s+1}\\ \dfrac{6.6e^{-7s}}{10.9s+1} & \dfrac{-19.4e^{-3s}}{14.4s+1}\end{bmatrix}.$$

Using Equation (3.45), the decoupler matrix is given by:

$$D(s)=\begin{bmatrix}1 & \dfrac{1.477(16.7s+1)e^{-2s}}{21s+1}\\ \dfrac{0.34(14.4s+1)e^{-4s}}{10.9s+1} & 1\end{bmatrix}.$$

The resulting diagonal system is:

$$Q(s)=diag\{q_1(s),q_2(s)\},$$
$$q_1(s)=\frac{12.8e^{-s}}{16.7s+1}-\frac{6.43(14.4s+1)e^{-7s}}{(10.9s+1)(21.0s+1)},$$
$$q_2(s)=\frac{-19.4e^{-3s}}{14.4s+1}+\frac{9.745(16.7s+1)e^{-9s}}{(10.9s+1)(21.0s+1)}.$$

In order to determine the NDT-PI controller, $q_1(s)$ and $q_2(s)$ should be approximated by FOPDT models. Using Equation (3.52), FOPDT models for $q_1(s)$ and $q_2(s)$ are determined as follows:

$$l_1(s)=\frac{6.37e^{-1.065s}}{5.411s+1},$$
$$l_2(s)=\frac{-9.655e^{-2.157s}}{4.684s+1}.$$

Substituting the delay time with a transfer function by using the Pade approximation, Figures 3.13 and 3.14 show the Nyquist plots of the diagonal elements of $Q(s)$ and their FOPDT approximate models.

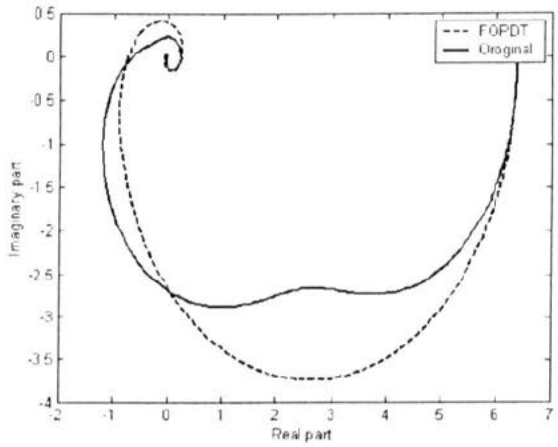

Fig. 3.13. Nyquist plots of $q_1(s)$ and $l_1(s)$.

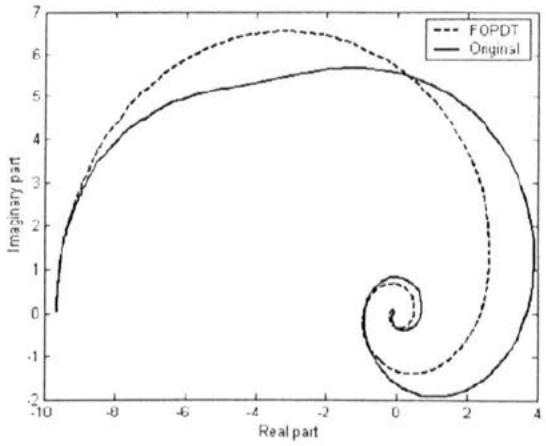

Fig. 3.14 Nyquist plots of $q_2(s)$ and $l_2(s)$.

Using Equations (3.20) and (3.21), the NDT controller is given by:

$$K_{NDT} = \begin{bmatrix} 0.41 + \dfrac{0.074}{s} & 0 \\ 0 & -0.12 - \dfrac{0.024}{s} \end{bmatrix}.$$

Applying three prevalent tuning methods, which are the BLT tuning technique (Luyben, 1986), the full-matrix multivariable (MV) method (Wang, Zou, Lee and Bi, 1997) and the Wang auto-tuning method (Wang, Huang and Guo, 2000), to $G_{10}(s)$ results in the following controllers:

$$K_{BLT} = \begin{bmatrix} 0.375 + \dfrac{0.045}{s} & 0 \\ 0 & -0.075 - \dfrac{0.003}{s} \end{bmatrix},$$

$$K_{MV} = \begin{bmatrix} 0.184 + \dfrac{0.047}{s} & -0.01 - \dfrac{0.023}{s} + 0.008s \\ -0.068 + \dfrac{0.016}{s} - 0.054s & -0.066 - \dfrac{0.015}{s} \end{bmatrix},$$

$$K_{Wang} = \begin{bmatrix} 0.216 + \dfrac{0.076}{s} + 0.017s & 0 \\ 0 & -0.068 - \dfrac{0.019}{s} - 0.064s \end{bmatrix}.$$

The BLT and MV methods do not use any decoupling strategy. In this example, the NDT and Wang techniques use the same decouplers. There are only four tuning parameters for the NDT decentralised PI controller, however, the MV and Wang controllers have ten and six parameters to tune, respectively. Output responses to unit step functions in the first or second input are shown in Figures (3.15)-(3.18).

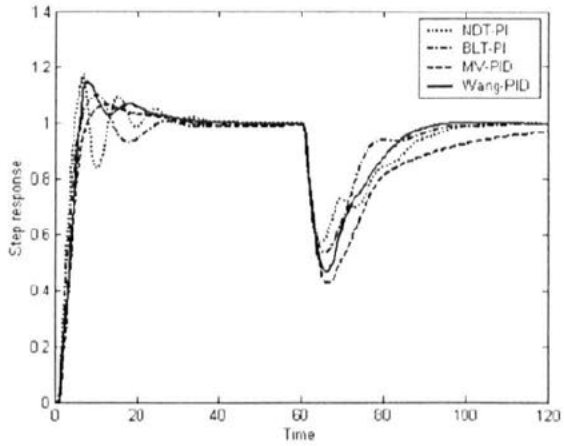

Fig. 3.15. First output response to a unit step in the first input.

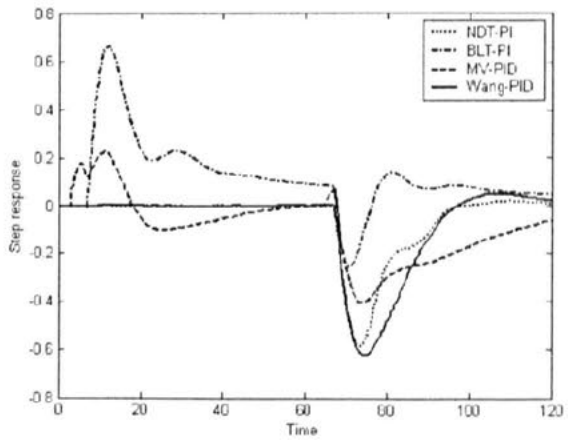

Fig. 3.16. Second output response to a unit step in the first input.

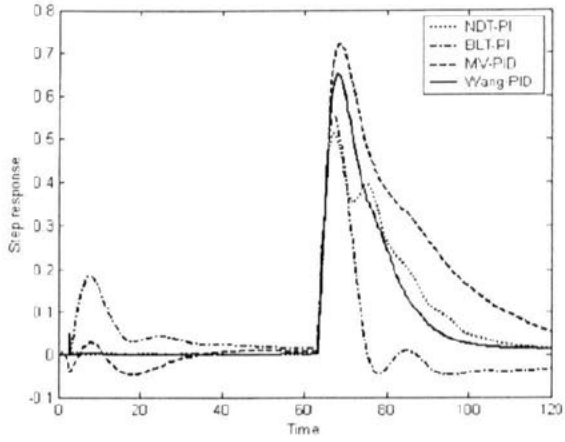

Fig. 3.17. First output response to a unit step in the second input.

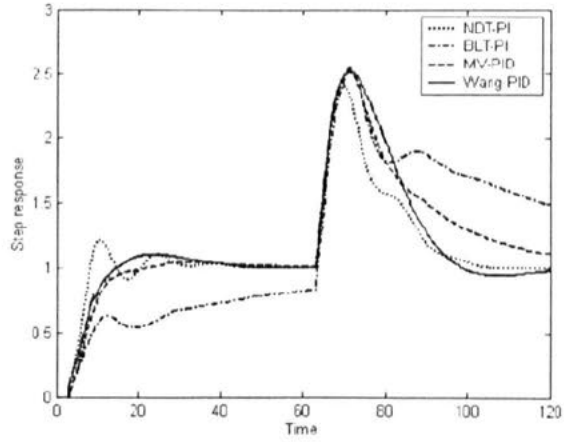

Fig. 3.18. Second output response to a unit step in the second input.

Figure 3.15 shows that although the NDT and BLT controllers are only PI, all the responses are satisfactory. It can be seen from Figures 3.16 and 3.17 that loop interactions are nearly zero for the NDT and Wang methods, however, other techniques, especially the BLT method, result in significant loop interactions. Figure 3.18 shows that the fastest response is given by the NDT controller.

Example 3.11.

Consider a modified Alatiqi subsystem (Luyben, 1986):

$$G_{11}(s)=\begin{bmatrix} \dfrac{-0.51e^{-7.5s}}{(32s+1)^2(2s+1)} & \dfrac{1.68e^{-2s}}{(28s+1)^2(2s+1)} \\ \dfrac{-1.25e^{-2.8s}}{(43.6s+1)(9s+1)} & \dfrac{4.78e^{-1.15s}}{(48s+1)(5s+1)} \end{bmatrix}.$$

The decoupler is given by:

$$D(s)=\begin{bmatrix} 1 & \dfrac{3.294(32s+1)^2}{(28s+1)^2} \\ \dfrac{0.262(48s+1)(5s+1)e^{-1.65s}}{(43.6s+1)(9s+1)} & e^{-5.5s} \end{bmatrix}.$$

The diagonal elements of $Q(s)$ are:

$$q_1(s)=\frac{-0.51e^{-7.5s}}{(32s+1)^2(2s+1)}+\frac{0.439(48s+1)(5s+1)e^{-3.65s}}{(28s+1)^2(43.6s+1)(9s+1)(2s+1)},$$
$$q_2(s)=\frac{4.78e^{-6.65s}}{(48s+1)(5s+1)}-\frac{4.118(32s+1)^2e^{-2.8s}}{(28s+1)^2(43.6s+1)(9s+1)}.$$

The FOPDT models for $q_1(s)$ and $q_2(s)$ are given by:

$$l_1(s)=\frac{-0.071e^{-77.24s}}{58.761s+1},$$
$$l_2(s)=\frac{0.662e^{-61.981s}}{32.133s+1}.$$

The Nyquist plots of $q_1(s)$and $q_2(s)$ and their FOPDT models are shown in Figures 3.19 and 3.20. The NDT-PI controller is given by:

$$K_{NDT}=\begin{bmatrix} -6.393-\dfrac{0.092}{s} & 0 \\ 0 & 0.499+\dfrac{0.012}{s} \end{bmatrix}.$$

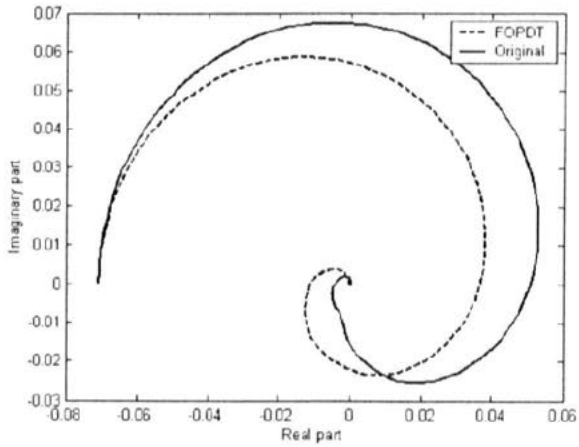

Fig. 3.19. Nyquist plots of $q_1(s)$ and $l_1(s)$.

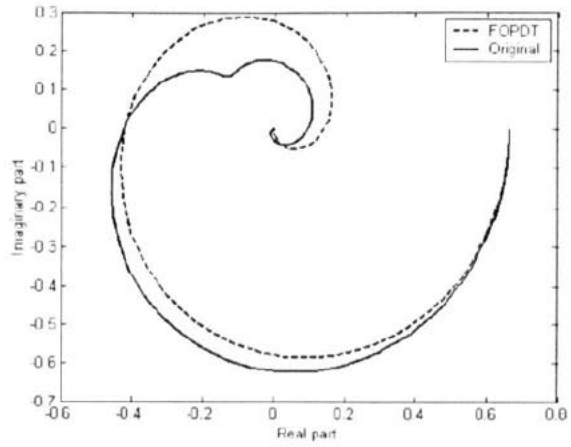

Fig. 3.20. Nyquist plots of $q_2(s)$ and $l_2(s)$.

Wang's decoupler and PID controller are:

$$D_{Wang} = \begin{bmatrix} 1 & \dfrac{3.22(61.71s+1)}{(48.365s+1)} \\ \dfrac{0.263(49.751s+1)e^{-3.474s}}{(48.781s+1)} & e^{-4.705s} \end{bmatrix},$$

$$K_{Wang} = \begin{bmatrix} -2.176 - \dfrac{0.059}{s} + 0.807s & 0 \\ 0 & 0.154 + \dfrac{0.005}{s} - 0.117s \end{bmatrix}.$$

The MV-PID controller is given by:

$$K_{MV} = \begin{bmatrix} -2.12 - \dfrac{0.034}{s} & -0.126 + \dfrac{0.013}{s} + 0.467s \\ -0.218 - \dfrac{0.009}{s} + 0.624s & 0.049 + \dfrac{0.004}{s} \end{bmatrix}.$$

Applying the NDT, MV and Wang controllers to $G_{11}(s)$, output responses to a unit step function in the first or second input are shown in Figures 3.21-3.24.

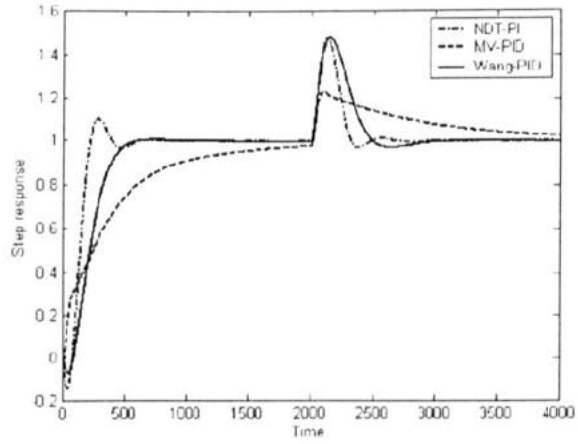

Fig. 3.21. First output response to a unit step in first input.

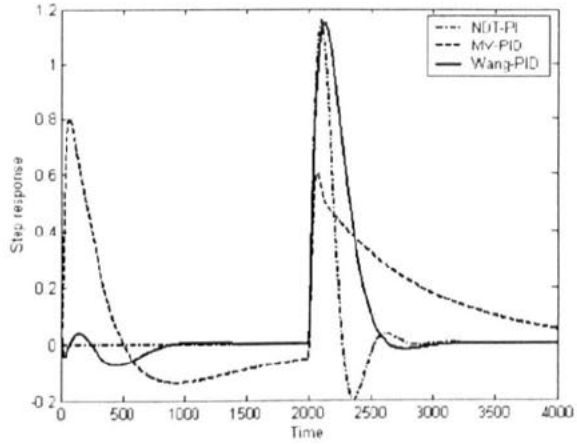

Fig. 3.22. Second output response to a unit step in first input.

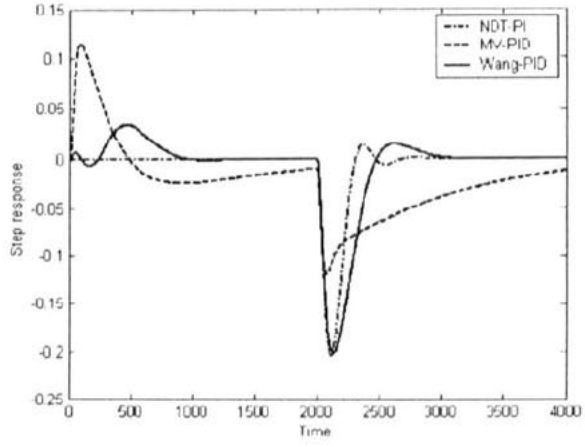

Fig. 3.23. First output response to a unit step in second input.

It can be seen from Figures 3.22 and 3.23 that loop interactions are nearly zero for the NDT method while other techniques give nonzero interactions. Large loop interactions are particularly given by the MV method. Figures 3.21 and 3.24 show that step responses resulting from the NDT method are faster than that of other techniques.

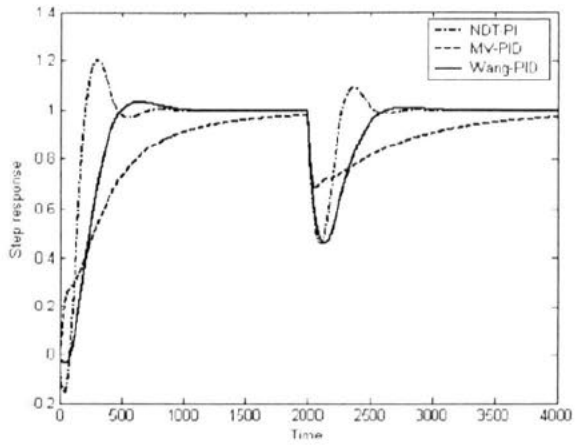

Fig. 3.24. Second output response to a unit step in second input.

Example 3.12.

Let the TITO process be:

$$G_{12}(s)=\begin{bmatrix} \dfrac{0.5}{(0.1s+1)^2(0.2s+1)^2} & \dfrac{-1}{(0.1s+1)(0.2s+1)^2} \\ \dfrac{1}{(0.1s+1)(0.2s+1)^2} & \dfrac{2.4}{(0.1s+1)(0.2s+1)^2(0.5s+1)} \end{bmatrix}.$$

Due to large interactions in this process, the performance of the decentralised PID controller based on the critical point (Palmor, Halevi and Krasney, 1993) is not satisfactory (Wang, Zou, Lee and Bi, 1997) and so is not considered for comparison.

Using Equation (3.45), the decoupler is:

$$D(s)=\begin{bmatrix} 1 & 2(0.1s+1) \\ -\dfrac{5}{12}(0.5s+1) & 1 \end{bmatrix}.$$

Using additional poles with small time constants, a practical decoupler is given by:

$$\hat{D}(s)=\begin{bmatrix} 1 & 2\dfrac{0.1s+1}{0.01s+1} \\ -\dfrac{\dfrac{5}{12}(0.5s+1)}{0.05s+1} & 1 \end{bmatrix}.$$

The diagonal elements of $Q(s)=G(s)\hat{D}(s)$ are:

$$q_1(s) = \frac{1}{(0.1s+1)(0.2s+1)^2}\left(\frac{0.5}{0.1s+1} + \frac{\frac{5}{12}(0.5s+1)}{0.05s+1}\right),$$
$$q_2(s) = \frac{1}{(0.2s+1)^2}\left(\frac{2.4}{(0.1s+1)(0.5s+1)} + \frac{2}{0.01s+1}\right).$$

The FOPDT and SOPDT models for these diagonal elements are as follows:

$$l_1(s) = \frac{0.917e^{-0.083s}}{0.591s+1},$$
$$l_2(s) = \frac{4.4e^{-0.252s}}{3.003s+1},$$
$$\tilde{l}_1(s) = \frac{32.674e^{-0.029s}}{s^2+11.349s+41.229},$$
$$\tilde{l}_2(s) = \frac{46.601e^{-0.008s}}{s^2+7.838s+9.443}.$$

Nyquist plots of $q_1(s)$ and $q_2(s)$ and their approximate models are shown in Figures 3.25 and 3.26.

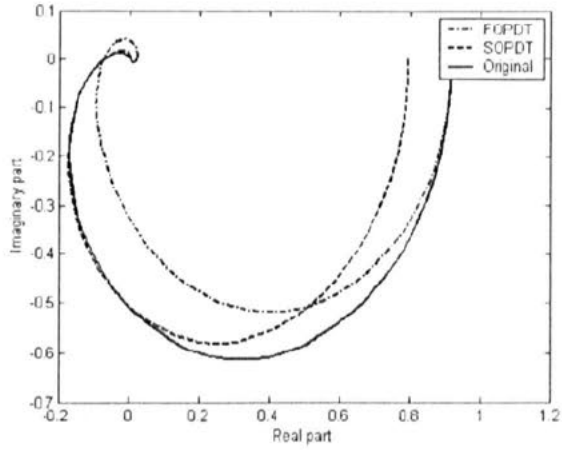

Fig. 3.25. Nyquist plots of $q_1(s)$, $l_1(s)$ and $\tilde{l}_1(s)$.

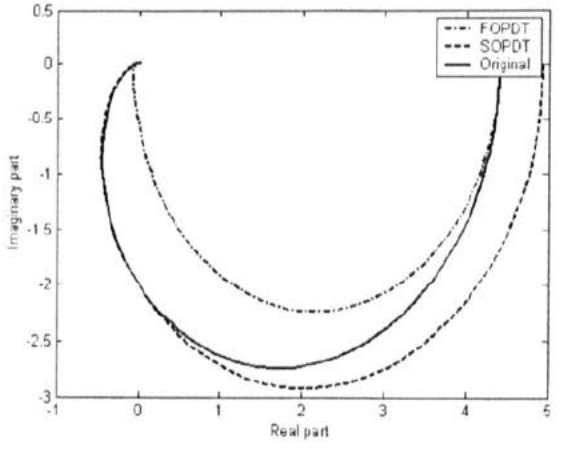

Fig. 3.26. Nyquist plots of $q_2(s)$, $l_2(s)$ and $\tilde{l}_2(s)$.

The NDT-PI and NDT-PID controllers are:

$$K_{NDT-PI} = \begin{bmatrix} 3.946 + \dfrac{6.551}{s} & 0 \\ 0 & 1.368 + \dfrac{0.602}{s} \end{bmatrix},$$

$$K_{NDT-PID} = \begin{bmatrix} 6.088 + \dfrac{22.113}{s} + 0.536s & 0 \\ 0 & 10.529 + \dfrac{12.686}{s} + 1.344s \end{bmatrix}.$$

The MV-PID controller is given by:

$$K_{MV} = \begin{bmatrix} 2.83 + \dfrac{9.93}{s} & 1.51 + \dfrac{1.746}{s} + 0.138s \\ -3.25 - \dfrac{4.14}{s} - 0.592s & 0.667 + \dfrac{0.86}{s} \end{bmatrix}.$$

Applying the NDT and MV controllers to $G_{12}(s)$, output responses to a unit step function in the first and second inputs are shown in Figures 3.27-3.30. Due to adding poles with small time constants to off-diagonal elements of the decoupler, the NDT controllers have non-zero interactions. Clearly, the NDT-PID controller gives the best response in terms of setpoint regulation and load disturbance rejection.

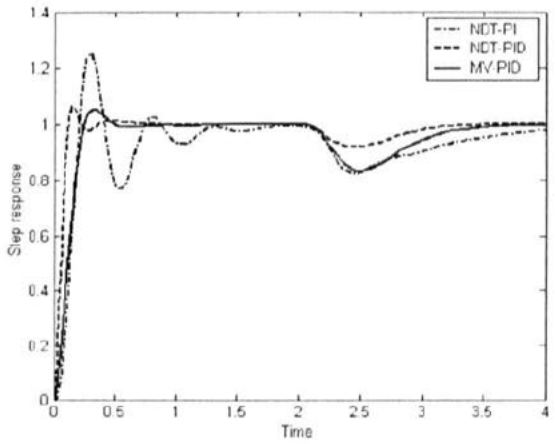

Fig. 3.27. First output response to a unit step in first input.

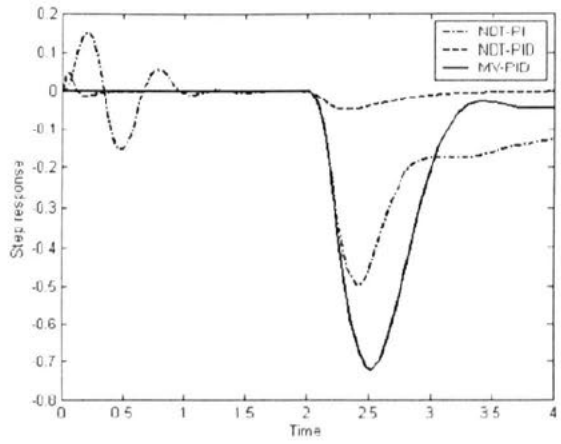

Fig. 3.28. Second output response to a unit step in first input.

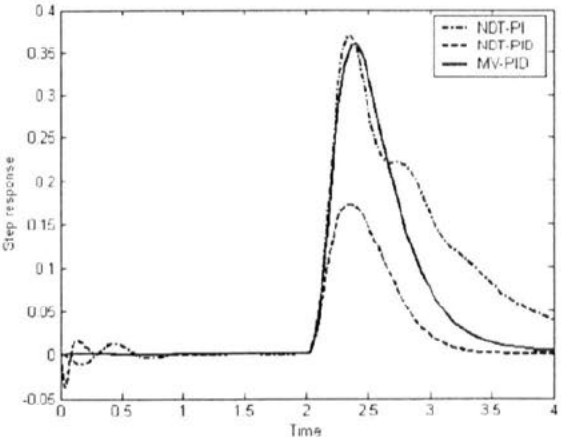

Fig. 3.29. First output response to a unit step in second input.

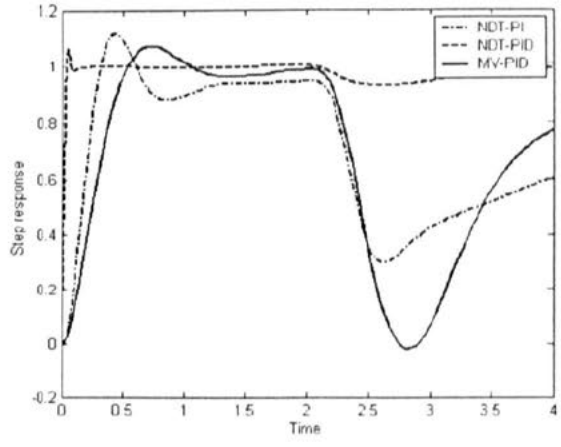

Fig. 3.30. Second output response to a unit step in second input.

3.4. Summary

A great number of industrial processes can approximately be modelled by FOPDT (SOPDT) processes. Having chosen to consider setpoint regulation as the primary design objective, an NDT method for designing PI (PID) controllers for this important category of processes is proposed in this chapter. Moreover, robustness constraints are taken into account to ensure that the resulting closed-

loop system is adequately robust against model uncertainties. In addition, for lag dominant and integrating processes, in which load disturbances are the major issue, the value of integral time of PI controller is revised.

The NDT method is simple, easy to understand and easy to apply. The procedure may be repeated for any objective function, any constraint and any process. The resulting tuning formulae are simple, easy to use and easy to memorise.

To extend the procedure to design a decentralised controller for a given TITO process, a stable decoupler is firstly introduced to decouple the process. The resulting diagonal elements are then approximated by FOPDT (SOPDT) processes using the proposed model reduction techniques. The decentralised controller is formed by two SISO controllers. Considering any diagonal element, the corresponding SISO controller is determined using the NDT tuning formulae as for the SISO case.

Assuming load disturbance rejection as the primary design objective, a simple analytical method for tuning PI controllers, which can be applied to a broad range of processes, is presented in Chapter 4. The design problem is constrained with a specified gain or phase margin.

Chapter 4

Analytical PI Tuning for Load Disturbance Rejection

4.1. Introduction

Most of the industrial controllers are PI as the derivative action is very often not used. As a result, good PI tuning methods are extremely desirable due to their widespread use. Generally, an efficient design method should deal with a wide range of systems. Not only should it satisfy the design requirements but it should also be robust against model uncertainties. Good load disturbance response is often the primary objective in process control applications. Good setpoint response can be considered as the secondary objective.

An analytical PI tuning method resulting in a set of tuning formulae is presented in this section. The design problem is aimed at optimisation of load disturbance rejection with a constraint either on the GM or on the PM. As a large number of industrial processes can approximately be modelled by FOPDT models, the tuning method is then applied to this category of processes to obtain a simple set of tuning formulae.

4.2. Control objectives

A process, $G_p(s)$, is controlled by the following PI controller:

$$G_c(s) = K_c + \frac{K_I}{s}, \tag{4.1}$$

where K_c and K_i are proportional and integral gains, respectively. Ignoring measurement noise, the output signal of a typical closed-loop system in the presence of a load disturbance signal is given by:

$$y = \frac{G_p G_c}{1 + G_p G_c} r + \frac{G_p}{1 + G_p G_c} d, \tag{4.2}$$

where r, d and y refer to the reference, load disturbance and output signals, respectively. Step disturbances are applied at the input to the process. A commonly chosen performance metric is the IAE. A significant drawback of this criterion is that it is not suitable for analytical approaches, as the evaluation requires the computation of time functions. In addition, it is necessary to simulate the process for a long time as the criterion is based on an infinite integral. However, if the sign of error signal does not change, the value of IAE can be obtained from the value of IE. Moreover, the value of IE may be a good approximation for the value of IAE for well-damped closed-loop systems. The reason for using IE is that it is appropriate for analytical approaches as, for a unit step at the load disturbance input, the value of IE is directly related to the integral gain, as shown below (Astrom and Hagglund, 1995):

$$IE = \frac{1}{K_i}. \tag{4.3}$$

In addition, robustness is a key issue in control systems. It is well-known that GM and PM are used as measures of robustness. To ensure the robustness of the closed-loop system, the optimisation problem is constrained so that a desired GM or a required PM is guaranteed. Moreover, because the PM is related to the damping of the system, it also serves as a measure of performance (Ho, Gan, Tay and Ang, 1996). Therefore, the design objective is to maximise K_i subject to satisfying the robustness constraint.

4.3. Tuning formulae for a constraint on GM or PM

Assume that the model of the process is given by:

$$G_p(j\omega) = A_p(\omega) e^{j\phi_p(\omega)}, \tag{4.4}$$

where $A_p(\omega)$ and $\phi_p(\omega)$ are the magnitude and phase of the process. Considering Equations (4.1) and (4.4), the loop transfer function is:

$$L(j\omega) = A_p(\omega) \frac{\sqrt{K_c^2\omega^2 + K_i^2}}{\omega} e^{j(\phi_p(\omega) - \tan^{-1}(\frac{K_i}{K_c\omega}))}. \tag{4.5}$$

In order to determine the controller parameters that obtain a desired GM or a desired PM, Equations (4.6) and (4.7) are considered.

$$|L(j\omega)| = \frac{1}{A_m}, \tag{4.6}$$

$$\pi + \angle L(j\omega) = \phi_m. \tag{4.7}$$

If $\phi_m = 0$, the optimisation problem guarantees a desired GM given by A_m. This is referred to as specified gain margin (SGM). Similarly, if $A_m = 1$, a desired PM given by ϕ_m is obtained. This is referred to as specified phase margin (SPM).

Inserting Equation (4.5) in Equations (4.6) and (4.7) results in the controller parameters:

$$K_c = \frac{-\cos(\phi_p - \phi_m)}{A_p A_m}, \tag{4.8}$$

$$K_i = \frac{-\omega \sin(\phi_p - \phi_m)}{A_p A_m}. \tag{4.9}$$

The necessary and sufficient conditions for maximising K_i and satisfying the constraint are given by Equations (4.10) and (4.11), respectively.

$$\frac{dK_i}{d\omega} = 0, \tag{4.10}$$

$$\frac{d^2 K_i}{d\omega^2} < 0. \tag{4.11}$$

Equation (4.9) can be written as:

$$K_i = \omega f(\omega), \tag{4.12}$$

where $f(\omega)$ is given by:

$$f(\omega) = \frac{-\sin(\phi_p - \phi_m)}{A_m A_p}. \tag{4.13}$$

Inserting Equation (4.12) into Equation (4.10) gives the necessary condition:

$$\frac{dK_i}{d\omega} = f(\omega) + \omega f'(\omega) = 0, \tag{4.14}$$

where $f'(\omega)$ is the derivative of $f(\omega)$ with respect to ω. Inserting $f(\omega)$ from Equation (4.13) and $f'(\omega)$ into Equation (4.14), results in:

$$\omega = \frac{1}{\frac{A_p'}{A_p} - \phi_p' \cot(\phi_p - \phi_m)}, \tag{4.15}$$

where A_p' and ϕ_p' are the derivatives of A_p and ϕ_p with respect to ω, respectively. An iterative technique, such as the Newton-Raphson method, is required to solve Equation (4.15). Inserting Equation (4.14) into Equation (4.11), the sufficient condition is obtained as follows:

$$\frac{d^2 K_i}{d\omega^2} = -2f(\omega) + \omega^2 f''(\omega) < 0. \tag{4.16}$$

The maximising ω is given by Equation (4.15) subject to satisfying Equation (4.16). The optimal controller parameters are given by inserting the maximising ω into Equations (4.8) and (4.9).

4.4. Tuning formulae for FOPDT processes

In this section, the tuning formulae are given for an important category of processes. A large number of industrial processes can approximately be modelled by a FOPDT transfer function:

$$G_p(s) = \frac{K_p e^{-\tau_d s}}{Ts + 1}. \tag{4.17}$$

The magnitude and phase of the process are given by:

$$A_p(\omega) = \frac{K_p}{\sqrt{1 + T^2\omega^2}}, \tag{4.18}$$

$$\phi_p(\omega) = -\omega\tau_d - \tan^{-1}(T\omega). \tag{4.19}$$

Inserting Equations (4.18) and (4.19) into Equations (4.8), (4.9) and (4.13) results in:

$$K_c = \frac{-\cos(\omega\tau_d + \phi_m) + \omega T \sin(\omega\tau_d + \phi_m)}{A_m K_p}, \tag{4.20}$$

$$K_i = \frac{\omega(\sin(\omega\tau_d + \phi_m) + \omega T\cos(\omega\tau_d + \phi_m))}{A_m K_p}, \tag{4.21}$$

$$f(\omega) = \frac{\sin(\omega\tau_d + \phi_m) + \omega T\cos(\omega\tau_d + \phi_m)}{A_m K_p}. \tag{4.22}$$

The maximising ω shown in Equation (4.23) is obtained by inserting $f(\omega)$ from Equation (4.22) and $f'(\omega)$ into Equation (4.14):

$$\omega = \frac{\sin(\omega\tau_d + \phi_m) + \omega T\cos(\omega\tau_d + \phi_m)}{-(T+\tau_d)\cos(\omega\tau_d + \phi_m) + \omega T\tau_d \sin(\omega\tau_d + \phi_m)}. \tag{4.23}$$

The sufficient condition for maximising K_i, shown in Equation (4.24), is obtained by inserting $f(\omega)$ from Equation (4.22) and $f''(\omega)$ into Equation (4.16):

$$A\sin(\omega\tau_d + \phi_m) + B\cos(\omega\tau_d + \phi_m) > 0, \tag{4.24}$$

where A and B are given by:

$$A = 2 + \omega^2\tau_d(2T + \tau_d), \tag{4.25}$$

$$B = \omega T(2 + \omega^2\tau_d^2). \tag{4.26}$$

It can be proven that the sufficient condition in Equation (4.24) always holds for $\phi_m \le \frac{\pi}{2}$.

4.4.1. Graphical proof

Equation (4.24) can equivalently be replaced by:

$$\sqrt{A^2 + B^2}\sin(\omega\tau_d + \phi_m + \tan^{-1}(\frac{B}{A})) > 0. \tag{4.27}$$

As a result, the sufficient condition is given by:

$$\delta(\omega) = \omega\tau_d + \phi_m + \tan^{-1}(\frac{B}{A}) < \pi. \tag{4.28}$$

Assuming the values of $\frac{\tau_d}{T}$ range from 10^{-4} to 10^{2}, Figure 4.1 shows $\delta(\omega)$ versus $\frac{\tau_d}{T}$.

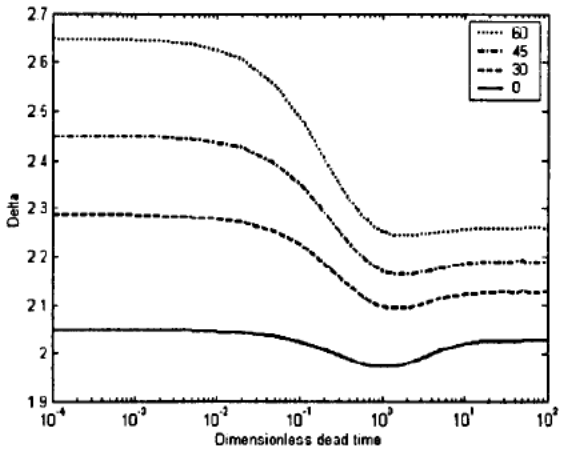

Fig. 4.1. $\delta(\omega)$ versus $\frac{\tau_d}{T}$ for different values of PM.

It shows that the sufficient condition for maximising K_I is satisfied for the selected phase margins, i.e. 0°, 30°, 45° and 60°. Moreover, a further investigation, detailed in Table 4.1, shows that the sufficient condition always holds for $\phi_m \leq \frac{\pi}{2}$.

Table 4.1. Values of $\delta(\omega)$ versus $\frac{\tau_d}{T}$ for $\phi_m = \frac{\pi}{2}$

$\frac{\tau_d}{T}$	ω	$\delta(\omega)$
10^{0}	0.4845	2.4361
10^{-1}	1.7895	2.6867
10^{-2}	5.7618	2.9721
10^{-3}	18.254	3.0869
10^{-4}	57.734	3.1243
10^{-5}	182.57	3.1361
10^{-6}	577.35	3.1399

4.4.2. Analytical proof

Finding $\cos(\omega\tau_d + \phi_m)$ from Equation (4.23) and substituting it into Equation (4.24), the sufficient condition is given by:

$$C\sin(\omega\tau_d + \phi_m) > 0, \tag{4.29}$$

where C is given by:

$$C = (2+\omega^2\tau_d^2)\frac{\tau_d(1+\omega^2T^2)+T}{2T+\tau_d} + 2\omega^2T\tau_d. \tag{4.30}$$

C is positive and it can be seen from Equation (4.7) that $\omega\tau_d + \phi_m < \pi$. As a result, the sufficient condition is always satisfied.

4.5. Simulation results

Tuning is a trade-off between conflicting design objectives. Good robustness and setpoint regulation are design goals that are in conflict with good load disturbance rejection. In this section, the SGM and SPM controllers are compared with the controller given by the method in (Astrom, Panagopoulos and Hagglund, 1998), which is one of the most prevalent techniques in PI tuning. For simplicity, the latter controller is referred to as APH.

Example 4.1.

As a simple example, consider the third order process:

$$G_1(s) = \frac{1}{(s+1)^3}.$$

Inserting $s = j\omega$ into $G_1(s)$ results in:

$$G_1(j\omega) = (1+\omega^2)^{-\frac{3}{2}} e^{-j3\tan^{-1}(\omega)}.$$

Considering $\phi_m = 0$, optimal PI parameters satisfying a desired GM are determined by solving Equation (4.15) and inserting the resulting ω into Equations (4.8), (4.9) and (4.31).

$$T_i = \frac{K_c}{K_i}. \tag{4.31}$$

Solving Equation (4.15) by a trial and error method results in $\omega = 1.225\ r/s$. Applying Equation (4.32):

$$f''(\omega) = \lim_{\Delta\to 0}\frac{f(\omega+2\Delta) - 2f(\omega+\Delta) + f(\omega)}{\Delta^2}. \tag{4.32}$$

to $f(\omega)$ in Equation (4.13), Equation (4.16) gives $\frac{d^2K_i}{d\omega^2} = \frac{-14.70}{A_m}$. Hence, the sufficient condition is satisfied. PI parameters are given by $K_c = \frac{3.5}{A_m}$ and $T_i = \frac{14}{9}$. Closed-loop step responses for different values of GM are shown in Figure 4.2.

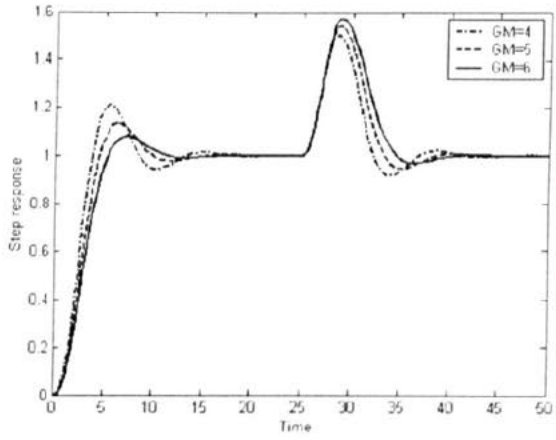

Fig. 4.2. Closed-loop step responses for different values of GM.

An interesting property of the SGM tuning formulae is that the value of GM can be indicated as a parameter to trade-off between performance and robustness. Figure 4.2 shows that a higher value of GM results in an inferior load disturbance rejection but a better setpoint regulation. Results of a robustness comparison are shown in Table 4.2.

Table 4.2. Robustness comparison of the SGM controllers to control $G_1(s)$

GM	3.000	4.000	5.000	6.000
K_c	1.167	0.875	0.700	0.583
T_i		1.556		
M_s	2.153	1.785	1.599	1.486
PM	37.45	47.52	54.72	60.02
$\frac{d^2K_i}{d\omega^2}$	-4.899	-3.675	-2.940	-2.450
$\frac{IE}{IAE}$	0.656	0.783	0.869	0.929

For a step load disturbance, the values of $\frac{IE}{IAE}$ are shown in Table 4.2. It should be noted that higher values of $\frac{IE}{IAE}$ are associated with less oscillatory systems. Considering $A_m = 1$, optimal PI parameters satisfying a desired PM are determined by solving Equation (4.15) and inserting the

resulting ω into Equations (4.8), (4.9) and (4.31). Considering $f(\omega)$ in Equation (4.13) and for $PM = 40°$, the SPM method results in $\omega = 0.697$, $K_c = 1.476$ and $T_i = 2.02$. The sufficient condition in Equation (4.16) is also satisfied as $\frac{d^2K_i}{d\omega^2} = -5.527$.

Table 4.3 summarises the results of a robustness comparison for different values of PM. It can be seen from this table that the sufficient condition is satisfied for the selected values of PM. Closed-loop step responses for different values of PM are shown in Figure 4.3.

Table 4.3. Robustness comparison of the SPM controllers to control $G_1(s)$

PM	40	45	50	55	60
ω	0.697	0.650	0.606	0.565	0.526
K_c	1.476	1.374	1.287	1.215	1.154
T_i	2.020	2.123	2.241	2.380	2.541
M_s	2.112	1.947	1.818	1.715	1.633
GM	2.963	3.296	3.646	4.006	4.374
$\frac{d^2K_i}{d\omega^2}$	-5.527	-4.948	-4.441	-3.994	-3.599
$\frac{IE}{IAE}$	0.812	0.894	0.965	1.000	1.000

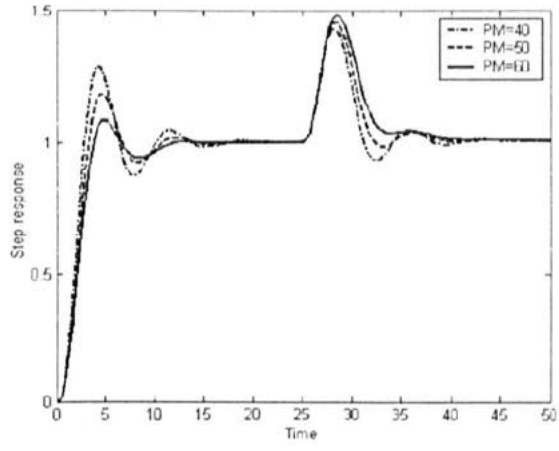

Fig. 4.3. Closed-loop step responses for different values of PM.

Clearly, a better setpoint regulation but an inferior load disturbance rejection is given by a higher value of PM. To compare the performance of the SGM, SPM and APH methods, closed-loop step responses are shown in Figure 4.4.

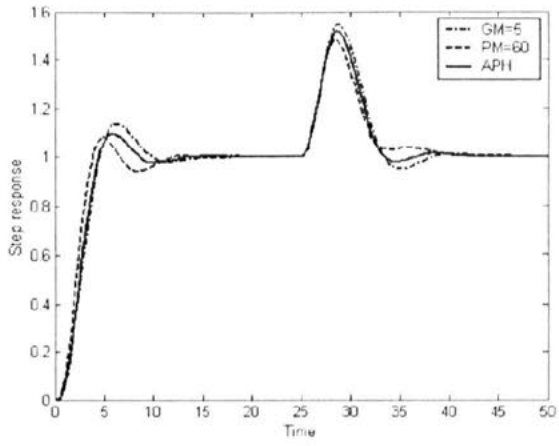

Fig. 4.4. Closed-loop step responses resulting from the SGM, SPM and APH design methods.

A slightly better setpoint regulation is given by the SPM due to a higher value of PM. To improve the setpoint response, the APH controller employs a two-degree of freedom structure, which needs an extra parameter. Table 4.4 shows the comparison results.

Table 4.4. Robustness comparison of the SGM, SPM and APH methods to control $G_1(s)$

Method	SGM	SPM	APH
K_c	0.700	1.154	0.862
T_i	1.556	2.541	1.870
b	1.000	1.000	0.930
M_s	1.599	1.633	1.600
GM	5.000	4.374	4.789
PM	54.72	60.00	56.90
$\frac{IE}{IAE}$	0.870	1.000	0.952

The SGM (SPM) controller is determined more easily than the APH controller. As soon as ω is determined and subject to satisfying the sufficient condition, the SGM (SPM) parameters are explicitly given by a set of tuning formulae. However, the APH parameters should be computed through a procedure, which may lead to very complicated situations for complicated systems (Astrom, Panagopoulos and Hagglund, 1998).

Example 4.2.

In this example, the SGM method is applied to a non-minimum phase process, a pure time delay unit, a long dead time process and a process with complex poles. These processes are not common in process control, however, they are included to demonstrate the wide applicability of the design procedure.

$$G_2(s) = \frac{1-2s}{(s+1)^3}. \qquad G_3(s) = e^{-s}.$$

$$G_4(s) = \frac{e^{-15s}}{(s+1)^3}. \qquad G_5(s) = \frac{9}{(s+1)(s^2+as+9)}.$$

Closed-loop step responses for different values of GM are shown in Figure 4.5.

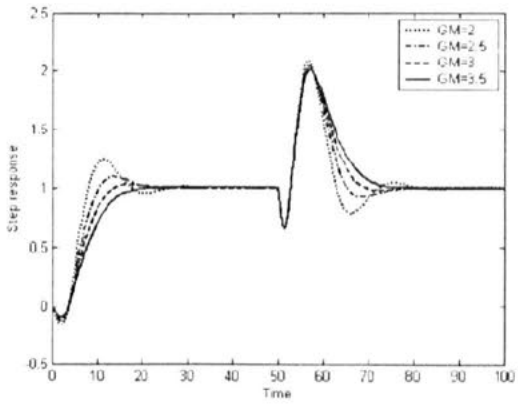

$G_2(s)$

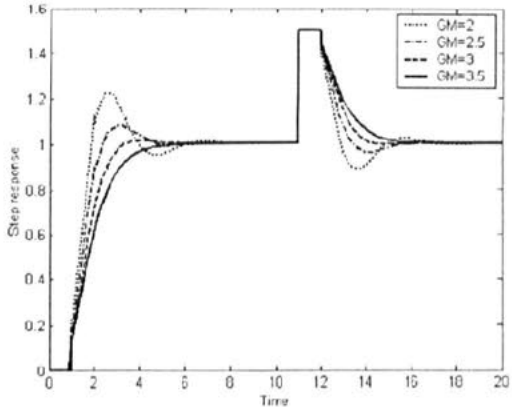

$G_3(s)$

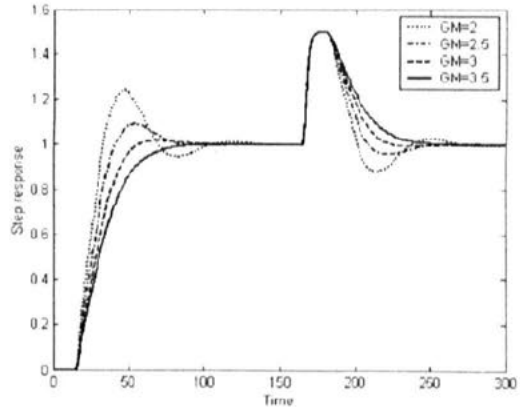

$G_4(s)$

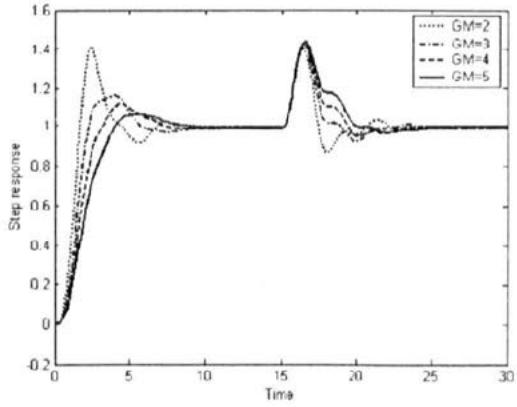

$G_5(s), a = 1$

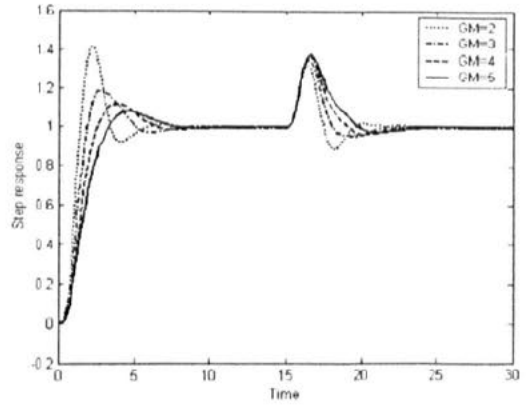

$G_5(s), a = 2$

Fig. 4.5. Closed-loop step responses for different values of GM.

Results of a robustness comparison are shown in Table 4.5.

Table 4.5. Results of a robustness comparison of the SGM controllers

Process	ω	K_c	T_i	M_s	GM	PM	$\frac{d^2K_i}{d\omega^2}$	$\frac{IE}{IAE}$
$G_2(s)$	0.491	0.268	1.319	2.225	2.000	46.18	-1.684	0.571
		0.214		1.825	2.500	55.19	-1.347	0.737
		0.179		1.624	3.000	61.12	-1.123	0.841
		0.153		1.502	3.500	65.31	-0.962	0.888
$G_3(s)$	2.029	0.177	0.243	1.772	2.500	57.84	-2.193	0.856
		0.147		1.584	3.000	63.35	-1.827	0.974
		0.126		1.470	3.500	67.23	-1.566	1.000
		0.111		1.394	4.000	70.12	-1.371	1.000
$G_4(s)$	0.114	0.231	4.486	2.155	2.000	48.94	-2.813	0.641
		0.185		1.778	2.500	57.48	-2.250	0.849
		0.154		1.589	3.000	63.05	-1.875	0.972
		0.132		1.474	3.500	66.97	-1.670	1.000
$G_5(s)$, $a=1$	2.236	0.056	0.040	2.088	2.000	37.58	-4.969	0.493
		0.037		1.648	3.000	48.55	-3.313	0.721
		0.028		1.479	4.000	55.68	-2.485	0.792
		0.022		1.384	5.000	60.88	-1.988	0.884
$G_5(s)$, $a=2$	2.345	0.417	0.248	2.221	2.000	37.04	-5.733	0.521
		0.278		1.671	3.000	47.76	-3.822	0.705
		0.208		1.488	4.000	54.59	-2.867	0.799
		0.167		1.391	5.000	59.54	-2.293	0.858

Figure 4.6 shows the fairly similar closed-loop step responses resulting from the SGM and APH methods.

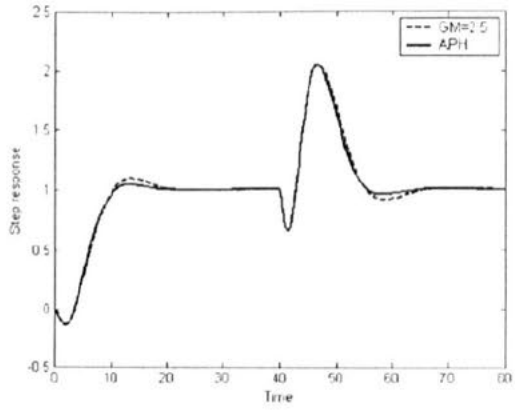

$G_2(s)$

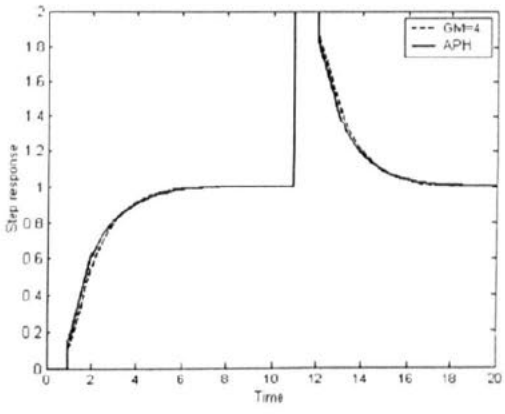

$G_3(s)$

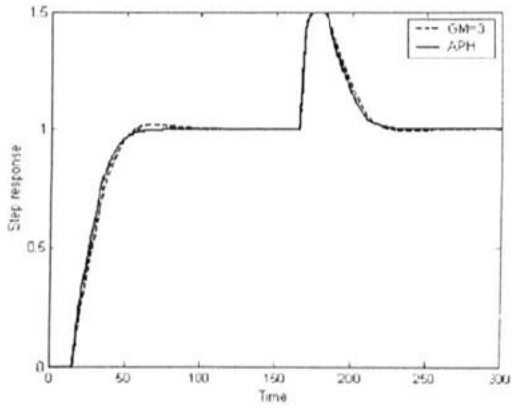

$G_4(s)$

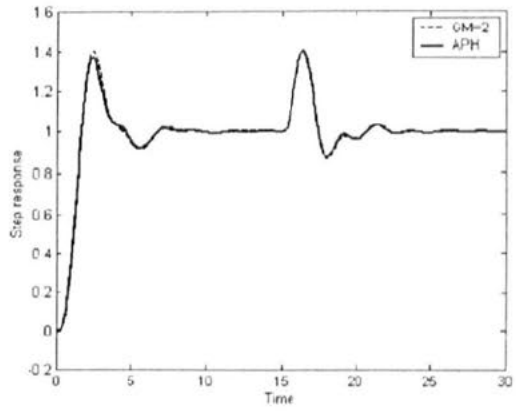

$G_5(s), a = 1$

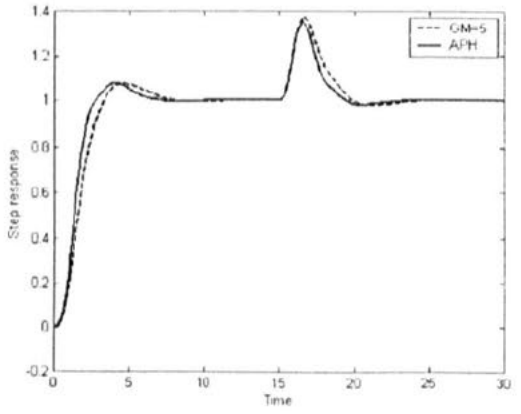

$G_5(s), a = 2$

Fig. 4.6. Closed-loop step responses resulting from the SGM and APH methods.

Table 4.6 shows results of a comparison of the SGM and APH methods. Results of applying the SPM method are shown in Table 4.7.

Table 4.6. Robustness comparison of the SGM and APH controllers

Process	Method	SGM	APH
$G_2(s)$	K_c	0.214	0.265
	T_i	1.319	1.640
	b	1.000	0.870
	M_s	1.825	1.797
	GM	2.500	2.476
	PM	55.19	57.93
	$\frac{IE}{IAE}$	0.737	0.798
$G_3(s)$	K_c	0.111	0.158
	T_i	0.243	0.335
	b	1.000	1.000
	M_s	1.394	1.400
	GM	4.000	3.846
	PM	70.12	71.71
	$\frac{IE}{IAE}$	1.000	1.000
$G_4(s)$	K_c	0.154	0.208
	T_i	4.486	5.870
	b	1.000	1.000
	M_s	1.589	1.599
	GM	3.000	2.888
	PM	63.05	64.70
	$\frac{IE}{IAE}$	0.972	1.000
$G_5(s)$, $a=1$	K_c	0.056	0.090
	T_i	0.040	0.065
	b	1.000	1.000
	M_s	2.090	2.002
	GM	2.000	2.005
	PM	37.55	39.24
	$\frac{IE}{IAE}$	0.493	0.510
$G_5(s)$, $a=2$	K_c	0.167	0.313
	T_i	0.248	0.373
	b	1.000	0.880
	M_s	1.391	1.400
	GM	5.000	3.843
	PM	59.54	59.16
	$\frac{IE}{IAE}$	0.858	0.867

Table 4.7. Robustness comparison of the SPM controllers

Process	PM	30	45	60
$G_2(s)$	ω	0.360	0.306	0.258
	K_c	0.560	0.594	0.639
	T_i	1.951	2.506	3.337
	M_s	4.280	3.347	3.090
	GM	1.339	1.457	1.500
	$\frac{d^2K_i}{d\omega^2}$	-2.797	-2.501	-2.202
	$\frac{IE}{IAE}$	0.319	0.519	0.722
$G_3(s)$	ω	1.605	1.404	1.213
	K_c	0.529	0.580	0.636
	T_i	0.388	0.507	0.680
	M_s	5.042	3.945	3.702
	GM	1.288	1.373	1.392
	$\frac{d^2K_i}{d\omega^2}$	-3.880	-3.234	-2.678
	$\frac{IE}{IAE}$	0.260	0.400	0.541
$G_4(s)$	ω	0.090	0.078	0.068
	K_c	0.543	0.591	0 644
	T_i	7.086	9.211	12.30
	M_s	4.904	3.800	3.512
	GM	1.284	1.379	1.412
	$\frac{d^2K_i}{d\omega^2}$	-3.946	-3.276	-2.704
	$\frac{IE}{IAE}$	0.283	0.425	0.589
$G_5(s)$, $a=2$	ω	1.919	1.717	1.500
	K_c	0.977	1.074	1.138
	T_i	0.412	0.569	0.802
	M_s	4.431	3.343	2.815
	GM	1.325	1.479	1.631
	$\frac{d^2K_i}{d\omega^2}$	-7.785	-5.972	-4.316
	$\frac{IE}{IAE}$	0.285	0.479	0.730

Unlike the corresponding SGM controller, each SPM controller gives a low gain margin and a high maximum sensitivity. Therefore, only the SGM method is suitable for processes in this example. Moreover, the SPM method fails to give a stabilising controller for $G_5(s), a=1$, for the desired values of PM.

Many traditional methods fail to give acceptable control for many of the more difficult control examples discussed in this section. For example, both the Ziegler-Nichols and Lambda tuning methods result in $K_c = 0$ for the pure delay process $G_3(s)$ (Astrom, Panagopoulos and Hagglund, 1998).

Example 4.3.

In this example, the SPM method is applied to the following processes:

$$G_6(s) = \frac{1}{s(s+1)^2}. \qquad G_7(s) = \frac{e^{-s}}{s}.$$

These processes are referred to as integrating processes. Closed-loop step responses for different values of PM are shown in Figure 4.7.

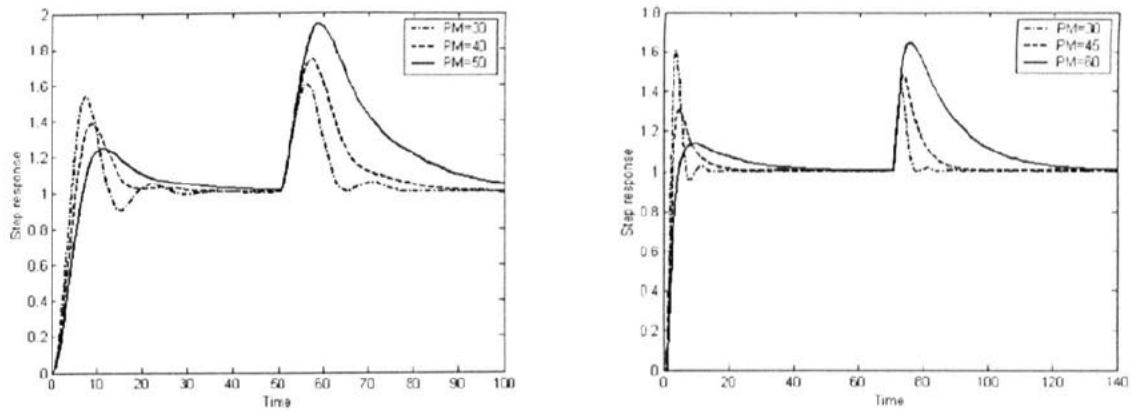

$G_6(s)$ $G_7(s)$

Fig. 4.7. Closed-loop step responses for different values of PM.

Results of a robustness comparison are shown in Table 4.8. Figure 4.8 shows the closed-loop step responses resulting from the SPM and APH methods. Unlike the APH method, which employs a two-degree of freedom structure and has an extra parameter, the SGM/SPM controller has only two parameters. As a result, the setpoint response resulting from an SGM/SPM controller may be improved using the extra parameter, b. Considering $G_6(s)$, Figure 4.8 shows that the setpoint response given by the SPM controller is improved by decreasing b from one, which is the value of setpoint weight for the SGM/SPM method, to 0.65. Results of a comparison of these methods are summarised in Table 4.9.

Table 4.8. Robustness comparison of the SPM controllers

Process	PM	30	40	50
$G_6(s)$	ω	0.396	0.317	0.246
	K_c	0.439	0.338	0.255
	T_i	8.372	11.93	18.54
	M_s	2.263	1.783	1.506
	GM	3.467	4.925	7.005
	$\frac{d^2K_i}{d\omega^2}$	-0.902	-0.584	-0.354
	$\frac{IE}{IAE}$	1.000	1.000	1.000
$G_7(s)$	PM	30	45	60
	ω	0.707	0.528	0.350
	K_c	0.667	0.510	0.345
	T_i	3.998	7.187	16.30
	M_s	2.429	1.742	1.395
	GM	2.068	2.899	4.464
	$\frac{d^2K_i}{d\omega^2}$	-1.533	-0.845	-0.370
	$\frac{IE}{IAE}$	0.998	1.000	1.000

Table 4.9. Robustness comparison of the SPM and APH controllers

Process	Method	SPM	APH
$G_6(s)$	K_c	0.338	0.286
	T_i	11.93	9.000
	b	1.000	0.570
	M_s	1.783	1.801
	GM	4.925	5.436
	PM	40.00	36.92
	$\frac{IE}{IAE}$	1.000	0.989
$G_7(s)$	K_c	0.345	0.282
	T_i	16.30	6.746
	b	1.000	0.660
	M_s	1.395	1.400
	GM	4.464	5.218
	PM	60.00	46.71
	$\frac{IE}{IAE}$	1.000	0.897

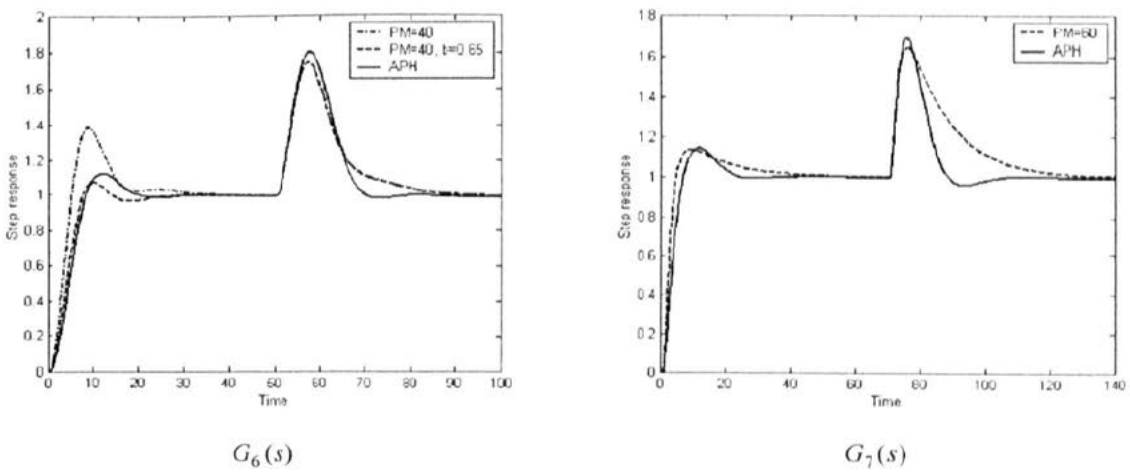

$G_6(s)$ $G_7(s)$

Fig. 4.8. Closed-loop step responses resulting from the SPM and APH methods.

A process with dead time and a single pole at the origin, given in Equation (3.15), is a special case of a FOPDT process when the time constant becomes infinite. For such a process, Equation (4.23) is simplified to:

$$\omega = \frac{2}{\tau_d}\cot(\omega\tau_d + \phi_m). \tag{4.33}$$

Controller parameters are given by inserting the resulting ω into Equations (4.34) and (4.35):

$$K_c = \frac{\omega \sin(\omega\tau_d + \phi_m)}{A_m K_p'}, \tag{4.34}$$

$$T_i = \frac{\tan(\omega\tau_d + \phi_m)}{\omega}. \tag{4.35}$$

The results shown in Table 4.8 for $G_7(s)$ can be obtained in a simpler manner using Equations (4.33)-(4.35).

Results of applying the SGM method to $G_6(s)$ and $G_7(s)$ are shown in Table 4.10. Compared to the corresponding SPM controller, the SGM controller does not have a large enough integral time, resulting in a low phase margin and a high maximum sensitivity.

Table 4.10. Robustness comparison of the SGM controllers

Process	GM	2.000	2.500	3.000
$G_6(s)$	ω		0.707	
	K_c	0.500	0.400	0.333
	T_i		4.000	
	M_s	5.115	4.203	3.788
	PM	11.81	14.24	15.64
	$\frac{d^2K_i}{d\omega^2}$	-1.414	-1.131	-0.943
	$\frac{IE}{IAE}$	0.324	0.352	0.357
$G_7(s)$	ω		1.077	
	K_c	0.474	0.379	0.316
	T_i		1.725	
	M_s	5.247	4.841	4.753
	PM	11.16	11.97	12.13
	$\frac{d^2K_i}{d\omega^2}$	-1.828	-1.462	-1.218
	$\frac{IE}{IAE}$	0.223	0.221	0.214

Example 4.4.

This example shows that the proposed PI controllers can be used for some unstable systems:

$$G_8(s) = \frac{a}{(s+a)(s-1)}.$$

To compare the results with the APH controller, the SPM method is used so that the desired PM, which corresponds with a maximum sensitivity of 2, is given. A two-degree of freedom structure is used to improve the setpoint response. For $a = 4$, the SPM method gives $\omega = 2.863$, $K_c = 3.719, T_i = 4.81$ and $PM = 31°$. The setpoint weight is chosen to be 0.6. For $a = 8$, the design procedure results in $\omega = 7.092$, $K_c = 9.469$, $T_i = 0.953$ and $PM = 32°$. A good setpoint response is given by $b = 0.6$.

Figure 4.9 shows the closed-loop step responses given by the SPM and APH methods.

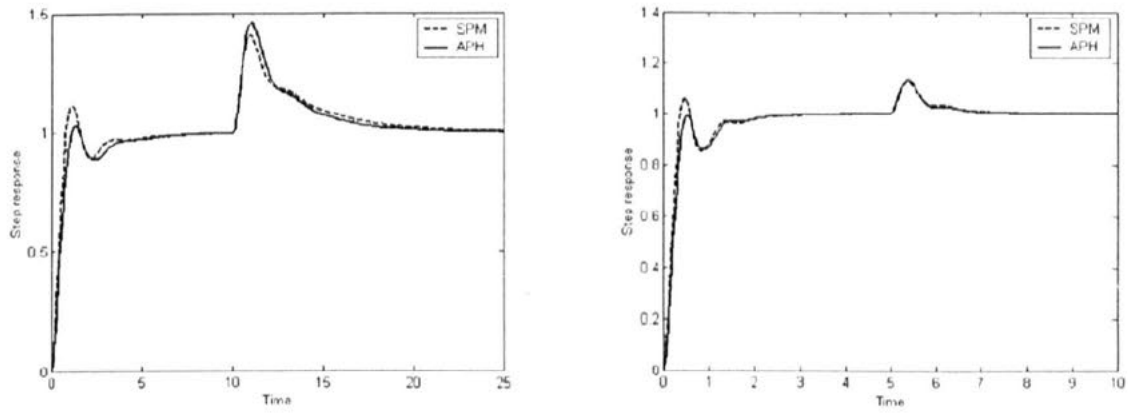

$G_8(s), a = 4$ $G_8(s), a = 8$

Fig. 4.9. Closed-loop step responses resulting from the SPM and APH method.

4.6. Discussions

If the gain of PI controller increases, the load disturbance response from a non-minimum phase process may exhibit a greater magnitude of fluctuation whereas a minimum phase process gives a lesser amplitude of deflection. This property is investigated through considering responses of the following transfer functions:

$$G_9(s) = \frac{s+1}{(2s+1)(3s+1)(4s+1)} \qquad G_{10}(s) = \frac{-s+1}{(2s+1)(3s+1)(4s+1)}$$

$$G_{11}(s) = \frac{10s+1}{(2s+1)(3s+1)(4s+1)} \qquad G_{12}(s) = \frac{-10s+1}{(2s+1)(3s+1)(4s+1)}$$

An SGM or SPM controller is designed for each process. Assuming a 30% deviation from the normal value of the controller gain, output and control signals are shown in Figures 4.10-4.13.

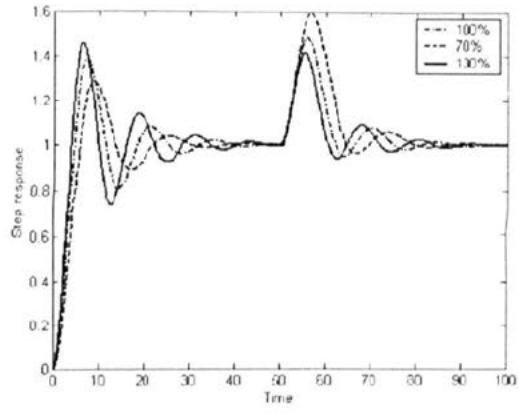

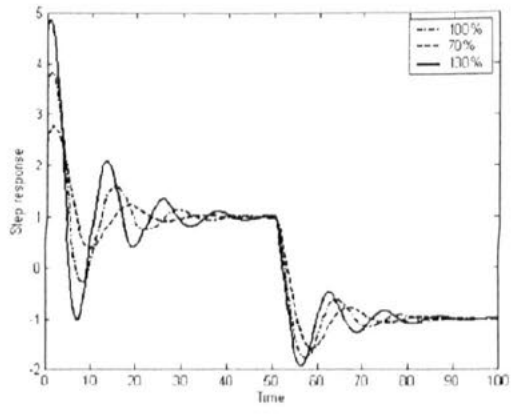

$G_9(s)$ $G_9(s)$

Fig. 4.10. Closed-loop step response (left) and control signal (right).

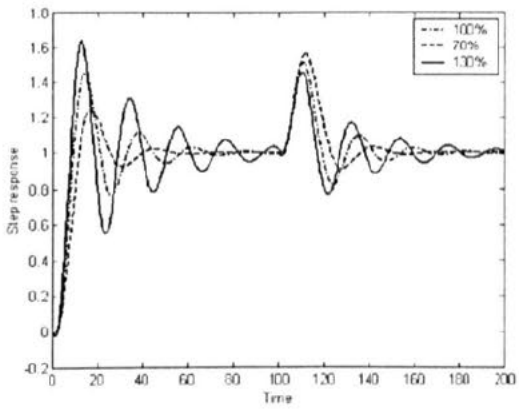

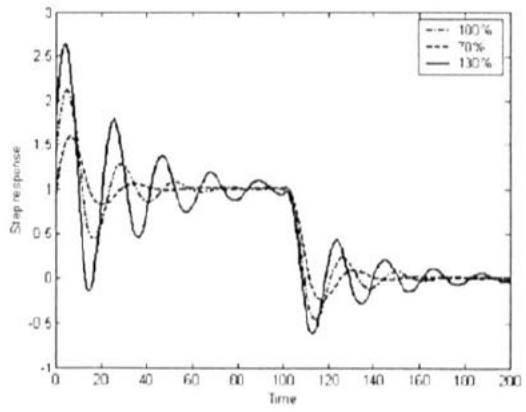

$G_{10}(s)$ $G_{10}(s)$

Fig. 4.11. Closed-loop step response (left) and control signal (right).

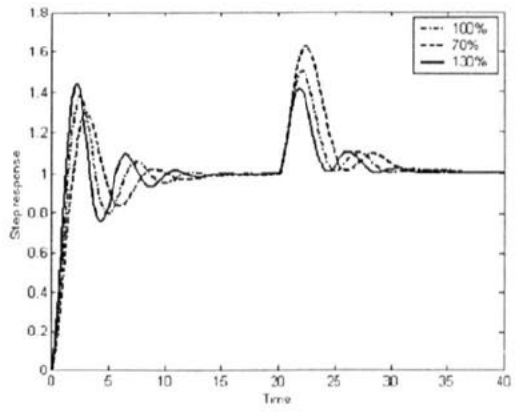

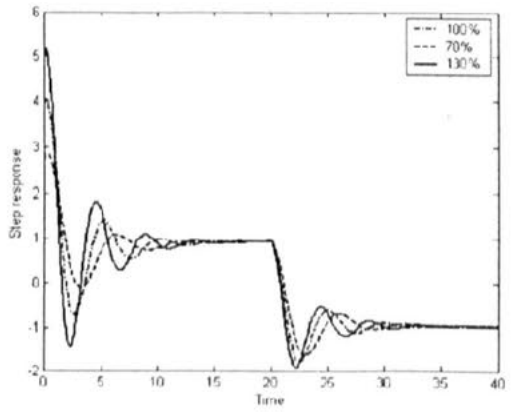

$G_{11}(s)$ $G_{11}(s)$

Fig. 4.12. Closed-loop step response (left) and control signal (right).

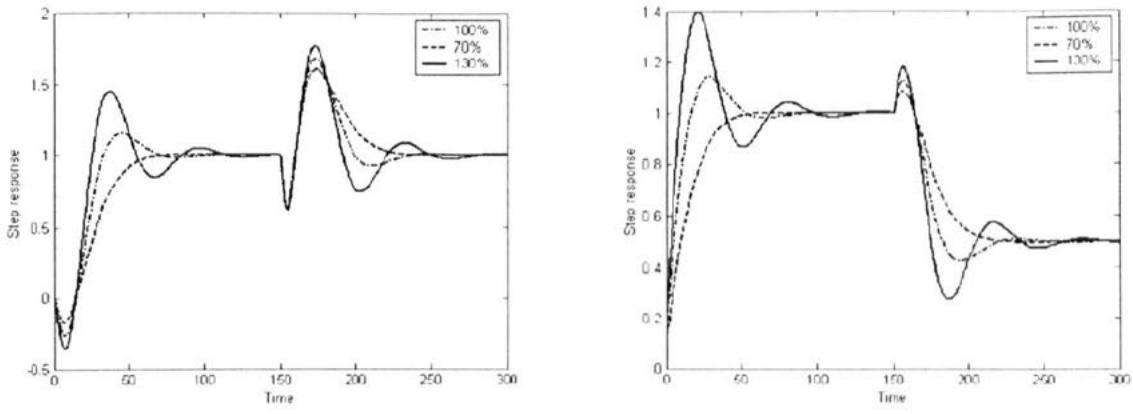

$G_{12}(s)$ $G_{12}(s)$

Fig. 4.13. Closed-loop step response (left) and control signal (right).

As can be seen from Figures 4.11 and 4.13, a greater controller gain does not necessarily result in a lesser fluctuation to load disturbance for a non-minimum phase process. To explore this situation, the role of integral action is reviewed.

In order for the process being controlled to be at steady state, $u(t)$ must be constant. Equation (2.4) implies that $u(t)$ changes with time unless the error signal is zero. Therefore, when integral action is used, $u(t)$ automatically changes until it attains the value required to make the steady state error zero.

Considering a step function in setpoint, Figure 4.14 shows typical closed-loop response and error signal of a non-minimum phase process to a setpoint step input.

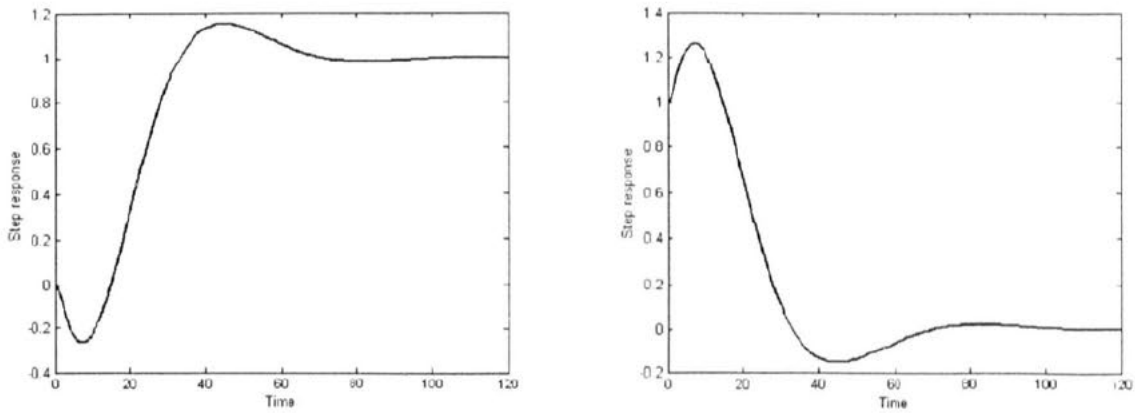

Output response Error signal

Fig. 4.14. Typical closed-loop step response and error signal of a non-minimum phase system.

Because of the initial increase in the error signal, the integral term continues to increase until the error signal changes sign. Only then does the integral term begin to decrease. This results in a large overshoot.

When the position of the RHP zero compared with the dominant pole is not close to the imaginary axis, e.g. in $G_{10}(s)$, the inverse response is not too harsh and, therefore, the problem of having a large overshoot is not serious. Hence, such non-minimum phase processes approximately behave like minimum phase processes in terms of having increased setpoint response and decreased

load disturbance response peaks to an increase in the controller gain. However, if the RHP zero is closer to the imaginary axis than the dominant pole, e.g. in $G_{12}(s)$, an increase in the controller gain leads to an increase in the load disturbance response peak.

As a result, there is a trade-off between the speed of the response and peak fluctuation to load disturbances for non-minimum phase processes whereas they are commensurate for minimum phase processes.

4.7. Summary

Selecting load disturbance rejection as the primary design objective, an analytical method for tuning PI controllers is proposed in this chapter. The optimisation problem includes a constraint either on the GM or on the PM to consider both performance requirements and robustness issues. The main advantage of the proposed method to other similar methods, such as the APH, is its simplicity. Determining ω by a trial and error method, the SGM (SPM) parameters are explicitly given by a set of tuning formulae. Simple tuning formulae for FOPDT processes are also determined and it is proven that the sufficient condition is always satisfied for such processes. Simulation results for a variety of examples including integrating, non-minimum phase, long dead time and unstable processes show that the proposed and APH methods perform fairly similarly and confirm the effectiveness of the proposed method in dealing with a wide range of processes.

In chapter 5, using a structure with two degrees of freedom, the NDT technique is used to obtain PI tuning rules, which are capable of satisfying conflicting design requirements, for FOPDT processes. Both single-objective and multi-objective approaches will be presented.

Chapter 5

PI Control for Conflicting Design Requirements

5.1. Introduction

There are many conflicting design objectives in a PI control problem. Considering setpoint regulation and load disturbance rejection as design requirements, the controller in a one-degree of freedom structure has to be designed either for good setpoint regulation or good load disturbance rejection. Otherwise, some compromise may be found, however, an acceptable compromise may not exist if there are severe requirements on both design objectives. A two-degree of freedom structure, which is more flexible and has different signal paths for the setpoint and the process output, decouples these conflicting requirements and can cope with them properly. In this chapter, the NDT technique is applied to a two-degree of freedom structure to design PI controllers for FOPDT processes.

5.2. Control requirements

In general, good load disturbance rejection is the primary design objective. The controller parameters are typically obtained from the model parameters. Due to model uncertainties, the controller parameters should be chosen in such a way that the closed-loop system is not too sensitive to variations in process dynamics. Therefore, robustness against model errors should also be taken into account.

Sensitivity to modelling errors can be expressed as the largest value of the sensitivity function. For SISO systems, M_s is the inverse of the shortest distance from the Nyquist curve of the loop transfer function to the critical point. Smaller values of M_s show little or no overshoot while larger ones result in faster responses.

The sensitivity can also be expressed as the largest value of the complementary sensitivity function, as shown in Equation (5.1). The maximum complementary sensitivity, M_T, is an indication of performance robustness.

$$M_T = \max_{\omega} |T(j\omega)| = \max_{\omega} \left| \frac{G_p(j\omega)G_c(j\omega)}{1+G_p(j\omega)G_c(j\omega)} \right| = \|T(j\omega)\|_{\infty}. \quad (5.1)$$

Although the primary design goal is load disturbance rejection it is also important to have good setpoint responses. Because responses to load disturbance and setpoint signals are usually conflicting, the first design goal may result in bad setpoint responses. As the secondary design goal, good setpoint regulation is achieved by using a structure with two degrees of freedom, which introduces an extra parameter, the setpoint weight.

5.3. A single-objective approach

Having a two-degree of freedom structure, the closed-loop system is described by:

$$y = \frac{G_p(s)G_{ff}(s)}{1+G_p(s)G_c(s)} r + \frac{G_p(s)}{1+G_p(s)G_c(s)} d, \quad (5.2)$$

where $G_{ff}(s)$, which is the feed-forward controller, is:

$$G_{ff}(s) = K_c(b + \frac{1}{T_i s}). \quad (5.3)$$

The design objective is to determine $G_c(s)$ and $G_{ff}(s)$ to obtain good load disturbance and setpoint responses. A constraint on maximum sensitivity, $M_s = 2$, is used to guarantee robustness to model uncertainties.

The design procedure has two main steps. In the first step, the setpoint signal is considered to be zero and $G_c(s)$ is determined so that load disturbances are attenuated and the robustness constraint is satisfied. For the $G_c(s)$ determined in the first step and in absence of load disturbances, $G_{ff}(s)$ is then tuned in the second step to achieve good setpoint responses.

The setpoint weight plays a significant role in improving the setpoint response. However, it has no influence on the load disturbance response and, therefore, it does not deteriorate good load disturbance response obtained in the first step.

5.3.1. Design procedure: step one

Using the non-dimensional tuning technique introduced in Chapter 3, Figures 5.1 and 5.2 show the optimal values of the dimensionless gain and the dimensionless integral time across the selected values of the dimensionless dead time, respectively.

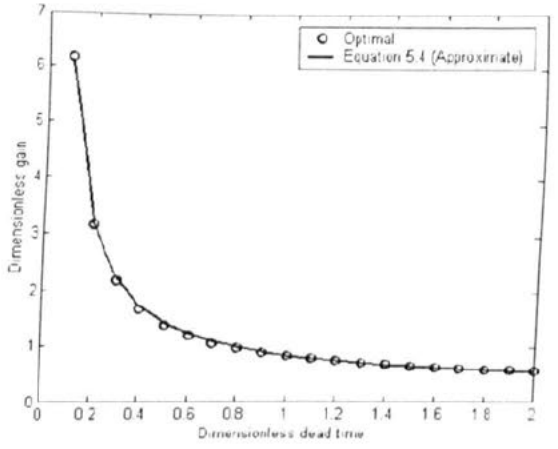

Fig. 5.1. Optimal values of the dimensionless gain, $K_p K_c$, and values of $K_p K_c$ given by Equation (5.4) versus the dimensionless dead time, $\frac{\tau_d}{T}$.

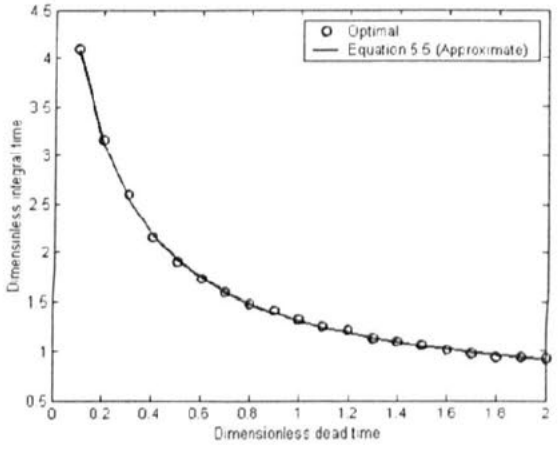

Fig. 5.2. Optimal values of the dimensionless integral time, $\frac{T_i}{\tau_d}$, and values of $\frac{T_i}{\tau_d}$ given by Equation (5.5) versus the dimensionless dead time, $\frac{\tau_d}{T}$.

It can be seen from Figure 5.1 that the dimensionless gain is a function of the dimensional dead time as follows:

$$K_p K_c = A_1 + \frac{B_1}{\frac{\tau_d}{T}}. \tag{5.4}$$

Similarly, the values of $\frac{T_i}{\tau_d}$ are determined from the values of $\frac{\tau_d}{T}$, using:

$$\frac{T_i}{\tau_d} = \frac{A_2 \frac{\tau_d}{T} + B_2}{\frac{\tau_d}{T} + C_2}. \tag{5.5}$$

Using the least-squares method, A_1, B_1, A_2, B_2 and C_2 are determined for the best match with optimal PI parameters. The optimal values of A_1, B_1, A_2, B_2 and C_2 are $\frac{3}{11}$, $\frac{4}{7}$, $\frac{9}{20}$, $\frac{13}{12}$ and $\frac{3}{17}$, respectively.

5.3.2. Design procedure: step two

In this step, the load disturbance signal is considered to be zero and $G_{ff}(s)$ is determined to obtain a good setpoint response. First, for each value of $\frac{\tau_d}{T}$, the optimal values of K_c and T_i are determined using Equations (5.4) and (5.5). Next, the optimal value of b is determined so that the IAE criterion to a step signal at the setpoint input is minimised. Figure 5.3 shows the optimal values of b versus $\frac{\tau_d}{T}$.

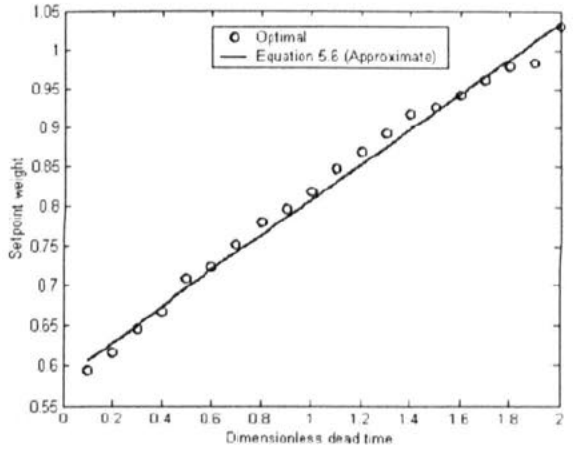

Fig. 5.3. Optimal values of the setpoint weight, b, and the values of b given by Equation (5.6) versus the dimensionless dead time, $\frac{\tau_d}{T}$.

Using the least-squares method, optimal value of b can be calculated from:

$$b = \frac{9}{40}\frac{\tau_d}{T} + \frac{7}{12}. \tag{5.6}$$

Obviously, there is no need to employ setpoint weighting if the setpoint response is already good. The setpoint signal is not weighted if the value of b is chosen equal to one. Hence, the setpoint

weight will not be far from one if the setpoint signal is fairly good. However, for small values of $\frac{\tau_d}{T}$, the dimensionless gain, $K_p K_c$, given by Equation (5.3) is large to reject load disturbance signals well. Therefore, the setpoint response is expected to be too oscillatory leading to a value of b which is far from one.

Equations (5.7)-(5.9) show PI tuning formulae for the integrating processes in Equation (3.15):

$$K_p' K_c = \frac{\frac{4}{7}}{\tau_d}, \tag{5.7}$$

$$T_i = \frac{\frac{13}{12}}{\frac{3}{17}} \tau_d \approx \frac{43}{7} \tau_d, \tag{5.8}$$

$$b = \frac{7}{12}. \tag{5.9}$$

5.3.3. Simulation results

In this section, performance of the proposed method is compared with that of the APH method. Both methods use a two-degree of freedom structure to reject load disturbance signals and improve setpoint responses through setpoint weighting whilst having a constraint on maximum sensitivity, $M_s = 2$.

Example 5.1.

The proposed PI tuning formulae are optimal for FOPDT processes, however, the following third order process is considered to show the efficient applicability of the proposed method to higher-order processes:

$$G_1(s) = \frac{1}{(s+1)^3}.$$

In order to obtain PI parameters suggested by the proposed method, the process is approximated by a FOPDT model. Using a simple method given in Toscano (2005), which is based on analysis of the open-loop step response, the FOPDT parameters are given by:

$$K_p = y_\infty, \tag{5.10}$$

$$\tau_d = 2.8t_1 - 1.8t_2, \tag{5.11}$$

$$T = 5.5(t_2 - t_1), \tag{5.12}$$

where y_∞ is the final value of the step response of the process and t_1 (t_2) is the time when the output attains 28% (40%) of its final value. Applying this model reduction method to $G_1(s)$, its FOPDT approximation is given by:

$$\hat{G}_1(s) = \frac{e^{-1.039s}}{2.448s + 1}.$$

The closed-loop step responses given by the proposed and APH methods are shown in Figure 5.4.

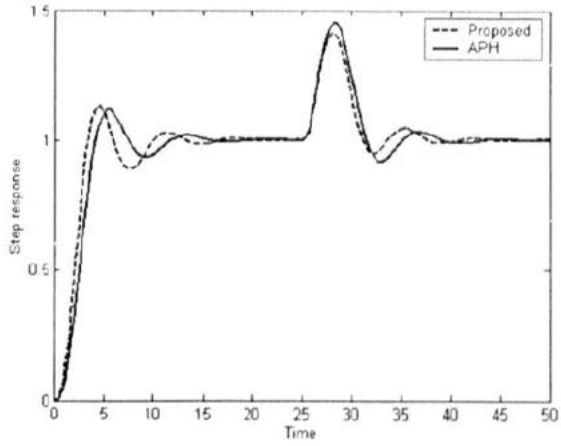

Fig. 5.4. Closed-loop step responses resulting from applying the proposed and APH methods to $G_1(s)$.

The comparison results are shown in Table 5.1:

Table 5.1. Comparison of the performance of the proposed and APH methods to control $G_1(s)$

Method	Proposed	APH
K_c	1.619	1.220
T_i	2.203	1.780
b	0.679	0.500
M_s	2.151	2.000
M_T	1.000	1.000
PO	12.77	11.94
T_s	12.23	11.07
Pd	0.418	0.458
Td	11.93	13.14

where Pd refers to the peak of the load disturbance response. Td is the time required for the disturbance response to settle to within a tolerance of ± 0.02.

Tuning is a trade-off between conflicting design objectives. Fast speed of response and good load disturbance rejection are design goals *in conflict with* good robustness (Skogestad, 2003). The proposed controller results in a faster response and a better disturbance rejection but at the cost of having a larger maximum sensitivity.

An advantage of the proposed method is that the controller parameters for FOPDT processes are directly given by Equations (5.4)-(5.6). For a higher-order process, the tuning formulae can be used after an appropriate model reduction. In contrast, parameters of the APH controller are not explicitly given by a set of tuning formulae. They should be computed through a procedure which may lead to complicated situations (Astrom, Panagopoulos and Hagglund, 1998).

Example 5.2.

Consider the integrating process with dead time:

$$G_2(s) = \frac{e^{-s}}{s}.$$

The proposed and APH methods result in closed-loop step responses shown in Figure 5.5.

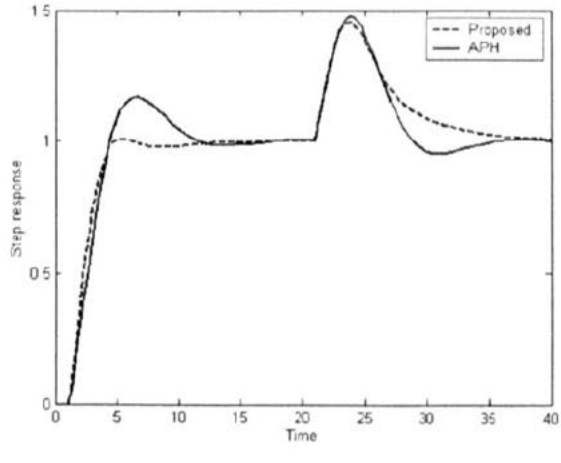

Fig. 5.5. Closed-loop step responses resulting from applying the proposed and APH methods to $G_2(s)$.

The proposed method performs better in setpoint regulation and gives a smaller M_s, however, a faster load disturbance rejection is given by the APH controller. The comparison results are shown in Table 5.2.

Table 5.2. Comparison of the performance of the proposed and APH methods to control $G_2(s)$

Method	Proposed	APH
K_c	0.571	0.488
T_i	6.140	3.725
b	0.583	0.460
M_s	1.913	2.003
M_T	1.444	1.821
PO	0.550	17.21
T_s	10.20	10.66
Pd	0.455	0.477
Td	16.21	13.80

5.4. Design parameter

The trade-off between performance and robustness varies for different control problems. Therefore, it is desirable to have a trade-off adjustment parameter to manipulate the specifications of the closed-loop system. The design parameter should not be process-oriented. Ideally, it should be directly related to the performance of the system. Moreover, the design parameter should have a good physical interpretation and good default values as well as natural limits to simplify its adjustment.

A numerical method to obtain optimal PI tuning formulae for FOPDT processes was presented in this chapter. The design method was based on optimal load disturbance rejection. To obtain a fairly robust controller, a constraint on the maximum sensitivity was used to guarantee $M_s = 2$. The design method dealt with setpoint response using a two-degree of freedom structure. The optimal tuning formulae were given by Equations (5.4)-(5.6). As fast speed of response and good load disturbance rejection are requirements conflicting with robustness, one can repeat the design procedure to obtain a more robust closed-loop system at the cost of slower responses and worse load disturbance rejection. If Equations (5.4) and (5.5) include a design parameter, they can be used to trade-off between performance and robustness. It can be done through replacing τ_d in these equations with $\alpha\tau_d$, where the default value of α is one. $\alpha < 1$ is corresponding to a larger closed-loop bandwidth, resulting in a faster response and a better load disturbance rejection. A better degree of robustness is given by choosing $\alpha > 1$.

Considering Example 5.1, different compromise solutions are obtained by choosing different values of α. The results are shown in Figure 5.6 and Table 5.3.

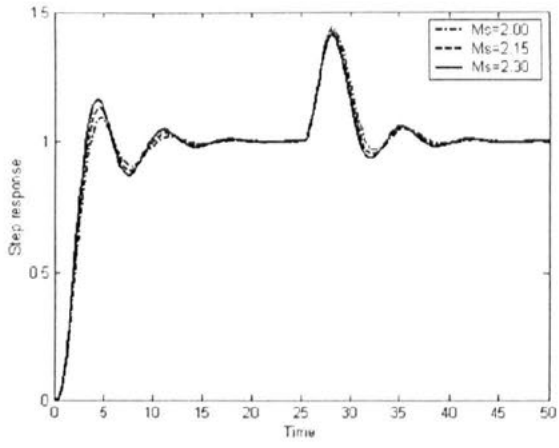

Fig. 5.6. Closed-loop step responses resulting from applying the proposed and APH methods to $G_1(s)$.

Table 5.3. Comparison of the performance of the proposed and APH methods to control $G_1(s)$

Method	Design 1	Design 2	Design 3
K_c	1.510	1.618	1.713
T_i	2.287	2.204	2.138
b	0.679	0.679	0.679
α	1.087	1.000	0.936
M_s	2.000	2.150	2.300

5.5. A multi-objective approach

Most practical design problems invariably require a number of design criteria to be satisfied simultaneously. Assuming a two-degree of freedom scheme, the closed-loop system is described by Equation (5.2). Considering a FOPDT process, the control aim is to determine $G_c(s)$ and $G_{ff}(s)$ so that the following objective functions are simultaneously minimised:

- IAE criterion to a setpoint step
- IAE criterion to a load disturbance step
- Maximum sensitivity (M_s)
- Maximum complementary sensitivity (M_T)
- Total variation (TV) of control signal

As a result, a multi-objective optimisation (MO) approach may be employed to address the inherent compromise between performance and robustness, which is prevalent in all control design approaches.

5.5.1. Multi-objective optimisation

Most real-world optimisation problems involve simultaneous optimisation of several conflicting objectives. The task of finding optimum solutions for such problems is known as multi-objective optimisation. Usually, some or all of these objectives are conflicting.

Considering two solutions from the search space for a two-objective optimisation problem, if solution x_2 is better than solution x_1 in both objectives, it can be said that solution x_1 is dominated by solution x_2. A solution is said to be non-dominated if there is no other solution that is better than it in all the objectives. For any two non-dominated solutions, one is better in terms of one objective but at the cost of sacrificing at least one of the remaining objectives. As a result, for multiple conflicting objectives, rather than a single optimum solution, there is a family of non-dominated (Pareto-optimal) solutions. These constitute a family of potential solutions from which the user may choose the solution that gives the desired compromise.

In many cases, multiple objective problems are aggregated into one single overall objective function. However, design engineers are often interested in identifying a Pareto-optimal set of alternatives when exploring a design space.

5.5.2. Multi-objective optimisation using genetic algorithms

The genetic algorithm (GA) is a stochastic global search technique inspired by the principles of natural selection and natural genetics. At each generation, a population of candidate solutions is evaluated in terms of their performance in the problem domain. Stronger individuals are given a greater chance of contributing to the production of new individuals (the offspring) than weaker ones. Offspring are produced through recombination, whereby they inherit features from each of the parents, and through mutation, which can confer some truly innovative features as well. In the next selection step, offspring are made to compete with each other and probably their parents. As this cycle repeats over a number of generations, the population becomes more refined as the weaker individuals are rejected and an optimal solution is approached (Fonseca, 1995).

Genetic algorithms have considerably broadened the scope of optimisation as they are able to handle complex problems. They are well-known for their ability to search multiple solutions in parallel and to handle complicated tasks such as discontinuities and multi-modality. In contrast to conventional search techniques, population-based search algorithms such as GAs are capable of evolving multiple solutions simultaneously, approaching the non-dominant Pareto front in a single run (Deb, 2001).

The multi-objective genetic algorithm (MOGA) makes no assumption about the nature of the decision variables in the search process. Therefore, the considerations made and the techniques proposed are largely domain-independent (Fonseca, 1995).

5.5.3. Design procedure

The design procedure has two main steps. In the first step, the setpoint signal is considered to be zero and $G_c(s)$ is determined so that load disturbances are appropriately attenuated and small values of M_s and TV are achieved. In the second step, the load disturbance signal is set to be zero and for the $G_c(s)$ determined in the first step, parameter b in $G_{ff}(s)$ is tuned to obtain good setpoint responses and small values of TV.

Using the non-dimensional tuning method, the multi-objective problem is solved to minimise conflicting objective functions. The optimal values of dimensionless gain across the values of dimensionless dead time are shown in Figure 5.7.

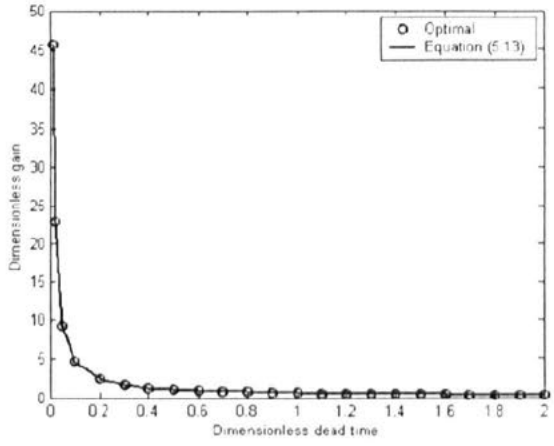

Fig. 5.7. Optimal values of dimensionless gain and the values of dimensionless gain given by Equation (5.13) versus dimensionless dead time.

It can be seen from this figure that the dimensionless gain is a function of dimensionless dead time as follows:

$$K_p K_c = A + \frac{B}{\frac{\tau_d}{T}}. \tag{5.13}$$

Using the least-squares method, optimal values of A and B for the best match with optimal PI parameters are $\frac{1}{6}$ and $\frac{5}{11}$, respectively. Similarly, the values of $\frac{T_i}{\tau_d}$ and b are given by:

$$\frac{T_i}{\tau_d} = \frac{\frac{3}{14}\frac{\tau_d}{T} + \frac{7}{6}}{\frac{\tau_d}{T} + \frac{1}{5}}, \tag{5.14}$$

$$b = \frac{4}{9}\frac{\tau_d}{T} + \frac{1}{2}. \tag{5.15}$$

PI tuning formulae for the integrating processes are:

$$K_p' K_c = \frac{\frac{5}{11}}{\tau_d}, \tag{5.16}$$

$$\frac{T_i}{\tau_d} = \frac{\frac{7}{6}}{\frac{1}{5}} = \frac{35}{6}, \tag{5.17}$$

$$b = \frac{1}{2}. \tag{5.18}$$

5.5.4. Decision making

Good robustness and small total variation of the control signal are design goals in conflict with good load disturbance rejection and fast response (Skogesatd, 2003). The trade-off graph for $\frac{\tau_d}{T} = 1$, resulting from applying the MOGA to the first step of the design procedure is shown in Figure 5.8.

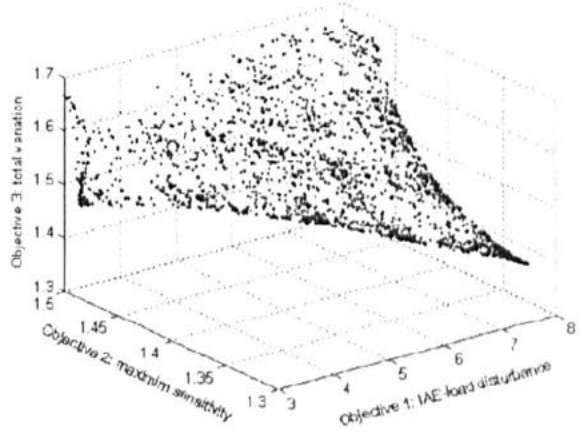

Fig. 5.8. Trade-off graph for the first step of the design procedure.

This figure shows the solutions from which an appropriate non-dominated solution should be chosen. The solution which gives the lowest value of the first objective has the highest value of the second objective and vice versa. Therefore, these two objectives are conflicting. Moreover, this figure shows that the second and third objectives are not conflicting with each other. However, the first and third objectives are conflicting.

The choice of a suitable compromise solution from all non-dominated alternatives is not only problem-dependent, but it generally depends on the subjective preferences of the decision maker. Therefore, the final solution to the problem is the result of both an optimisation process and a decision process (Fonseca, 1995). The final controller is determined by choosing the solution which appropriately satisfies the design goals. This solution should give the desired trade-off between fast response (small IAE) on the one hand, and smooth input usage (small TV) as well as robustness (small M_s) on the other. For a given $\frac{\tau_d}{T}$, the solution which gives $IAE < A$, $TV < B$ and $M_s < C$ is chosen from the Pareto-optimal surface. The values of A, B and C are determined appropriately by the designer.

Figure 5.9 shows the trade-off graph given by applying the MOGA to the second step of the design procedure. The appropriate value of b is determined by selecting the compromise solution satisfying the conflicting objectives.

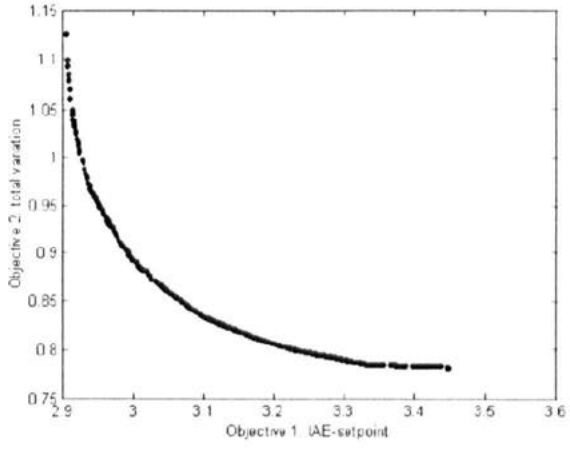

Fig. 5.9. Trade-off graph for the second step of the design procedure.

5.5.5. Simulation results

In this section, performance of the proposed multi-objective technique is compared with that of the APH method.

Example 5.3.

Consider the third order process:

$$G_3(s) = \frac{1}{(s+1)^3}.$$

In order to determine the MO controller, $G_3(s)$ is approximated by the following FOPDT model:

$$\hat{G}_3(s) = \frac{e^{-1.039s}}{2.448s+1}.$$

The closed-loop step responses given by the MO and APH methods are shown in Figure 5.10. The comparison results are shown in Table 5.4, where PR denotes the peak of the unit step response. Moreover, T_s for load disturbance is the time required for the disturbance response to settle to within a tolerance of ± 0.02. The proposed controller results in a better response but at the expense of having a larger maximum sensitivity.

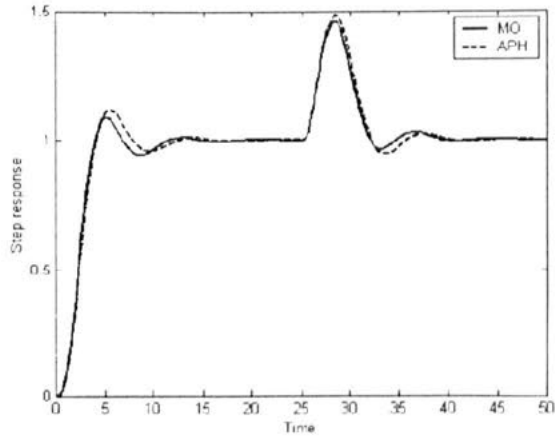

Fig. 5.10. Closed-loop step responses resulting from applying the MO and APH controllers to $G_3(s)$.

Table 5.4. Comparison of the performance of the MO and APH methods to control $G_3(s)$

Method	MO		APH	
	Setpoint	Load disturbance	Setpoint	Load disturbance
K_c	1.245		1.060	
T_i	2.087		1.820	
b	0.687		0.700	
M_s	1.839		1.793	
IAE	3.620	1.150	3.812	1.309
TV	1.475	1.068	1.418	1.143
PR	1.105	0.462	1.117	0.481
T_s	10.67	12.81	11.36	13.35

Although the MO tuning formulae have been obtained for FOPDT processes, this example shows that it can also be applied to higher-order processes.

Example 5.4.

Consider the fourth order process:

$$G_4(s) = \frac{1}{(s+1)(0.2s+1)(0.04s+1)(0.008s+1)}.$$

Using Equations (5.10)-(5.12), $G_4(s)$ is approximated by:

$$\hat{G}_4(s) = \frac{e^{-0.224s}}{1.084s+1}.$$

The MO and APH methods result in closed-loop step responses shown in Figure 5.11. The comparison results are shown in Table 5.5. The APH controller performs better in terms of setpoint regulation and load disturbance rejection. However, the MO controller is better in terms of robustness and total variations of the control signal.

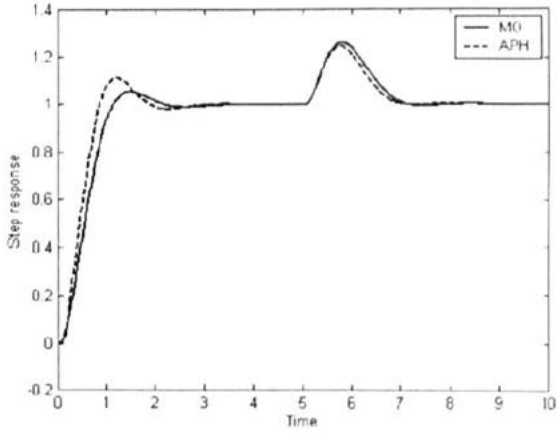

Fig. 5.11. Closed-loop step responses resulting from applying the MO and APH methods to $G_4(s)$.

Table 5.5. Comparison of the performance of the MO and APH methods to control $G_4(s)$

Method	MO		APH	
	Setpoint	Load disturbance	Setpoint	Load disturbance
K_c	2.401		2.740	
T_i	0.661		0.672	
b	0.590		0.750	
M_s	1.541		1.600	
IAE	0.846	0.107	0.715	0.088
TV	1.896	0.544	2.613	0.508
PR	1.054	0.264	1.111	0.247
T_s	1.920	1.910	2.390	1.780

Example 5.5.

Consider the non-minimum phase process:

$$G_5(s)=\frac{-2s+1}{(s+1)^3}.$$

Using the half rule approximation method, the approximate FOPDT model for this process is given by:

$$\hat{G}_5(s) = \frac{e^{-3.5s}}{1.5s+1}$$

The closed-loop step responses of the MO and APH methods are shown in Figure 5.12.

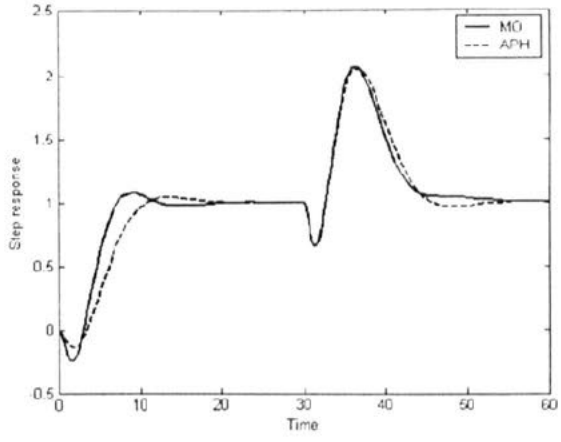

Fig. 5.12. Closed-loop step responses resulting from applying the MO and APH methods to $G_5(s)$.

Table 5.6 shows the results of the comparison. A better setpoint regulation is given by the MO controller whereas the load disturbance responses are fairly similar. Also, the APH controller results in a better degree of robustness. In the design procedure, dimensionless dead time is considered to vary from 0.1 to 2. The dimensionless dead time for $\hat{G}_{17}(s)$ is 2.33, however, the MO controller has a good performance.

Table 5.6. Comparison of the performance of the MO and APH methods to control $G_5(s)$

Method	MO		APH	
	Setpoint	Load disturbance	Setpoint	Load disturbance
K_c	0.362		0.265	
T_i	2.303		1.640	
b	1.537		0.870	
M_s	1.838		1.797	
IAE	10.34	10.47	11.80	11.17
TV	0.771	2.820	0.889	2.876
PR	1.077	1.064	1.046	1.023
T_s	16.67	22.83	17.03	21.58

The simulation studies show that the MO method can effectively cope with conflicting design objectives. Moreover, the performance of the MO and APH methods are fairly similar for the simulation examples.

5.6. Single-objective versus multi-objective techniques

Optimisation techniques provide powerful tools for the tuning of controllers. Optimisation-based design methods are very popular as they can capture many different aspects of the design problem. The mathematical modelling of a real-world design problem often results in multiple design objectives. The optimisation problem can then be tackled by using either a single-objective or a multi-objective technique.

To deal with the optimisation problem by using a single objective technique, it is common to use a weighted sum approach. In this method, a weighting factor is given to any objective function. Then, a single cost function is formed by aggregating weighted objective functions. This method is simple and gives one optimal solution, however, the critical stage is to define suitable weighting factors prior to starting the optimisation process. As a result, to change the trade-off between conflicting design objectives, the optimisation process has to be repeated with different weighting factors.

The use of multi-objective optimisation algorithms enhances the design procedure by enabling optimisation of several design objectives. Unlike the weighted sum approach which only gives one individual as the optimal solution, a multi-objective technique investigates the whole trade-off surface in a single run resulting in a family of solutions. Therefore, the user can finally select a desired compromise solution from this non-dominated set.

5.7. Summary

Using a two-degree of freedom structure, the NDT technique is employed to design PI controllers for FOPDT processes. The design objectives are good load disturbance rejection, good setpoint regulation, good degree of robustness and small total variation of the control signal. Both single-objective and multi-objective approaches are presented.

Multivariable control enables reduction of margins provided for safe operation and, therefore, improves engine efficiency. Alternatively, it may be used to provide similar safety requirements compared to a corresponding SISO controller whilst offering better performance. In Chapter 6, a simple and efficient decentralised control scheme proposed in chapter 3 is applied to a rolls-Royce civil engine to improve its safety requirements.

Chapter 6

Multivariable Jet Engine Control

6.1. Introduction

Most modern civil and military aircraft are powered by gas turbine engines. These engines come in a wide variety of shapes and sizes because of the many different aircraft missions. Some aircraft, such as military planes, require a very high power-to-weight ratio to accelerate quickly and to overcome the high drag associated with high speeds. For these airplanes, engine efficiency is not as important as very high thrust. Some aircraft, like civil airplanes, spend most of their life in a cruise condition. For these airplanes, excess thrust is not as important as high engine efficiency resulting in low fuel usage. Figure 6.1 shows some different types of gas turbine engines.

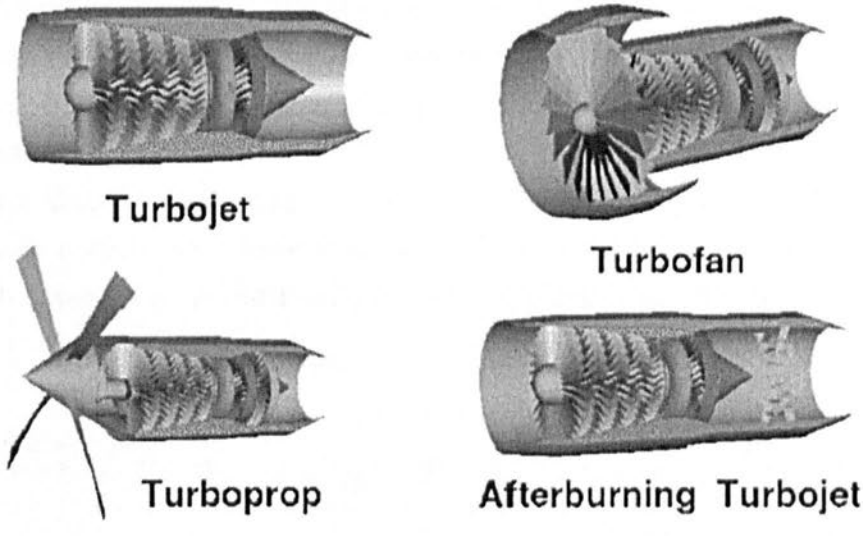

Fig. 6.1. Common types of jet engines.

Since thrust depends on both the amount of gas moved and its overall level of acceleration, high thrust can be generated by accelerating a large mass of gas by a small amount, or by accelerating a small mass of gas by a large amount. Propellers develop thrust by moving a large mass of air with a small acceleration and thus have a high propulsive efficiency at low air speed. Many low speed transport aircraft and small commuter aircraft use turboprop engines. As propellers become less efficient as air speed increases, high speed transports usually use high bypass ratio turbofans because of their higher fuel efficiency at higher air speed.

A turbofan engine has a large fan at the front, which sucks in air. In a basic turbojet all the air entering the intake passes through the core of the engine, which is composed of the compressor(s), combustion chamber, and turbine(s). However, in a turbofan engine only a portion of the incoming air goes into the combustion chamber. The remainder, which passes through the fan, is ejected directly through the cold nozzle or is mixed with the engine core exhaust before exiting the engine. The objective of this sort of bypass system is to increase thrust without increasing fuel consumption. This is achieved by increasing the total mass flow and reducing the velocity within the same total energy supply. Further detail on the applicability of gas turbine configurations can be found in Rolls-Royce (2005).

6.2. Traditional jet engine control strategies

Feedback control has always been an essential part of jet engines, because they operate at near their mechanical or aero-thermal limitations (Spang III and Brown, 1999). Although early jet engines were controlled by hydro-mechanical control systems, modern engines are controlled by digital electronic or combinations of digital electronic and hydro-mechanical control systems (Harefors, 1997). Since the jet engine is a highly non-linear process, it is normal for several linear controllers to be designed at different operating points and the control parameters to be scheduled across the flight envelope.

The primary engine variable to be controlled is the thrust. Other variables such as compressor surge margin(s) are important for safety, see Appendix C. The main strategy in jet engine control is to use fuel flow to control the thrust. Open-loop scheduling is often used for other control signals (Harefors, 1997).

A typical SISO jet engine control scheme is shown in Figure 6.2. The conventional SISO controller uses multiple SISO loops in selector control for the thrust. The safety variables are subsequently controlled by open-loop schedules driven from other measured engine outputs.

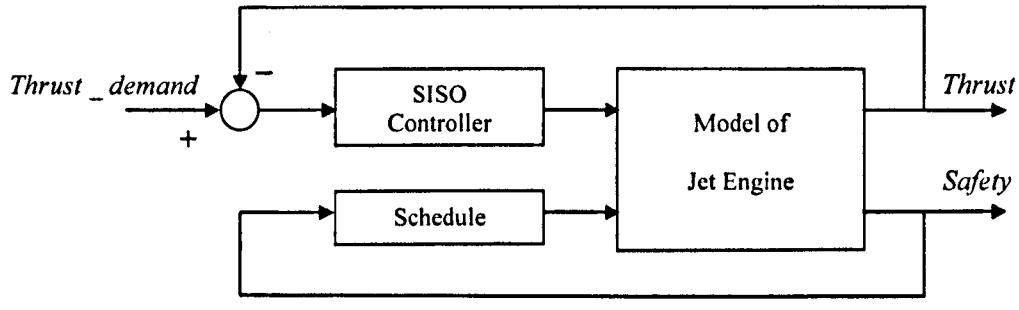

Fig. 6.2. Schematic representation of SISO control scheme.

Apart from the variables being controlled, there are a number of variables that should be kept within given ranges. As the number of parameters to be controlled and/or limited exceeds the number of variable inputs, all these parameters cannot be controlled independently at the same time. To solve this problem, a selector control, which consists of many measured signal and only one actuator, can be used. The idea is to design several scheduled controllers for different sets of output variables. Depending on the most significant limit, the selector chooses the most appropriate controller at any given time.

There are two types of selectors: maximum and minimum. For a maximum selector the output is the largest of the input signals. As shown in Figure 6.3, the switching procedure is usually done by means of lowest-wins highest-wins gates, which serve to propagate the output of the most suitable controller to the process input. As a result, a switched gain scheduled controller is designed to cover the full operating range and all possible configurations (Skogestad and Postlethwaite, 2001).

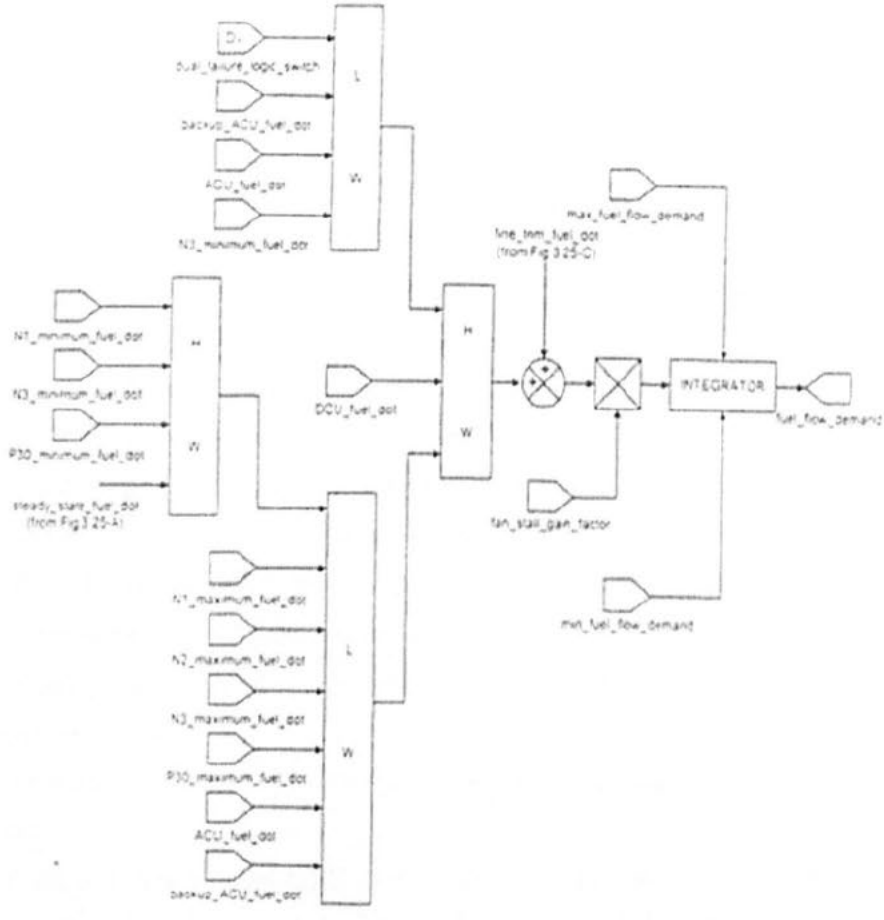

Fig. 6.3. Lowest-wins highest-wins gates.

6.3. Overview of modern jet engine control

Jet engines are becoming more complex to meet future demands. Modern jet engines, which have more control variables, are able to improve engine performance and safety. Reducing fuel consumption and increasing engine life can also be considered as objectives in jet engine design. In order to utilise the potential of these engines, it is necessary to use more advanced control strategies

rather than conventional control techniques. To this end, strong collaboration among control theory, fluid mechanics and experimental methods is required.

Research projects focusing on multivariable engine control have been under way since 1970. Leininger (1979) designed a multivariable controller for a jet engine using Nyquist array methods. Another multivariable frequency domain method proposed by Edmunds (1979) has been frequently used by General Electric. This method was also applied to the GE16 experimental engine by Polley, Adibhatla and Hoffman (1988). In 1974, the US Air Force and NASA initiated a major research programme to evaluate the applicability of LQ design methods to jet engine control. DeHoff, Hall, Adams and Gupta (1977) and Soeder (1984) are examples originating from this programme. LQG and LQG/LTR techniques were applied to jet engines by Athans, Kapasouris, Kappos and Spang III (1986) and Garg (1989). In the 1990s, H_∞ control design techniques were applied to jet engines in many research projects. One example is the work by Postlethwaite, Samar, Choi and Gu. (1995), where an H_∞ controller was designed for a Rolls-Royce Spey engine, which is a two-spool turbofan engine. Extensive work has been published on various control strategies for such an engine (Dadd, Sutton and Greig, 1995; Samar, 1995; Silva, 1999). Another application of H_∞ control to a General Electric engine was described by Frederic, Garg and Adibhatla (1996). Watts and Garg (1995) carried out a comparison between LQG/LTR and H_∞ multivariable design techniques for application to a linear model of a jet engine. H_∞ methodology has also been used in integrated flight and propulsion control (IFPC) system design methods (Garg, 1993; Hyde and Glover, 1993). Bates, Gatley, Postlethwaite and Berry (1999) designed a robust integrated flight and propulsion controller for an experimental V/STOL aircraft configuration, using H_∞ loop shaping method.

Performance requirements of jet engines vary according to mission characteristics. Good commercial aircraft operation requires minimum running and maintenance costs. Military aircraft require maximum available thrust and speed of response for combat missions (Silva, Khatib and Fleming, 2005). Dodd and Martin (1997) defined performance optimisation of a gas turbine engine to be one, or a combination of the following cases:

- Minimising fuel consumption while maintaining thrust levels
- Maximising thrust
- Maximising engine life by reducing turbine blade temperature while maintaining thrust levels

Examples of research works on jet engine performance optimisation can be found in (Silva, Khatib and Fleming, 2000; Silva, Khatib and Fleming, 2003; Silva, Khatib and Fleming, 2005).

Research works carried out by Frederick, Garg and Adibhatla (2000); Lyantsev, Breikin, Kulikov and Arkov (2004) are examples of recent studies on multivariable control of jet engines. In addition, Rees, Mu and Chiras (2003) applied a multivariable PID controller to the linear and non-linear NARMAX and neural network models of Rolls-Royce Spey MK202 aircraft gas turbine. This research work showed that a gain scheduling is necessary, because the engine dynamics change significantly when considering all operating conditions (Ruano, Fleming, Teixeira, Rodriguez-Vazquez and Fonseca, 2003).

Proposing advanced control strategies for modern civil or military jet engines is currently an important subject for research at General Electric, NASA, Volvo and Rolls-Royce. For engines with two shafts the safety issue relating to surge should only be considered during acceleration, while for three-spool jet engines surge during both acceleration and deceleration should be dealt with. This research work aims to investigate multivariable control for Rolls-Royce three-spool high bypass ratio turbofan engine. In this chapter, a case study, which is a model of the above-mentioned engine, is considered to explore the application of the proposed decentralised tuning method for TITO processes.

6.4. Model description

The highly cross-coupled linear models of the Rolls-Royce turbofan engine derived from the non-linear model have 4 inputs, 147 outputs and 35 states. It was shown in Jackson (1988) that for a given stationary point, the higher order non-linear thermodynamic models derived from the engine physics could be reduced to linear models of the same order as the number of engine shafts. The turbofan engine is a three-spool gas turbine with low pressure (LP), intermediate pressure (IP) and high pressure (HP) shafts. Therefore, the linear models of the turbofan can be reduced to 3 states. The applicability of the design technique to a gas turbine engine is, of course, depending upon the validity of the model used.

A Rolls-Royce three-spool jet engine is shown in Figure 6.4. It consists of three major moving parts. They are concentrically mounted, cylindrical shafts. Each shaft has a compressor mounted on the front and a turbine mounted on the rear. The LP shaft is of greatest length and, therefore, innermost in the concentric arrangement whilst the HP shaft is the shortest and outermost.

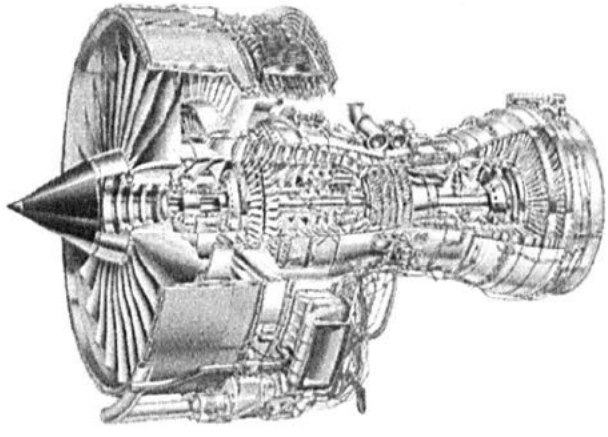

Fig. 6.4. A Rolls-Royce three-spool high bypass ratio jet engine.

The LP compressor is a single stage configuration, however, the IP and HP compressors consist of eight and five stages, respectively. Each stage has two parts, a set of rotating blades and a set of stationary vanes. The rotating blades impart kinetic energy by accelerating the air flow. The flow is diffused by the stator vanes to convert the kinetic energy to pressure.

The engine core is surrounded by a bypass duct, which contains no moving parts and exhausts its airflow rearwards to the atmosphere. The airflow for both the core and the surrounding bypass duct is

provided by the LP compressor, or fan. In high bypass ratio turbofans the airflows from the core and the bypass duct exhaust to atmosphere through either separate or common propelling nozzles at the rear of the engine. In the case of a common propelling nozzle, the airflows from the bypass duct and the core are mixed before exiting the engine. However, the engine studied here has separate ducts. The majority of the intake air passes through the bypass duct and exits through the cold nozzle towards the rear. The airflow experiences a relatively small acceleration from the fan, however, it involves a high mass flow rate. Therefore, a large thrust is produced.

Jet engines are required to operate in steady state with the highest possible level of fuel efficiency. Whilst turbines are stable at all operating points, compressors have unstable regions. During transient manoeuvres, jet engines are required to move between one steady state condition and another in as short a time as possible whilst retaining acceptable stability margins for the compressors. In traditional control strategies, compressor instabilities are avoided by having conservative working conditions. Some engine configurations employ variable stator vanes (*VSVs*) and/or bleed valves, which are controlled by means of some open-loop scheduling, to assist in compressor stabilisation.

In the engine studied here, *VSVs* are situated in the front three stages of the IP compressor. These vanes, which are adjusted according to the IP compressor speed and inlet temperature, deflect the airflow into the subsequent stages of IP rotor blades at an angle of incidence appropriate to the operating conditions. Opening up these vanes increases the angle of incidence of the airflow onto the rotor blades, raising the pressure ratio across the stage and hence the whole IP compressor. At a condition, this raises the inlet pressure of the HP compressor, thereby reducing its pressure ratio. The effect of raising the IP and lowering the HP pressure ratios means that opening the *VSVs* has deteriorated the IP surge margin whilst improving the HP surge margin for a given inlet flow. Closing the *VSVs* will have the opposite effect and therefore the *VSVs* can be used to effectively redistribute the surge risk between the core compressors.

Figure 6.5 shows velocity triangles in an axial compressor at the design operating point as well as near to surge and in choke (Walsh and Fletcher, 1998).

Bleed valves, which in the engine under consideration are located at IP stage 8 and HP stage 3, can be used to alleviate surge risk. They allow the air to escape from the core at certain stages of the compressors into the bypass duct. For the engine configuration studied here, bleed valves are actuated such that they are either open or closed. The control law is an open-loop schedule based on the relevant compressor speed. When open they lessen the pressure at that point in the core airflow and, therefore, reduce the surge risk to upstream compressor stages. Note that this may have the effect of increasing the pressure ratio across downstream stages, thereby deteriorating their surge risk. Overall compressor handling therefore requires careful scheduling of bleed valves. Whilst open handling bleed valves result in noise pollution and reduced engine efficiency.

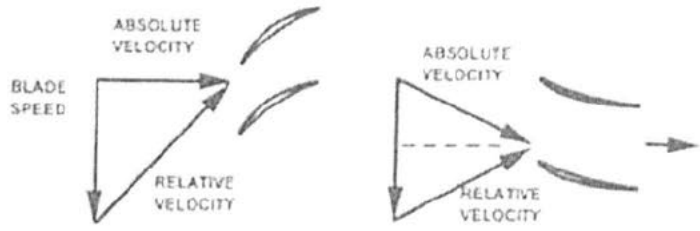

(a) Design operating point

Notes:
For stators vane angles match air absolute inlet and outlet angles.
For rotors blade angles match air relative inlet and outlet angles.

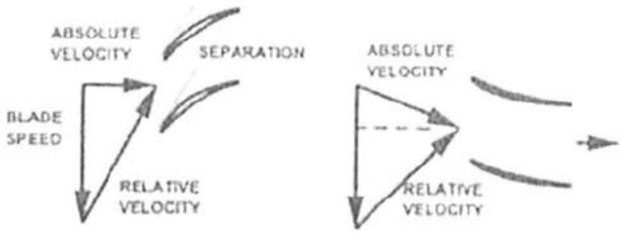

(b) Operation close to surge

Notes:
Axial velocity is reduced due to lower flow.
Rotor blade is stalled with flow separation from suction surface due to high positive incidence onto rotor blades.

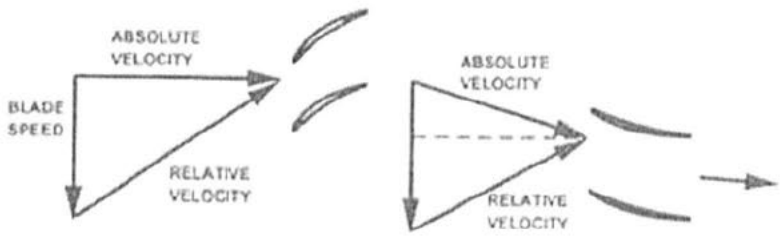

(c) Operation close to choke

Notes:
Axial velocity increased due to higher flow.
Throat at inlet to rotor blade is choked.
Negative incidence onto rotor blades.

Fig. 6.5. Axial compressor velocity triangles.

6.5. Multivariable control of a three-spool engine

In order to satisfy performance requirements and safety issues, the jet engine control configuration should have at least two outputs (Tavakoli, Griffin and Fleming, 2004). For the chosen outputs in this study, the first output infers engine thrust whilst the second one represents safety. These outputs are turbofan power ratio (TPR) and $\overline{SM}$. The second output is representative of the overall surge risk to the engine. The first input, which manipulates the thrust, is the engine fuel flow rate (WFE). Another input should contribute to dealing with compressor instabilities. In this study, $VSVs$ are selected as the second input. Figure 6.6 shows the schematic representation of multivariable control scheme.

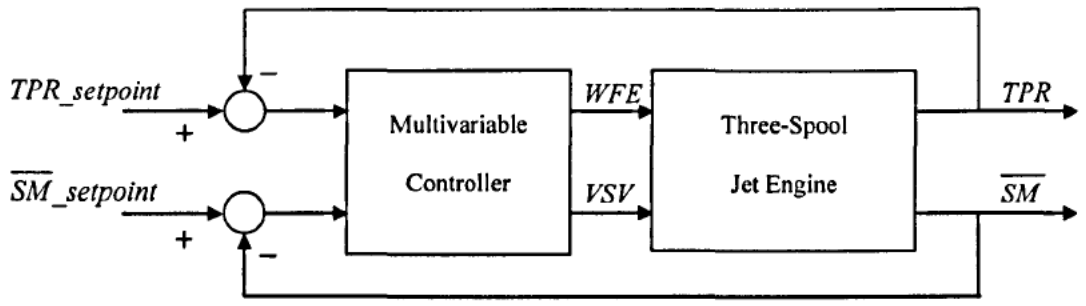

Fig. 6.6. Multivariable control configuration.

6.5.1. Design 1

The TITO turbofan linear model derived from a non-linear simulation at 80% of maximum HP compressor shaft speed is as follows:

$$G_1(s)=\frac{1}{d(s)}\begin{bmatrix} g_{11}(s) & g_{12}(s) \\ g_{21}(s) & g_{22}(s) \end{bmatrix},$$

$$g_{11}(s)=\frac{1}{344.284}(s^3+7.931s^2+21.31s+18.876),$$

$$g_{12}(s)=\frac{-1}{108.582}(s^3+2.238s^2-0.357s-1.667),$$

$$g_{21}(s)=\frac{1}{59195}(s^3+31.135s^2+100.163s+91.732),$$

$$g_{22}(s)=\frac{1}{376.507}(s^3+3.786s^2+3.128s-0.942),$$

$$d(s)=(s^3+6.206s^2+13.093s+9.292).$$

As $g_{12}(s)$ and $g_{22}(s)$ have RHP zeros, both decouplers represented in Equations (3.45) and (3.48) are unstable. Applying the method described in Appendix B to the above-mentioned TITO model results in the following process:

$$\overline{G_1}(s)=G_1(s)A=\frac{1}{d(s)}\begin{bmatrix} \overline{g}_{11}(s) & \overline{g}_{12}(s) \\ \overline{g}_{21}(s) & \overline{g}_{22}(s) \end{bmatrix},$$

$$A=\begin{bmatrix} -100 & 200 \\ 300 & 100 \end{bmatrix},$$

$$\overline{g}_{11}(s)=-3.053s^3-8.489s^2-5.202s-0.879,$$

$$\overline{g}_{12}(s)=-0.34s^3+2.546s^2+12.708s+12.499,$$

$$\overline{g}_{21}(s)=0.795s^3+2.964s^2+2.323s-0.906,$$

$$\overline{g}_{22}(s)=0.269s^3+1.111s^2+1.169s+0.06.$$

The decoupler is given by:

$$D(s)=\begin{bmatrix} 1 & -\dfrac{\bar{g}_{12}(s)}{\bar{g}_{11}(s)} \\ -\dfrac{\bar{g}_{21}(s)}{\bar{g}_{22}(s)} & 1 \end{bmatrix}.$$

Diagonal elements of $Q(s)$ are as follows:

$$q_1(s)=20.283\frac{(-3.823s+1)(0.499s+1)(0.238s+1)}{(18.581s+1)(0.533s+1)(0.455s+1)},$$
$$q_2(s)=-1.377\frac{(-3.823s+1)(0.238s+1)}{(3.338s+1)(2.082s+1)}.$$

Using the specified phase margin (SPM) method of loop design, *TPR* responses resulting from applying a unit step in *TPR_setpoint* followed by a step load disturbance decrease of 50 lb/hr in *WFE* are shown in Figure 6.7. As expected, more robust controllers, which are corresponding to larger values of PM, lead to slower responses and worse load disturbance rejection. Figure 6.7 clearly shows the drop in thrust for a step load disturbance decrease in fuel flow.

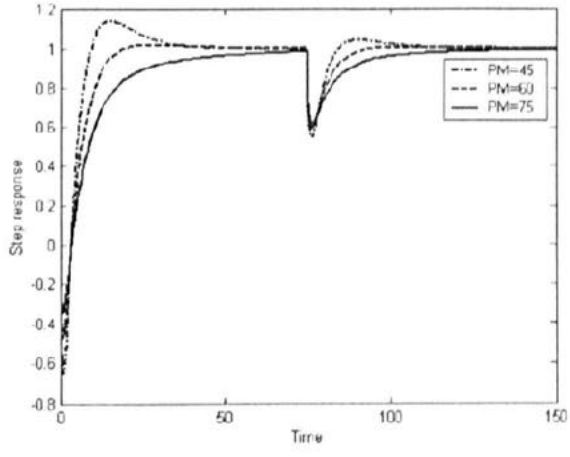

Fig. 6.7. *TPR* responses for different values of PM.

Zeros of elements of the resulting open-loop diagonal matrix, $\bar{G}_1(s)D(s)$, can be found from roots of $|G_1(s)|=0$. Considering the model of TITO turbofan engine given in Section 6.5.1, $g_{12}(s)$ and $g_{22}(s)$ have RHP zeros. Therefore, $|G_1(s)|=0$ may have some RHP roots, which is the case in this example. As a result, Figure 6.7 shows inverse responses at the beginning.

Figure 6.8 shows the initial part of Figure 6.7. As expected, a faster response is given by a higher controller gain, K_c. Since an inverse response in *TPR* is undesirable, there is a trade-off between speed of *TPR* response and amount of its inverse response.

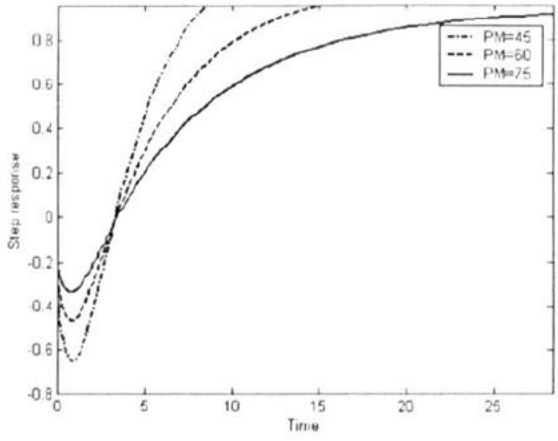

Fig. 6.8. Initial part of Fig. 6.7.

Table 6.1 summarises the results of a robustness comparison for different values of PM.

Table 6.1. Robustness comparison of the SPM controllers to control $q_1(s)$

PM	45	60	75
ω	0.174	0.127	0.090
K_c	0.125	0.103	0.083
T_i	11.76	16.68	23.63
M_s	2.117	1.747	1.518
GM	2.006	2.479	3.116
$\frac{d^2K_i}{d\omega^2}$	-0.211	-0.168	-0.124
$\frac{IE}{IAE}$	0.831	0.903	0.945

As $q_2(s)$ has a negative gain, the integral gain, K_i, should be negative too. Therefore, optimal load disturbance rejection results in maximising - K_i, i.e. minimising K_i. As a result, the sufficient condition is satisfied if $\frac{d^2K_i}{d\omega^2}$ is positive.

Using the specified gain margin (SGM) method, $\overline{SM}$ responses resulting from applying a unit step in $\overline{SM}\_setpoint$ followed by a step load disturbance decrease of 10° in *VSV* are shown in Figure 6.9. This figure shows that $\overline{SM}$ has an inverse response due to the RHP zeros. It also shows a decrease in the overall surge risk to the engine resulting from step load disturbance decrease in *VSV* angle indicating a benefit to the HP compressor of opening the vanes with negligible detriment caused to the IP compressor.

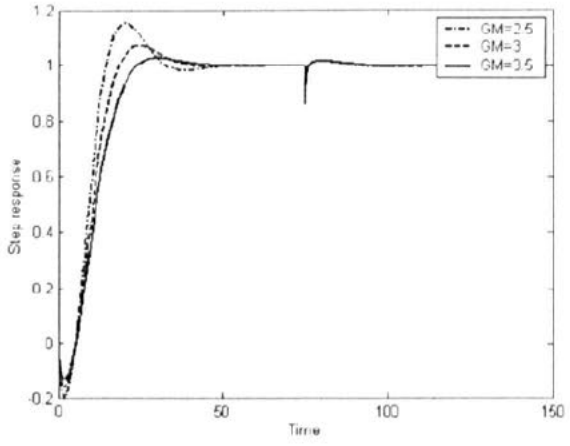

Fig. 6.9. $\overline{SM}$ responses for different values of GM.

The results of a robustness comparison for different values of GM are summarised in Table 6.2.

Table 6.2. Robustness comparison of the SGM controllers to control $q_2(s)$

GM	2.500	3.000	3.500
ω		0.345	
K_c	-0.233	-0.186	-0.160
T_i		2.688	
M_s	1.941	1.712	1.574
PM	49.28	55.89	60.67
$\frac{d^2 K_i}{d\omega^2}$	0.699	0.583	0.499
$\frac{IE}{IAE}$	0.652	0.750	0.819

As an option, the decentralised SPM/SGM controller can be given by:

$$K_{SPM/SGM} = \begin{bmatrix} 0.103 + \dfrac{0.006}{s} & 0 \\ 0 & -0.186 - \dfrac{0.069}{s} \end{bmatrix}.$$

Figure 6.10 shows $\overline{SM}$ response resulting from applying a unit step in *TPR_setpoint* followed by a step load disturbance decrease of 50 lb/hr in *WFE*.

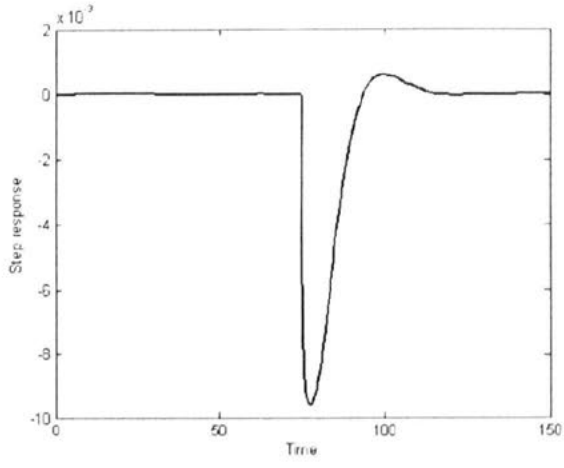

Fig. 6.10. $\overline{SM}$ response to a unit step in *TPR_setpoint* followed by a step load disturbance of -50 lb/hr in *WFE*.

The improvement in the overall surge risk resulting from a step load disturbance decrease in *WFE* can be seen in Figure 6.10. This surge risk returns to its original equilibrium point as the spool speeds rematch.

TPR response resulting from applying a unit step in $\overline{SM}$*_setpoint* followed by a step load disturbance decrease of 10° in *VSV* is shown in Figure 6.11.

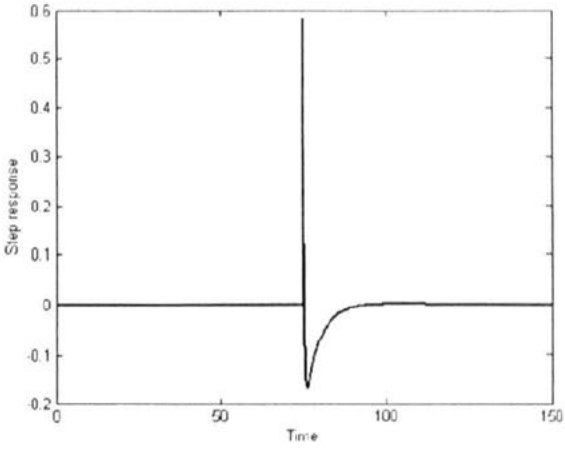

Fig. 6.11. *TPR* response to a unit step in $\overline{SM}$*_setpoint* followed by a step load disturbance of -10° in *VSV*.

Figure 6.11 shows the instantaneous response of gas dynamics to a step load disturbance decrease in *VSV* angle. The decrease in *VSV* angle denotes an opening of the guide vanes leading to an increase in the pressure ratio across the IP compressor. This results in raising power following the load disturbance event. Thrust is then restored to its reference value through the closed-loop action on *WFE*.

The decoupler has effectively decoupled the TITO jet engine transfer matrix, as Figures 6.10 and 6.11 show that interactions are negligible for the nominal system. It means that each output can be regulated independently of another.

6.5.2. Design 2

Clearly, an inverse response in TPR is undesirable. To prevent a large inverse response, one solution is to add some additional poles to the decoupler, or equivalently to matrix A. The additional poles can be located at $s=-\frac{1}{0.238}$, $s=-\frac{1}{0.499}$ and $s=-\frac{1}{3.823}$. Such a choice cancel left half plane zeros of diagonal elements of $Q(s)$ and eases the model reduction procedure. Consequently, diagonal elements of $Q(s)$ are given by:

$$q_1(s)=9.212\frac{-3.823s+1}{(18.577s+1)(3.823s+1)(0.533s+1)(0.455s+1)},$$
$$q_2(s)=-0.628\frac{-3.823s+1}{(3.823s+1)(3.345s+1)(2.081s+1)(0.5s+1)}.$$

Using Equation (3.52), the FOPDT models for these elements are:

$$l_1(s)=9.212\frac{e^{-7.058s}}{18.879s+1},$$
$$l_2(s)=-0.628\frac{e^{-8.899s}}{11.83s+1}.$$

Using the half rule approach, the FOPDT models are given by:

$$\hat{l}_1(s)=9.212\frac{e^{-6.721s}}{20.488s+1},$$
$$\hat{l}_2(s)=-0.628\frac{e^{-8.076s}}{5.495s+1}.$$

Figures 6.12 and 6.13 show the Nyquist plots of diagonal elements of $Q(s)$ and their approximate FOPDT models.

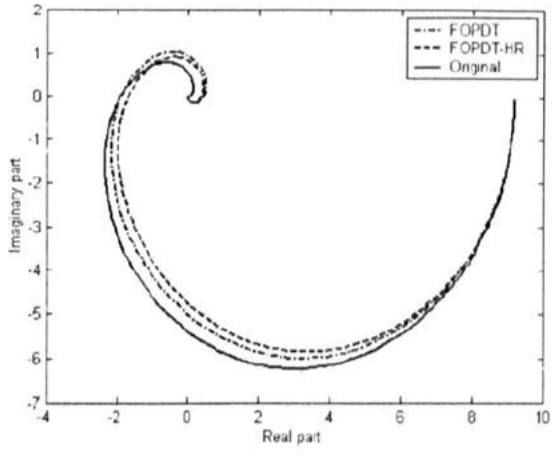

Fig. 6.12. Nyquist plots of $q_1(s)$, $l_1(s)$ and $\hat{l}_1(s)$.

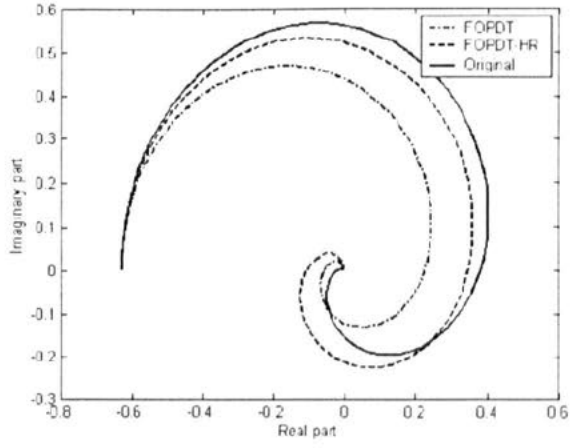

Fig. 6.13. Nyquist plots of $q_2(s)$, $l_2(s)$ and $\hat{l}_2(s)$.

Using Equations (3.20) and (3.21), the NDT controllers are given by:

$$K_{NDT} = \begin{bmatrix} 0.153 + \dfrac{0.008}{s} & 0 \\ 0 & -1.173 - \dfrac{0.09}{s} \end{bmatrix},$$

$$K_{NDT-HR} = \begin{bmatrix} 0.173 + \dfrac{0.008}{s} & 0 \\ 0 & -0.657 - \dfrac{0.099}{s} \end{bmatrix}.$$

Using the NDT tuning formulae, the *TPR* and $\overline{SM}$ responses resulting from applying a unit step in *TPR_setpoint* or $\overline{SM}$*_setpoint*, followed by a step load disturbance of -50 lb/hr in *WFE* or -10° in *VSV* are shown in Figures 6.14-6.17.

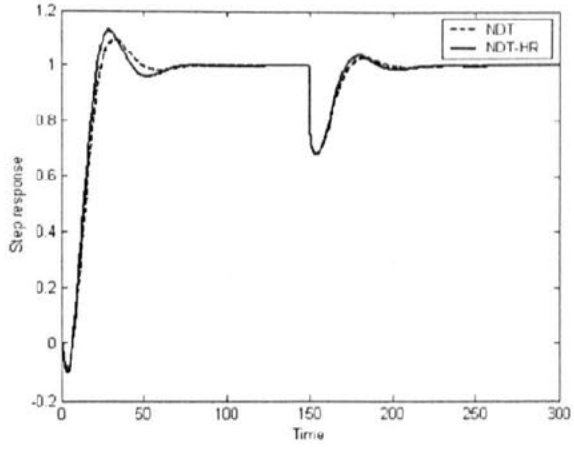

Fig. 6.14. *TPR* response to a unit step in *TPR_setpoint* followed by a step load disturbance of -50 lb/hr in *WFE*.

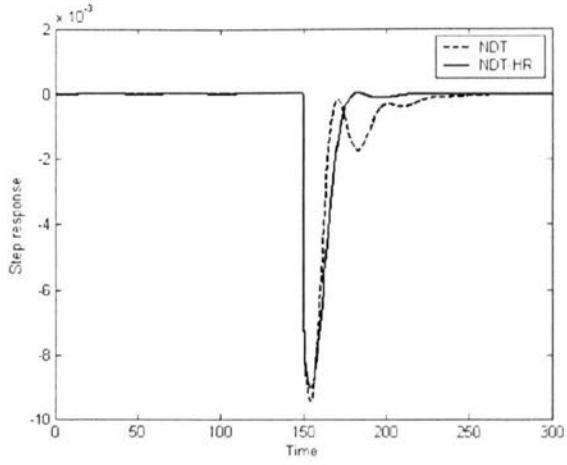

Fig. 6.15. $\overline{SM}$ response to a unit step in *TPR_setpoint* followed by a step load disturbance of -50 lb/hr in *WFE*.

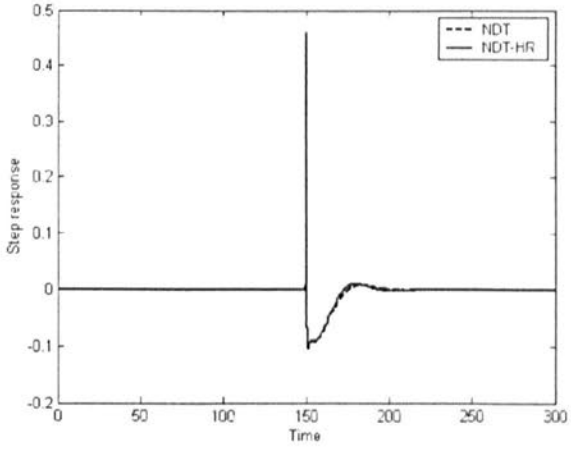

Fig. 6.16. *TPR* response to a unit step in $\overline{SM}$*_setpoint* followed by a step load disturbance of -10° in *VSV*.

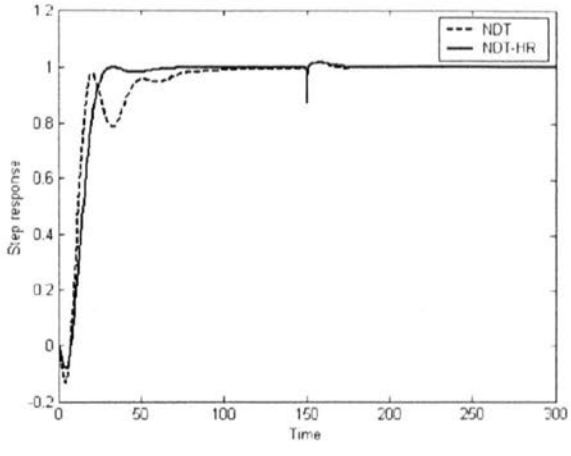

Fig. 6.17. $\overline{SM}$ response to a unit step in $\overline{SM}$*_setpoint* followed by a step load disturbance of -10° in *VSV*.

6.5.3. Design 3

The jet engine is a non-linear, highly cross-coupled, numerically ill-conditioned process having a dominant input, namely *WFE*. In Appendix D, a condition number minimisation approach is proposed to improve the numerical conditioning of the ALSTOM gasifier. It is shown that the resulting controller is able to satisfy the performance requirements whilst making sure that the multivariable effects of uncertainty are not severe. In this design, the condition number minimisation approach is applied to the TITO model of the jet engine.

The pre and post-plant scaling matrices, D_1 and D_2, are placed after the decoupler and after the process, respectively. Considering G_p and G_c as the process and controller transfer matrices, Figure 6.18 shows the closed-loop system:

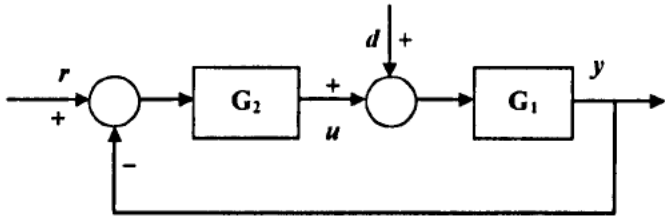

Fig. 6.18. Block diagram of one-degree of freedom feedback control system.

where $G_1 = D_2 G_p$, $G_2 = Z_a D_1 D_e G_c$, and Z_a and D_e are zero assignment and decoupler matrices, respectively.

Considering three additional poles at $s = -\frac{1}{0.238}$, $s = -\frac{1}{0.499}$ and $s = -\frac{1}{3.823}$, proposed in Section 6.5.2, the zero assignment technique is applied to the TITO model given in Section 6.5.1 to obtain the following process:

$$\overline{G_1}(s) = \frac{1}{d(s)}\begin{bmatrix} \overline{g}_{11}(s) & \overline{g}_{12}(s) \\ \overline{g}_{21}(s) & \overline{g}_{22}(s) \end{bmatrix},$$

$$\overline{g}_{11}(s) = -3.053s^3 - 8.489s^2 - 5.202s - 0.879,$$

$$\overline{g}_{12}(s) = -0.34s^3 + 2.546s^2 + 12.708s + 12.499,$$

$$\overline{g}_{21}(s) = 0.795s^3 + 2.964s^2 + 2.323s - 0.906,$$

$$\overline{g}_{22}(s) = 0.269s^3 + 1.111s^2 + 1.169s + 0.06,$$

$$d(s) = (s^3 + 6.206s^2 + 13.093s + 9.292)(s + .2616)(s + 2)(s + 4.2).$$

To improve the numerical conditioning of $\overline{G_1}(s)$, scaling matrices are determined through minimising the condition number over a specified range of frequencies. The objective function for optimising the condition number is:

$$\begin{aligned} &\underset{D_1,D_2}{Min}[cond(\tilde{G}_1(s))], \\ &\tilde{G}_1(s) = D_2\overline{G_1}(s)D_1. \end{aligned} \tag{6.1}$$

Minimising condition number over frequencies less than $\omega = 4.2r/s$, results in the following scaling matrices.

$$\begin{aligned} D_1 &= diag(0.486,0.495), \\ D_2 &= diag(1,7.468). \end{aligned}$$

$\tilde{G}_1(s)$ is given by:

$$\begin{aligned} \tilde{G}_1(s) &= \frac{1}{d(s)}\begin{bmatrix} \tilde{g}_{11}(s) & \tilde{g}_{12}(s) \\ \tilde{g}_{21}(s) & \tilde{g}_{22}(s) \end{bmatrix}, \\ \tilde{g}_{11}(s) &= -1.483s^3 - 4.123s^2 - 2.527s - 0.427, \\ \tilde{g}_{12}(s) &= -0.168s^3 + 1.26s^2 + 6.288s + 6.184, \\ \tilde{g}_{21}(s) &= 2.884s^3 + 10.752s^2 + 8.427s - 3.285, \\ \tilde{g}_{22}(s) &= 0.994s^3 + 4.105s^2 + 4.32s + 0.221, \\ d(s) &= (s^3 + 6.206s^2 + 13.093s + 9.292)(s + .2616)(s + 2)(s + 4.2). \end{aligned}$$

The decoupler is:

$$D(s) = \begin{bmatrix} 1 & -\dfrac{\tilde{g}_{12}(s)}{\tilde{g}_{11}(s)} \\ -\dfrac{\tilde{g}_{21}(s)}{\tilde{g}_{22}(s)} & 1 \end{bmatrix}.$$

Diagonal elements of $Q(s)$ are given by:

$$\begin{aligned} q_1(s) &= 4.477\frac{-3.823s + 1}{(18.577s + 1)(3.823s + 1)(0.533s + 1)(0.455s + 1)}, \\ q_2(s) &= -2.32\frac{-3.823s + 1}{(3.823s + 1)(3.345s + 1)(2.081s + 1)(0.5s + 1)}. \end{aligned}$$

Applying the SPM method to $q_1(s)$ and the SGM method to $q_2(s)$, Table 6.3 summarises the results of a robustness comparison for different values of PM or GM.

Table 6.3. Robustness comparison of the SPM (SGM) controllers to control $q_1(s)$ ($q_2(s)$)

	SPM controllers for $q_1(s)$		SGM controllers for $q_2(s)$	
ω	0.089	0.071	0.184	
K_c	0.363	0.311	-0.134	-0.111
T_i	17.04	21.84	4.237	
M_s	2.024	1.69	1.888	1.674
GM	2.394	2.972	2.5	3
PM	45	60	51.3	57.62
$\frac{d^2K_i}{d\omega^2}$	-1.067	-0.785	0.91	0.758
$\frac{IE}{IAE}$	0.958	0.972	0.712	0.826

Again, as $q_2(s)$ has a negative gain, the integral gain should be negative resulting in a positive value for $\frac{d^2K_i}{d\omega^2}$ in case of satisfying the sufficient condition.

As a choice, the decentralised SPM/SGM controller can be given by:

$$K_{SPM/SGM} = \begin{bmatrix} 0.311 + \frac{0.014}{s} & 0 \\ 0 & -0.111 - \frac{0.026}{s} \end{bmatrix}.$$

To design a decentralised NDT controller, Equation (3.52) is used to determine the FOPDT models for Diagonal elements of $Q(s)$. The approximate models are given by:

$$l_1(s) = 4.477\frac{e^{-7.058s}}{18.879s+1},$$
$$l_2(s) = -2.32\frac{e^{-8.899s}}{11.83s+1}.$$

Using the half rule approach, the FOPDT models are as follows:

$$\hat{l}_1(s) = 4.477\frac{e^{-6.721s}}{20.488s+1},$$
$$\hat{l}_2(s) = -2.32\frac{e^{-8.076s}}{5.495s+1}.$$

Using Equations (3.20) and (3.21), the NDT controllers are given by:

$$K_{NDT} = \begin{bmatrix} 0.315 + \dfrac{0.016}{s} & 0 \\ 0 & -0.317 - \dfrac{0.024}{s} \end{bmatrix},$$

$$K_{NDT-HR} = \begin{bmatrix} 0.356 + \dfrac{0.017}{s} & 0 \\ 0 & -0.177 - \dfrac{0.027}{s} \end{bmatrix}.$$

Figures 6.19-6.22 show the TPR and $\overline{SM}$ responses resulting from applying a unit step in $TPR\_setpoint$ or $\overline{SM}\_setpoint$, followed by a step load disturbance of -50 lb/hr in WFE or -2° in VSV.

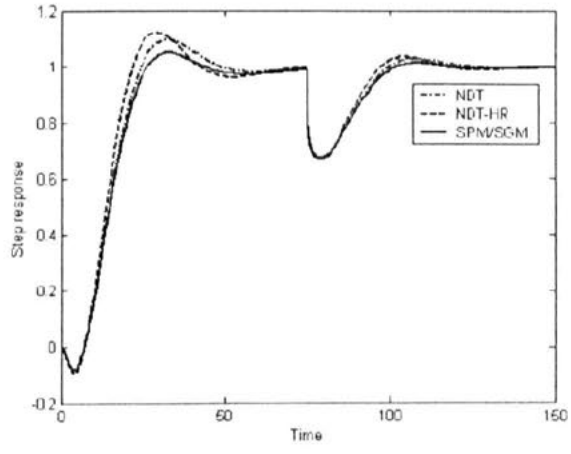

Fig. 6.19. TPR response to a unit step in $TPR\_setpoint$ followed by a step load disturbance of -50 lb/hr in WFE.

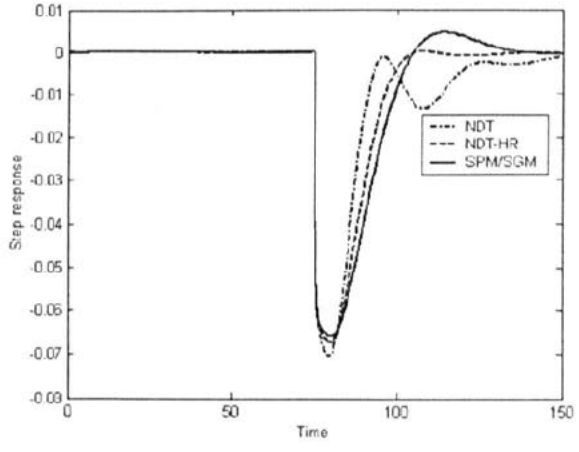

Fig. 6.20. $\overline{SM}$ response to a unit step in $TPR\_setpoint$ followed by a step load disturbance of -50 lb/hr in WFE.

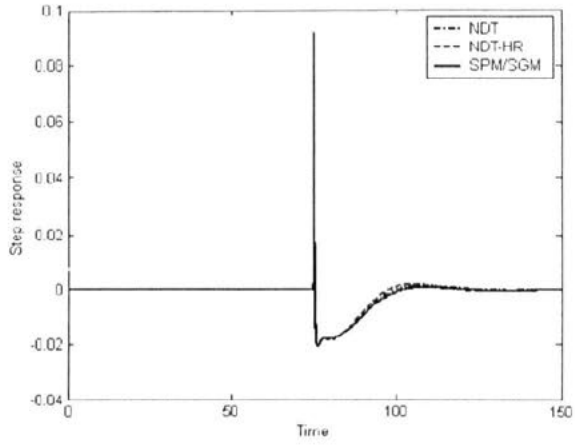

Fig. 6.21. *TPR* response to a unit step in $\overline{SM}\_setpoint$ followed by a step load disturbance of -2° in *VSV*.

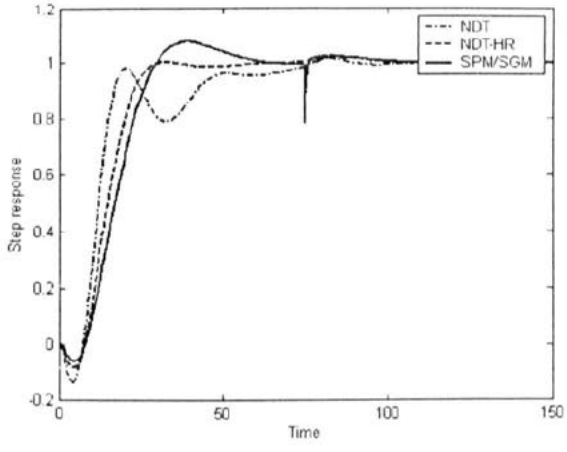

Fig. 6.22. $\overline{SM}$ response to a unit step in $\overline{SM}\_setpoint$ followed by a step load disturbance of -2° in *VSV*.

6.5.4. Robustness studies

In order to investigate the robustness issues, model parameters are deviated from their nominal values to represent uncertainties in the model. Then, the previously designed controllers are applied to the perturbed model.

6.5.4.1. Uncertainty in the process gain

Considering the controllers designed in Section 6.5.3, an increase of 20% in the process gain is considered as uncertainty in the model. Applying a unit step in *TPR_setpoint* or $\overline{SM}\_setpoint$, followed by a step load disturbance of -50 lb/hr in *WFE* or -2°, Figures 6.23-6.26 show the *TPR* and $\overline{SM}$ responses. Clearly, all the proposed controllers show a good degree of robustness and satisfactorily cope with uncertainty in the process gain.

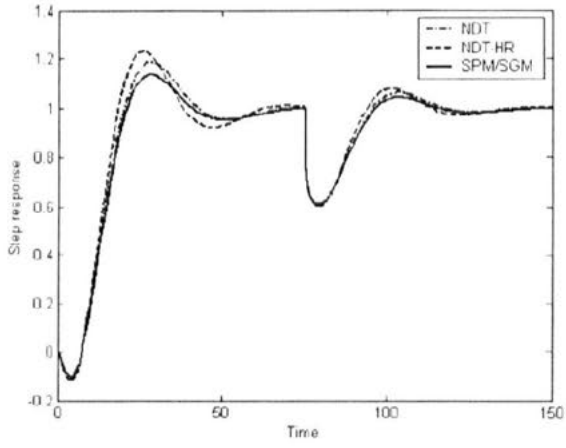

Fig. 6.23. *TPR* response to a unit step in *TPR_setpoint* followed by a step load disturbance of -50 lb/hr in *WFE*.

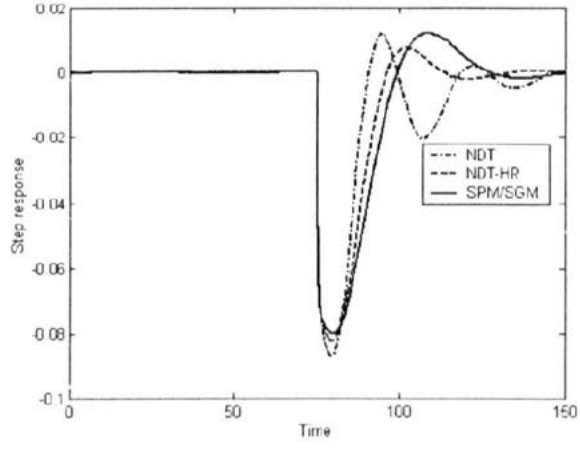

Fig. 6.24. $\overline{SM}$ response to a unit step in *TPR_setpoint* followed by a step load disturbance of -50 lb/hr in *WFE*.

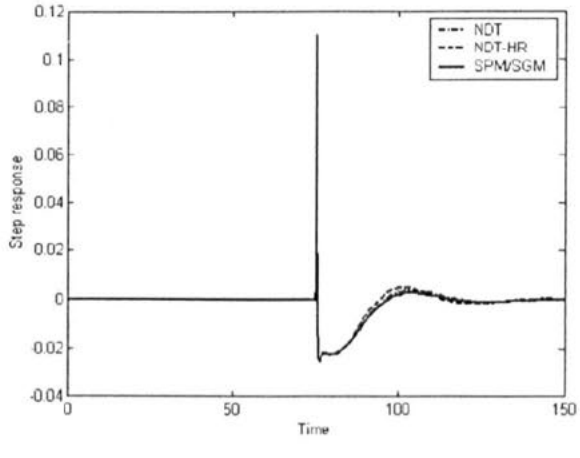

Fig. 6.25. *TPR* response to a unit step in $\overline{SM}$_*setpoint* followed by a step load disturbance of -2° in *VSV*.

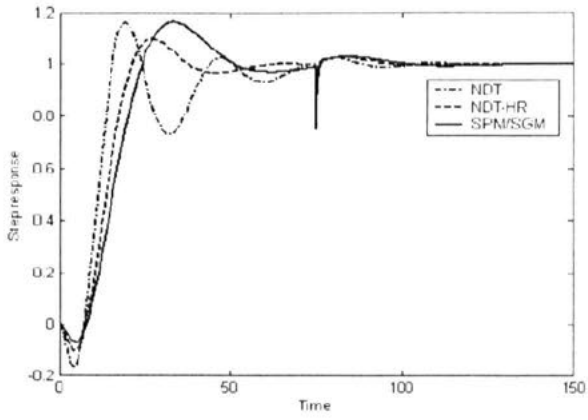

Fig. 6.26. $\overline{SM}$ response to a unit step in $\overline{SM}\_setpoint$ followed by a step load disturbance of -2° in VSV.

6.5.4.2. Uncertainty in the real pole of process

The process has one real and two complex conjugate poles, located at $s=-1.8$ and $s=-2.203\pm j0.555$. Assume that due to uncertainty, the real pole is moved to $s=-1.44$, i.e. 20% closer to the imaginary axis. TPR and $\overline{SM}$ responses are shown in Figures 6.27-6.30.

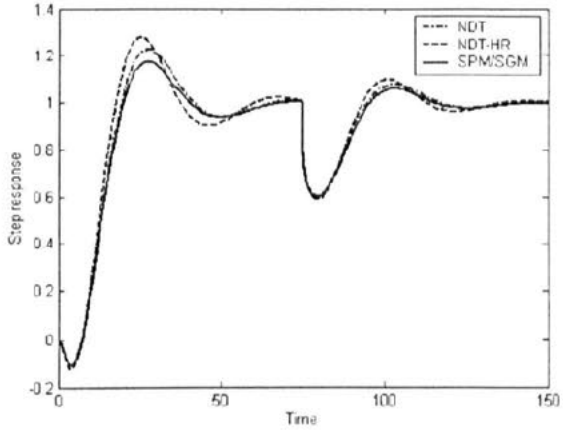

Fig. 6.27. TPR response to a unit step in $TPR\_setpoint$ followed by a step load disturbance of -50 lb/hr in WFE.

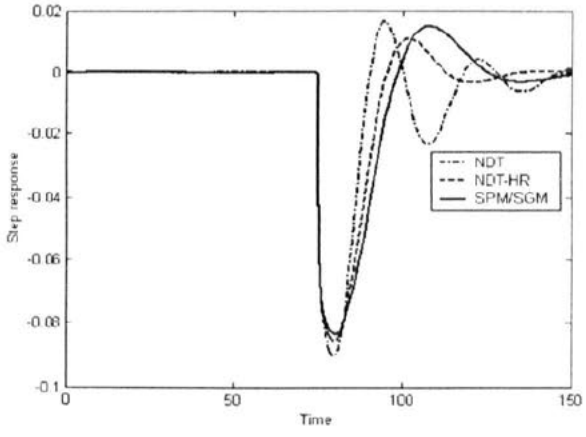

Fig. 6.28. $\overline{SM}$ response to a unit step in $TPR\_setpoint$ followed by a step load disturbance of -50 lb/hr in WFE.

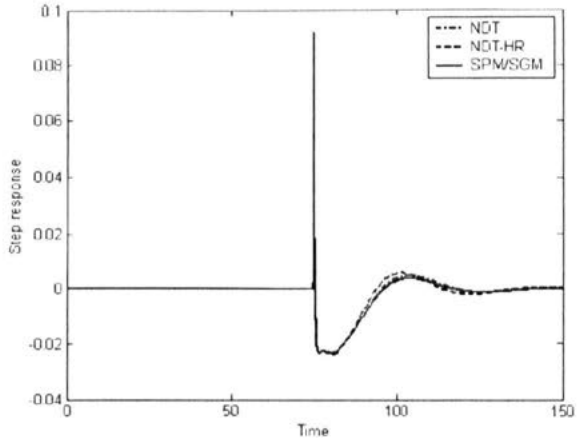

Fig. 6.29. *TPR* response to a unit step in $\overline{SM}\_setpoint$ followed by a step load disturbance of -2° in *VSV* .

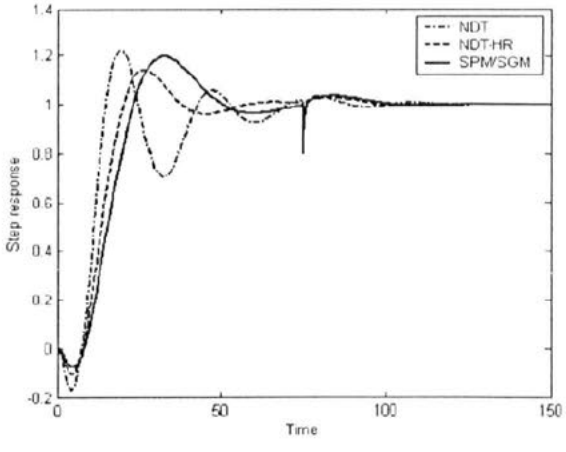

Fig. 6.30. $\overline{SM}$ response to a unit step in $\overline{SM}\_setpoint$ followed by a step load disturbance of -2° in *VSV* .

Again, the proposed controllers satisfactorily deal with the model uncertainty.

6.5.4.3. Uncertainty in both the gain and real pole of process

The model uncertainty introduced by an increase of 20% in the process gain and a decrease of 20% in the value of the real pole of the model. *TPR* and $\overline{SM}$ responses are shown in Figures 6.31-6.34. These figures show that the proposed controllers satisfactorily deal with this significant model uncertainty.

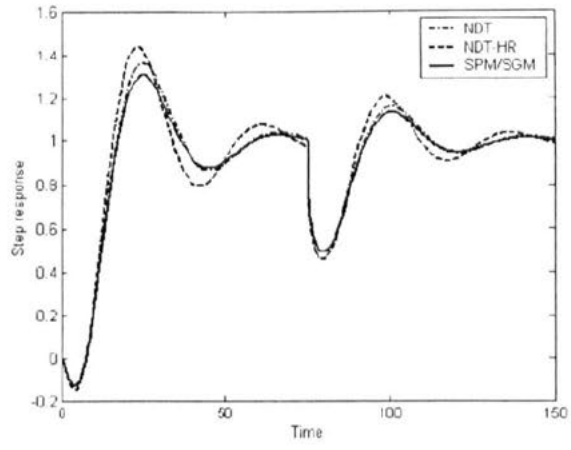

Fig. 6.31. *TPR* response to a unit step in *TPR_setpoint* followed by a step load disturbance of -50 lb/hr in *WFE*.

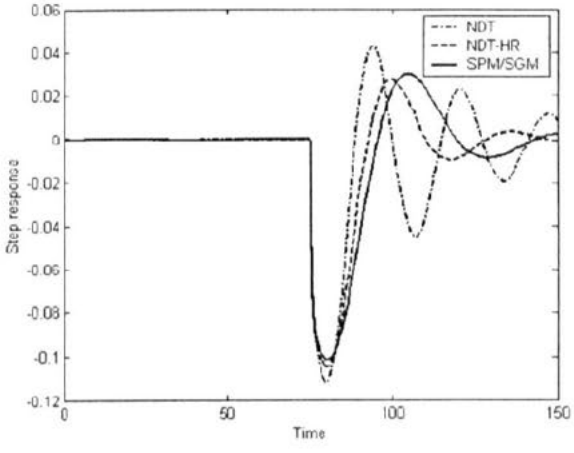

Fig. 6.32. $\overline{SM}$ response to a unit step in *TPR_setpoint* followed by a step load disturbance of -50 lb/hr in *WFE*.

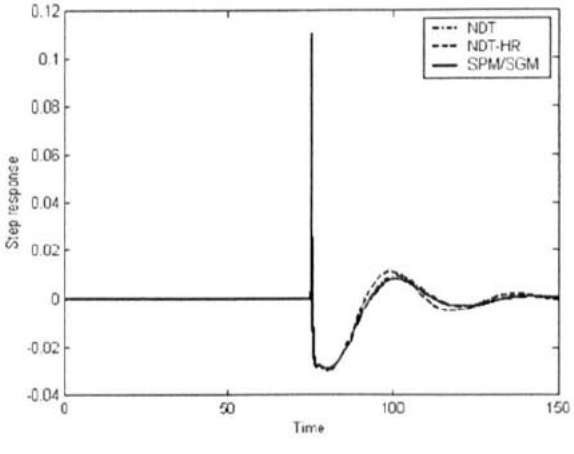

Fig. 6.33. *TPR* response to a unit step in $\overline{SM}$_*setpoint* followed by a step load disturbance of -2° in *VSV*.

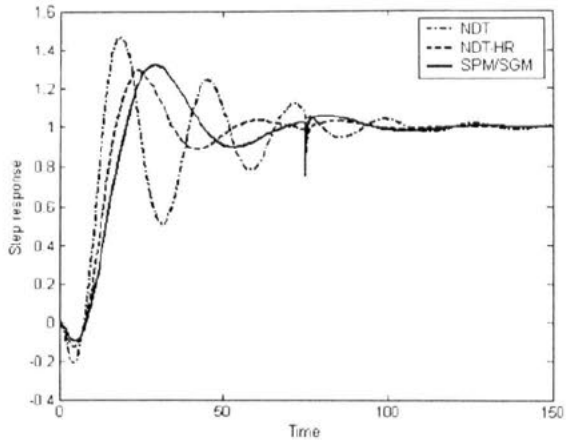

Fig. 6.34. $\overline{SM}$ response to a unit step in $\overline{SM}\_setpoint$ followed by a step load disturbance of -2° in VSV.

6.6. Discussions

The open-loop dynamics of the jet engine vary widely both with the operating point and the flight condition. For small perturbations about a given operating point the departure from the linear dynamics is small enough to be ignored, whereas between idle and maximum thrust there are six other operating points used in a standard design. The design approach is to design linear multivariable controllers at specific operating points. Then, a gain scheduled controller accommodates non-linearity in engine dynamics and characteristics using eight design points over the thrust range. Whist results have been presented only for an operating point, similar responses were achieved at other operating points and flight conditions.

The SISO controller offers simplicity of structure but restricts tight control to only one engine output, namely the engine thrust. On the other hand, the multivariable controller offers tight control of two engine outputs, which are representatives of the engine thrust and safety. However, this is obtained at the expense of a more complex design procedure.

While this study shows a successful application of multivariable control, this application raises a number of issues that need addressing. A vital issue is to keep the current conventional lowest-wins highest-wins control scheme and, therefore, to minimise the variations in the control structure. This allows the limiter loops, which protect other engine parameters from going out of range, to remain within the controller structure.

6.7. Summary

Requirements for improved performance and/or safety issues of current jet engines indicate a need for more comprehensive closed-loop jet engine control. The application of multivariable control to jet engines, which enables simultaneous closure of multiple control loops around the engines, offers the prospect of lower safety margin requirements leading to more efficiency and lower fuel consumption. The multivariable control may be used in civil engines to offer better safety margin whilst providing similar thrust compared to corresponding SISO control strategies. In military engines, however, the

multivariable control may be employed to offer more agility in combat through improved engine responses and prolonged engine life through more precise control of engine parameters.

Applying a simple decentralised control strategy to the Rolls-Royce three-spool turbofan engine, it was shown that the multivariable controllers were capable of improving efficiency of the corresponding conventional SISO controllers through offering greater control flexibility by virtue of the increased number of loops.

The summary of the research work carried out in this PhD and some recommendations for further work are given in Chapter 7.

Chapter 7

Conclusions and Future Work

7.1. Introduction

This thesis has introduced a new multivariable PID control technique and demonstrated its application, especially, to the jet engine control problem. The purpose of this chapter is to summarise the research work carried out in this thesis and to give recommendation for future work. A review of the work undertaken during this research and proposals for further work in the particular subject area is provided by each section.

Jet engines perform efficiently when they can be operated at or near their mechanical, thermal, flow or pressure limitations such as rotor speeds, turbine temperatures, internal pressures, etc. The closer the operating point is to the unstable region, the greater the jet engine efficiency, but the greater the risk of compressor instabilities. Therefore, there is a trade-off between performance and safety.

In order to meet increasing demands on performance, stability, fuel consumption and functionality, modern jet engines are becoming more complex. To utilise the potential of these engines, which have more control variables, it is necessary to use more advanced control strategies.

Having motivated by improving performance and/or safety of jet engines, a study on multivariable jet engine control has been addressed by this thesis. As a case study, the proposed multivariable control technique has been explored on a Rolls-Royce three-spool high bypass ratio turbofan engine. The linear models of the engine can be represented by third order transfer functions. As the design requirements are not too rigorous, a multivariable PID controller is sufficient. In order to have a simple and efficient design and to prevent the complexity caused by using full matrix multivariable controllers, a systematic decentralised PID control design procedure has been proposed and has been successfully applied to the jet engine.

7.2. Review of PID control design

Considering the need for simple, flexible and extendable PID tuning methods and in view of the necessity of having a tuning method capable of properly dealing with conflicting design requirements, a step-by-step PID design technique has been developed in Chapters 3, 4 and 5. As many industrial processes can approximately be modelled by FOPDT (SOPDT) transfer functions, the design method aims to present a systematic approach to derive multi-objective PI (PID) tuning formulae for such processes. Assuming setpoint regulation as the primary design objective, the NDT tuning method for designing PI (PID) controllers for FOPDT (SOPDT) processes has been proposed in Chapter 3. To ensure that the resulting closed-loop system is sufficiently robust against model uncertainties, robustness constraints have also been considered. This approach has then been extended to design a decentralised controller for a given two input two output process.

In addition, the value of integral time of PI controller has been revised for lag dominant and integrating processes to cope with load disturbances properly. However, further work is required to give a compromise solution for a PID controller when applying to a SOPDT process with small $\xi\omega_n\tau_d$. To do so, obtaining PID tuning formulae resulting in optimisation of both setpoint regulation and load disturbance rejection for such processes by means of multi-objective optimisation is a straightforward solution. Alternatively, load disturbance rejection can be considered as the main design objective instead of setpoint regulation when values of $\xi\omega_n\tau_d$ are small.

Selecting load disturbance rejection as the prime design objective, a simple analytical PI tuning method, which is applicable to a broad range of processes, has been proposed in Chapter 4. To consider both performance requirements and robustness issues, the optimisation problem includes a constraint either on the GM or PM. These robustness constraints can be interpreted as design parameters. In addition, simple tuning formulae for FOPDT processes have also been provided and satisfaction of the sufficient condition for such processes has been proven. However, an iterative method is still required to obtain the value of ω. For further work, a simple set of PI tuning formulae for FOPDT processes can be obtained using the SGM (SPM) technique in conjunction with dimensional analysis and curve-fitting methods to form approximate SGM (ASGM) and approximate SPM (ASPM) tuning formulae.

Chapter 5 presents the design of NDT-PI controllers for FOPDT processes using a two-degree of freedom structure. The design objectives are good load disturbance rejection, good setpoint regulation and good degree of robustness, whilst both single-objective and multi-objective approaches are taken into account.

Chapters 3 and 4 address the design of PI (PID) controllers for stable FOPDT (SOPDT) processes. However, if these processes are unstable the NDT method will not directly be applicable. For future work, an IMC structure, which is able to decouple design of the setpoint response from the load disturbance response, is recommended to provide a stable closed-loop system for unstable FOPDT (SOPDT) processes. Considering good load disturbance rejection, good setpoint regulation

and good degree of robustness as control objectives, a multi-objective optimisation approach can be used to obtain tuning rules.

7.3. Review of multivariable control design

Trade-off between performance and safety is an important issue in feedback control design. The performance and effectiveness of jet engines are limited by the unstable regions of their compressors. In order to improve engine performance and safety, the study of compressor instabilities has received much attention in recent years. Many advanced control strategies have been employed to suppress compressor instabilities and extend their stable operating range and, therefore, improve the engine performance and efficiency. An overview of the fundamentals of compressor instabilities, surge and rotating stall, has been presented in Appendix C. In addition, the major recent developments in surge and rotating stall avoidance, detection and avoidance and control techniques have been reviewed.

In order to address a number of important issues in multivariable control design, a non-linear, highly cross-coupled and numerically ill-conditioned case study plant has been considered in Appendix D. To improve the numerical conditioning of the process, minimal realization, model order reduction and scaling techniques are used. A multivariable control design procedure based on condition number minimisation strategy is proposed to successfully tackle this ill-conditioned process.

Compared to the SISO control strategy, the application of multivariable control to jet engines offers better performance and/or better safety. Applying a decentralised control strategy, which offers greater control flexibility by virtue of the increased number of loops, to a Rolls-Royce three-spool turbofan engine, it has been shown in Chapter 6 that the multivariable controllers improve safety margins in comparison with the corresponding conventional SISO controllers.

Due to the non-linearity in a jet engine model, which results in significant changes in the model dynamics when considering all operating conditions, gain scheduling is necessary. Designing decentralised controllers at specific operating points, the gain scheduled controller accommodates the non-linearity in engine dynamics through introducing a suitable controller for any operating point over the thrust range.

The subject of future work is to address consideration of large scale transients, which is a more challenging test for the controller, enabling major changes in thrust. The conflicting design objectives such as minimisation of fuel consumption, safety maximisation and maximisation of engine life should be addressed through applying the proposed NDT method in conjunction with the decentralised control strategy. In addition, the task of structure change to accommodate actuator failure or saturation has to be tackled.

This research work shows that multivariable control is an advantageous enabling technology for jet engines, however, its complexity and the consideration of actuator failure accommodation limit the number of variables controlled in a closed-loop sense. Figure 7.1 shows a MIMO jet engine control structure. To control both performance and safety effectively, at least two loops should be

closed, whilst the other loops remain scheduled. However, the possibility of having more than two loops may be the scope of further work.

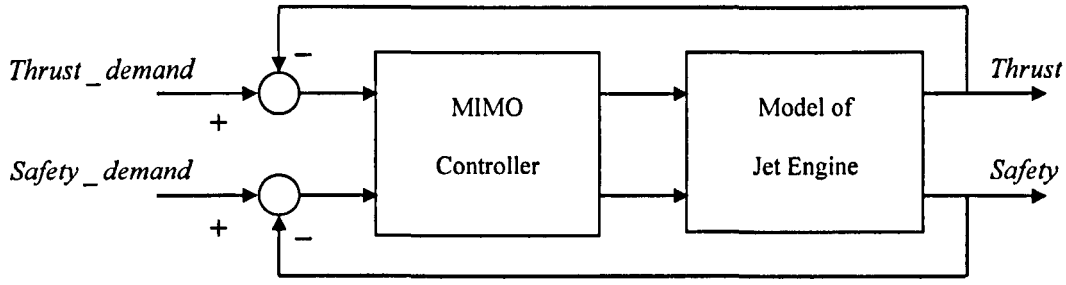

Fig. 7.1. Schematic representation of MIMO control scheme.

This thesis offers a decentralised control scheme which is applicable to both civil and military gas turbines. Some gas turbine engines use more advanced engine structures. A possible additional feature is the variable nozzle guide vanes (*VNGVs*). The under-study Rolls-Royce turbofan engine also has these vanes located at entry to the IP turbine. Opening up the *VNGVs* causes the HP spool to speed up whilst the IP spool slows down. As a result, the IP compressor is feeding less air into the gap between the two compressors whilst the HP compressor is sucking more out. This reduces the pressure at this point in the engine and avoids the need for opening the bleed valves at IPC delivery when surge has to be avoided. The study of coping with safety issues through *VNGVs* instead of *VSVs* can be a subject for future research. Also, the performance of a 3-by-3 MIMO control structure consisted of *WFE*, *VSV* and *VNGV* as actuators along with outputs representing thrust and safety, or thrust, safety and engine life can be investigated.

7.4. Jet engine control using advanced model-based schemes

Jet engines are complex multivariable processes with demanding requirements. Some objectives to control non-linear models of jet engines are as follows:

- To prevent violations of input and output constraints
- To drive some output variables to their optimal values, while maintaining other outputs within specified ranges
- To prevent excessive movement of the input variables
- To control as many process variables as possible when a sensor or actuator is not available

Model predictive control (MPC) is an important model-based control strategy devised for large MIMO control problems with inequality constraints on the inputs and/or outputs. It can fulfil the above-mentioned objectives (Qin and Badgwell, 2003) and has been a popular subject for academic and industrial research. For example, a survey by Qin and Badgwell (2003) reported that there were over 4500 applications worldwide by the end of 1999, primarily in oil refinements and petrochemical plants.

If a reasonably accurate dynamic model of the process is available, the model and current measurements can be used to predict future values of the outputs. Then, the appropriate changes in the input variables can be calculated based on both measurements and predictions. The MPC produces a sequence of control moves, i.e. manipulated input changes, so that the predicted response moves toward its target in an optimal manner. Clearly, the success of any model-based approach, such as MPC, depends on the accuracy of the process model. Inaccurate predictions can make matters worse, instead of better.

Due to recent developments of more efficient and reliable computational algorithms and having access to fast computers, the application of online optimisation approaches, such as MPC, in conjunction with reasonably accurate real-time simulation technologies may become more popular in jet engine control in the future.

Appendix A

Dimensional analysis

Dimensional analysis is often used to simplify a problem by reducing the number of its variables to the smallest number of essential parameters (Zlokarnik, 1991). Using this technique, relations between variables in a physical system can be defined as relations between dimensionless numbers in the system with no change in the system behaviour. A dimensionless number is a pure number without any physical unit. Such a number is typically defined as a product or ratio of quantities that do have units, in such a way that all units can be cancelled.

Assume that a system is expressed by:

$$x_1 = f(x_2, x_3, ..., x_n), \tag{A.1}$$

with non-zero $x_1, x_2, ..., x_n$. Based on Buckingham's pi-theorem (Taylor, 1974; Zlokarnik, 1991), Equation (A.1) can be written as follows:

$$\pi_1 = g(\pi_2, \pi_3, ..., \pi_{n-m}), \tag{A.2}$$

where $\pi_2, ..., \pi_{n-m}$ are independent dimensionless numbers and m is the minimum number of $x_2, x_3, ..., x_n$, which includes all the units in $x_1, x_2, ..., x_n$.

Appendix B

Zero assignment

Assuming a stable $G(s)$, if both diagonal and off-diagonal elements of $G(s)$ have RHP zeros, a stable decoupler cannot be obtained using decouplers in Equations (3.45) or (3.48). The objective is to find $\overline{G}(s)$ so that its diagonal or off-diagonal elements have no RHP zeros. This may be done through multiplying $G(s)$ by A as shown below:

$$\begin{aligned} &\overline{G}(s) = G(s)A, \\ &A = \begin{bmatrix} a_{11} & a_{12} \\ a_{21} & a_{22} \end{bmatrix}. \end{aligned} \tag{B.1}$$

Considering the $\overline{G}(s)$ requirements, the range of elements of A can be analytically determined. This is illustrated through considering the following stable $G(s)$:

$$G(s) = \frac{1}{(s+b)(s+c)} \begin{bmatrix} s+d_1 & s-d_2 \\ s+d_3 & s-d_4 \end{bmatrix}.$$

Using Equation (B.1), $\overline{G}(s)$ is obtained as follows:

$$\overline{G}(s)=\frac{1}{(s+b)(s+c)}\begin{bmatrix}\bar{g}_{11}(s) & \bar{g}_{12}(s)\\ \bar{g}_{21}(s) & \bar{g}_{22}(s)\end{bmatrix},$$

$$\bar{g}_{11}(s)=(a_{11}+a_{21})s+a_{11}d_1-a_{21}d_2,$$

$$\bar{g}_{12}(s)=(a_{12}+a_{22})s+a_{12}d_1-a_{22}d_2,$$

$$\bar{g}_{21}(s)=(a_{11}+a_{21})s+a_{11}d_3-a_{21}d_4,$$

$$\bar{g}_{22}(s)=(a_{12}+a_{22})s+a_{12}d_3-a_{22}d_4.$$

Then, range of elements of matrix A can be determined so that $\overline{G}(s)$ satisfies the requirements.

Appendix C

An Overview of Compressor Instabilities: Basic Concepts and Control

C.1. Introduction

In recent years, the study of airflow through turbomachines has attracted the attention of a large number of academic and industrial researchers. These machines have a wide range of applications such as in submarines and natural gas pumps in pipelines. However, they are most commonly known as jet engines, propelling the majority of modern aircraft.

The main reason for this interest in turbomachines is due to the fact that when the machine operates close to its optimal operating point, the flow can become unstable. These instabilities put a major stress on the engine and in some cases the engine has to be turned off in order to recover original operation. For this reason, turbomachines are currently operated far away from their optimal operating points.

In a complex machine like a jet engine there are many things that must be kept under control. The airflow can exhibit various modes of undesirable behaviour. In addition, components of the engine can start to vibrate and overheat and the burning of the fuel can become unstable.

Since the first jet engine was made, scientists have tried to improve the performance of the engine by increasing fuel efficiency, making lighter engines, increasing the thrust produced and improving the stability and safety.

A jet engine is composed of four main parts. First, there is a fan that sucks and accelerates the air into the front of the engine. In commercial jet engines the fan generates most of the thrust that the engine produces. Then, incoming air is compressed by the compressors. The third main part is the combustion chamber, where the air is mixed with fuel and then this compressed mixture is ignited. As a result, the pressure increases dramatically and the air rushes to the back of the engine after passing through the turbines. The turbines extract energy from the flow to drive the fan and compressors.

C.2. Compressor stability

Stability in a compressor is the ability of a compressor to recover from disturbances that alter the compressor operation about an operational equilibrium point. Disturbances may be considered as transient or deliberate changes to the operating points. In the case of transient disturbance, the system is stable if it returns to its original operating point. However, if the disturbances drive the compressor away from the original point such that it is unable to return, the system is unstable. When there are deliberate changes to the operating point, the performance is considered as stable if a new operating equilibrium point can be achieved, e.g. shifting the operating point by changing the compressor shaft speed. If steady state operation at a new operating point is not possible, the system will be unstable.

Axial and centrifugal compressors are two types of continuous flow compressors. For the axial compressors, flow leaves the compressor in the direction parallel to the rotational axis, while it is in the direction perpendicular to the rotational axis for centrifugal compressors. The stable range of operation for axial and centrifugal compressors is limited at both very high and very low mass flow rates. If the mass flow rate is too high, the flow through the compressor will be chocked meaning that the airflow has reached the local speed of sound. On the other hand, as the mass flow rate through the compressor decreases, flow instabilities will occur.

These instabilities include rotating stall and surge. If they are allowed to persist or grow, catastrophic damage to the compressor and the engine will occur. Surge, in particular, should be avoided at any cost. Rotating stall and surge particularly occur in axial compressors and limit their efficiency, effectiveness and usefulness. Therefore, preventing these instabilities from occurring would benefit the large community of users of turbomachines.

Traditionally, surge is avoided using passive surge avoidance schemes. In this method, a recirculation path fed from a recycle valve is usually constructed around the compressor and used to regulate the pressure gradient to keep the operating point of the compressor far enough from the surge line. This method works well, as has been proven by numerous installations. Typically, a surge avoidance line is drawn at a specified distance from the surge line to ensure that the operating point does not cross the surge line under any conditions. In other words, the surge avoidance line provides a safety margin for the compressor operation and prevents the compressor from operating in a region where stall or surge is more likely to occur. However, due to the increased surge margin, the method restricts the operating range of the machine and, therefore, achievable efficiency is limited. The closer the operating point is to the surge line, the greater the pressure rise achieved by the compressor, but the greater the risk of stall or surge. Examples of surge avoidance schemes may be found in Staroselsky and Ladin (1979), Nisenfeld (1982) and Botros and Henderson (1994).

The stability margin is usually considered very conservatively, as it may be reduced by many influences on the engine. The transient trajectory of the high pressure compressor working line during engine acceleration moves toward the surge line. Other significant factors in the reduction of the stability margin are inlet flow distortion, manufacturing tolerances, compressor deterioration and foreign object damage (FOD). Moreover, many jet engine variables cannot be measured when flying or can only be measured with complex and, hence, unreliable instrumentation systems. This includes

variables that are important for the safe operation of the engine such as the surge margin of the compressors or those related to the engine life, such as the temperature of the high pressure turbine blades. As a result, current control systems have to transform limits on these variables into limits on other variables that can be measured by the engine's sensors. This leads to increased safety margins and more conservatism. Furthermore, because of the engine build tolerances, the compressor working and surge line may be different from one engine to another. These lines may also be changed due to aging and engine deterioration. Finally, combinations of the above effects must also be handled. Therefore, during engine design a significant portion of the pressure rise capability of the compressor is dedicated to the 'surge margin', resulting in decreasing the engine efficiency.

Compromise between the performance and safety has been an important research topic over the past decade and many advanced control strategies have been employed to reduce the surge margin requirements in order to improve the performance and efficiency. Przybylko (1997) showed that for an aircraft engine, if one stage in the compressor would be eliminated due to margin-reduction technologies, 5% increase in thrust-to-weight ratio, 1.5% decrease in fuel consumption, 3.2% and 1% reduce in acquisition and operating cost would be achieved, respectively.

C.3. Fundamentals of rotating stall

During normal operation of a compressor, the airflow through the compressor is essentially steady and axisymmetric in a rotating coordinate system. Resulting from a change in a factor such as rotor speed, flow separation at the inlet or other type of flow distortion, flow instability is somehow introduced into the system. As a result, instabilities may develop and the compressor performance may deteriorate. The stability manifests itself as either a rotating stall or surge.

Rotating stall is inherently a steady local phenomenon in which the flow is no longer uniform. At rotating stall inception, the mean pressure rise of the compressor drops dramatically, after which it remains relatively fixed. This is sometimes termed "deep stall", because recovery from the rotating stall condition can be very difficult, sometimes requiring engine restart. It often takes only a few seconds for rotating stall to build up and the compressor can operate under rotating stall for several minutes before damage develops.

In manufacturing and assembly, blades may be produced with slightly different profiles or with higher stagger angles than specified. These imperfections would cause the inlet air to see these blades at slightly different angles of attack compared to the other blades. When one of the blades stalls, the angle of the flow relative to the shaft increases. This increase in flow angle in addition to blockage attributed to the stalled region cause part of the oncoming flow to be diverted towards the neighbouring blades, resulting in causing an increase in their angles of attack and leading them to the stall. As a result, a local region or local regions appear where the flow is stagnant. The region of the stalled flow is known as a stall cell and continues moving from blade to blade and propagates around the annulus in the same direction as the rotor motion. This region may also grow exponentially with time until a certain size is reached, depending on the slope of the pressure rise/mass flow characteristic for a constant speed in the compressor performance map, as shown in Figure C.1.

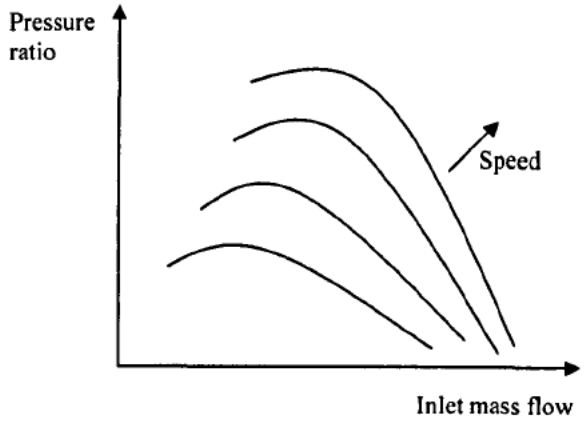

Fig. C.1. Compressor map with constant speed lines.

The rotational speed of rotating stall around the annulus of the compressor varies from 20% to 50% of the rotor speed. In addition, the incipient rotating stall cells move faster (Day, 1993). Typical frequencies for rotating stall are 10 to 50 times larger than those of the surge. The number of stall cells is usually between one and nine, depending on the compressor.

Two types of stall associated with the number of stalled cells are progressive and abrupt stall. In progressive stall, a phenomenon involving multiple stalled cells, the pressure rise after stall reduces gradually. Abrupt stall results in a sudden drop in the pressure rise and always appears to involve a single stalled cell.

There are several types of rotating stall (Day, 1993), as follows:

- **Part-span:** Only a restricted region of the blade passage, usually the tip, is stalled
- **Full-span:** The entire height of the annulus is stalled
- **Small/large scale:** In this case, a small/large part of annular flow path is blocked

Figure C.2 shows a typical rotating stall pattern. When rotating stall occurs at point A on the unstalled branch, the operating point proceeds to the so-called stalled characteristic at point B through a straight line AB. If point B is stable, the compressor will remain and operate there until measures are taken to bring it back to the unstalled branch.

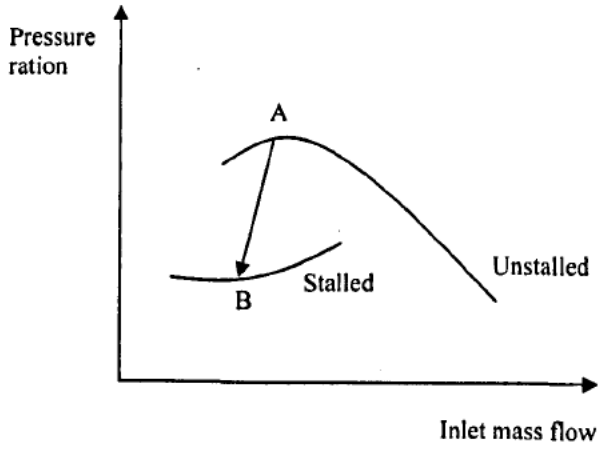

Fig. C.2. Compressor map with stalled flow characteristics.

C.4. Fundamentals of surge

Surge is a global self-excited instability that can affect the whole compression system. Surge is characterised by large amplitude limit cycle oscillations in mass flow rate and pressure rise. It starts to occur in a region of the compressor map where the pressure rise/mass flow characteristics for a constant speed have a positive slope that exceeds a certain value determined by characteristics of the compressor and the slope of the load line (Fink, Cumpsty and Greitzer, 1992). Essentially, the slope of the instantaneous pressure rise/mass flow characteristic plays the major role. As a consequence, the onset of surge not only depends on the compressor characteristics, but it also depends on the pressure rise/mass flow characteristic of the system that it discharges into. An answer for the question 'Why does the compressor map have a region with positively sloped speed lines' can be found in (Wo and Bons, 1994).

In centrifugal compressors, rotating stall often has little effect on pressure rise and, therefore, on surge. There is no consensus on whether rotating stall is important for centrifugal or single stage axial compressors, or surge is only important for these machines. At least for axial machines, each surge cycle begins with rotating stall, which causes the pressure rise through the machine to drop dramatically (Fink, Cumpsty and Greitzer, 1992). This catastrophic loss of pumping capability allows the flow through the machine to decelerate rapidly, sometimes reversing. In addition, flame-out is often another consequence of surge. For multistage axial compressors, it seems that rotating stall is more prevalent at low shaft speeds, while surge occurs more frequently at high speeds (Day, 1994; Gysling, Dugundji and Greitzer, 1991).

The essential difference between rotating stall and surge is that the average flow in pure rotating stall is steady in time, but the flow has a circumferentially non-uniform mass deficit, whereas in pure surge the flow is unsteady but circumferentially uniform. Because it is steady, rotating stall may be local to the compressor or to parts of the compressor. Due to its unsteadiness, surge involves the entire compression system. Rotating stall and surge phenomena are related as they are natural oscillatory modes of the compression system (Paduano, Epstein, Valavani, Longley, Greitzer and Guenette, 1993; Simon and Valavani, 1991). Rotating stall is often more difficult to recover from than surge (Copenhaver and Okiishi, 1993).

Many of the conditions that a compression system experiences during rotating stall are also present in surge. The rotor blades are stressed by the oscillating flow and the uneven distribution of shaft work. The compressor's noise characteristic changes and pressure rise fluctuations occur throughout the compressor. In high speed compressors, the flow reversal can be triggered by a shock wave. The high pressures behind the shock may deform the casing and inlet and the twist of the rotor/stator blades. In low speed compressors, the surge appears as a moderate pulsing of the flow.

Based on the flow and pressure rise fluctuations, at least four different categories of surge can be distinguished (Fink, Cumpsty and Greitzer, 1992; Kim and Fleeter, 1994; Day, 1994).

- **Mild surge:** No flow reversal; small periodic pressure rise fluctuations
- **Classic surge:** No flow reversal; larger oscillations at a lower frequency than mild surge

- **Modified surge:** Combination of classic surge and rotating stall; entire annulus flow fluctuations in axial direction, unsteady and non-axisymmetric flow
- **Deep surge**: Strong version of classic surge; possibility of flow reversal; unsteady but axisymmetric limit cycle flow

In both axial and centrifugal compressors a mild surge can occur when increasing the pressure at the compressor exit at a constant rotor speed. The mild surge may be followed by rotating stall or modified surge. A classic or a deep surge may then follow (Day, 1994). Figure C.3 gives an example of a deep surge cycle in the compressor map. The cycle starts at point A, where the flow becomes unstable. Then, it goes very rapidly to the negative flow characteristic at point B. Then it descends until the flow is approximately zero, point C. Finally, it proceeds very rapidly to the normal characteristic at point D, where it starts to climb to point A and repeat itself until measures are taken to avoid it.

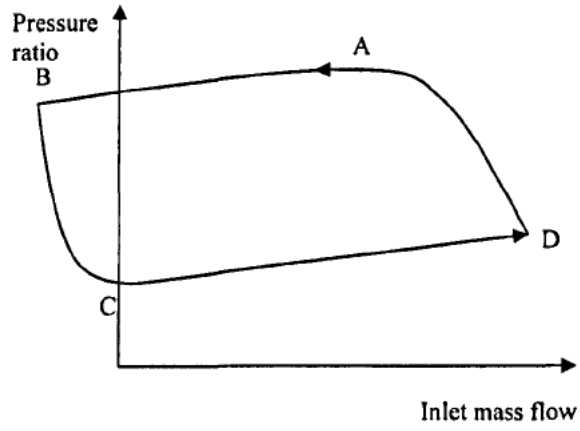

Fig. C.3. Compressor map with deep surge cycle.

Rotating stall can subsequently lead to surge if the system arrives at a new stable operating point on the stalled characteristic with severely reduced performance and efficiency, or the stalled area grows until it occupies the total annular circumference. The transfer of mild surge to other types of surge or rotating stall is characterised by increasing amplitudes of the pressure rise and flow fluctuations. Small fluctuations may be used to detect the onset of a rotating stall or surge phenomenon.

Rotating stall and surge phenomena may lead to rapid heating of the blades and an increase in the exit temperature of the compressor. Moreover, the unsteady fluid dynamic excitation results in additional periodic loads on the blades, causing blade vibrations and fatigue and may even cause severe damage to the machine due to unacceptable levels of system vibration (Kim and Fleeter, 1994; Pinsley, Guenette, Epstein and Greitzer, 1991). If rotating stall occurs in isolated parts of the machine, it may cause acoustic resonances (Cargill and Freeman, 1991).

C.5. Surge line

In order to determine the surge line, the barrier that separates the stable and unstable regions in the compressor map, at least three variables should be considered. They are compressor speed, mass flow and pressure rise that are connected according to relations expressed in the compressor map. Therefore, only two variables are really independent.

An example of a compressor map with the surge line is shown in Figure C.4. The operating point is uniquely determined by knowing pressure rise and mass flow, or mass flow and spool speed. Due to the non-linearity of the characteristics, the pair pressure rise and spool speed cannot necessarily determine the operating point uniquely.

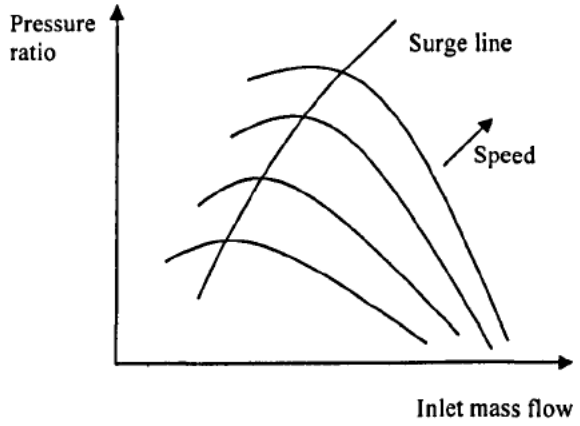

Fig. C.4. Compressor map with surge line.

C.6. Rotating stall/surge avoidance/control approaches

Rotating stall and surge may be avoided by operating away from the surge line. On the other hand, due to the high performance and efficiency obtained near the surge line, it is desirable to operate the compressor closer to the surge line. To overcome this dilemma, two different approaches exist, as follows:

- Surge/rotating stall avoidance
- Surge/rotating stall control

C.6.1. Surge/rotating stall avoidance

Surge/rotating stall avoidance methods are divided into two different categories. They are surge/rotating stall avoidance and surge/rotating stall detection and avoidance. Surge/rotating stall avoidance techniques are known and have been used for a long time in industrial and commercial systems. In this approach, the control systems do not allow the compressor to operate on the left side of the surge avoidance line. To locate the surge avoidance line on the compressor map, a safety margin should be specified. This safety margin may be defined based on pressure ratio, mass flow or a combination between them. A common safety margin, SM, is based on total pressure ratio and is defined as follows:

$$SM = \frac{(\frac{P_o}{P_i})_{Surge} - (\frac{P_o}{P_i})_{Surge\ avoidance}}{(\frac{P_o}{P_i})_{Surge\ avoidance}}, \qquad (C.1)$$

where P_o and P_i are total pressure at the compressor exit and inlet, respectively. In a multistage axial compressor of a turbojet it is typical to have a safety margin of as much as 25% (Ucer, Show and Hirsch, 1985), whereas for a centrifugal pipeline compressor the safety margin is 10% (Botros and Henderson, 1994). A surge/rotating stall avoidance technique can be regarded as an open-loop strategy.

There are many measures to avoid surge/rotating stall in turbomachinery (Botros and Henderson, 1994). Because the operating point is established by pressure rise, mass flow and spool speed, all measures aim to influence at least one of these variables. As these variables are connected according to relations shown in the compressor map, influencing one of them implicitly influences the others. Some measures aim to increase the flow rate by discharging into a bypass, by feeding back excess flow through a recirculation loop or by dumping the excess flow via a vent (bleeding). This may be done after the compressor or between compressor stages. Other measures aim to reduce or increase the spool speed by modifying the torque on the compressor through changing the fuel consumption of a driving turbine or through changing the voltage of a motor. The last possibility is to influence the pressure rise. This can be achieved by manipulating bleed valves in the flow.

The measures can also be divided into those changing the compressor characteristic and those changing the operating line (Pinsley, Guenette, Epstein and Greitzer, 1991). Both of them lead to operating points further away from the unstable region.

Characterising surge/rotating stall and detecting its onset is necessary for surge/rotating stall detection and avoidance methods. The most successful techniques to detect the onset of stall are based on monitoring the pressure and temperature variations or their time derivative and oscillation frequency at the compressor inlet or exit. These measurements are compared to the expected values at the surge condition, stored in the control computer. When surge or stall is detected, corrective measures (bleed) are applied.

In order to prevent the machine entering into the deep surge, a quick response is needed after detecting the onset of surge/rotating stall. Therefore, the sensors and actuators should have small time constants and delays. Also, the instrumentation should be as limited as possible to restrict investment and maintenance costs. As a result, the advantage of this technique is that it is not necessary to define a large safety margin and, therefore, the compressor can operate close to the surge line. The disadvantages of this method are the need for large control forces and very fast-acting control systems. A surge/rotating stall detection and avoidance method can be categorised as a closed-loop strategy.

The main difference between different surge/rotating stall detection and avoidance methods arise in the area of detection of the flow condition, pressure rise and flow rate, and in the instrumentation used to do that. In 1993, Dadd and Porter showed that for a jet engine, measuring the Mach number at

the exit of the turbomachine could be a reliable way of detecting surge/rotating stall. It is not known whether or not this measure is also suitable for other types of turbomachines. A fault detection approach to identify rotating stall and surge was used by Vachtsevanos, Kang, Cheng and Kim (1992).

A compressor map with its surge and surge avoidance lines is shown in Figure C.5. As discussed in section C.2, a specific gap between these lines is needed. In addition, due to uncertainties in detection of flow conditions or surge/rotating stall, the time constant of sensors and actuators and the delay in reacting to the onset of surge/rotating stall, a larger safety margin is needed (Botros and Henderson, 1994). The aim of the margin is to ensure that despite all uncertainties and under the worst conditions, the machine does not go into surge. On the other hand, this restriction of the feasible operating region unduly restricts the capabilities of the machine.

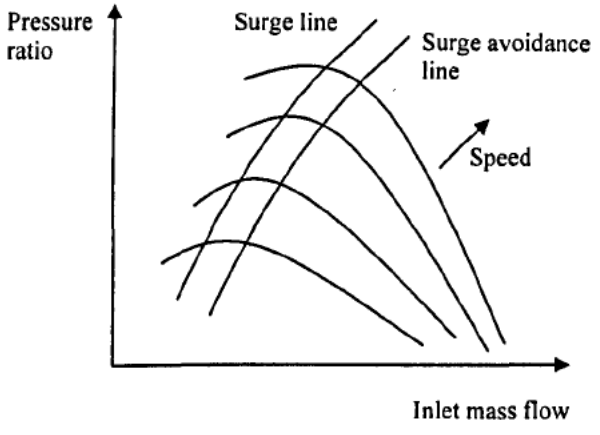

Fig. C.5. Compressor map with surge avoidance line.

Surge/rotating stall avoidance methods have many important limitations (Kim and Fleeter, 1994). Surge/rotating stall avoidance measures such as recycle and bleed have significant negative effects on energy consumption and should preferably be avoided. Also, the point of peak pressure rise for constant speed that represents the peak compressor performance is often near the surge line and cannot be reached if a safety margin is introduced, see Figure C.5. This limits the effectiveness of the compression system.

Figure C.6 shows that the region of lowest specific power consumption or highest efficiency is close to the surge line. This region may even encompass the surge line. Therefore, introducing a safety margin moves the feasible operating region of the machine away from the region of lowest specific power consumption, resulting in decreasing efficiency and increasing the operational costs.

During acceleration, the operating point of the high pressure compressor moves closer to the surge line. When the machine crosses the surge avoidance line and enters the safety region, the acceleration is limited by surge avoidance measures. Therefore, a safety margin effectively limits the achievable transient performance of the machine, see Figure C.7.

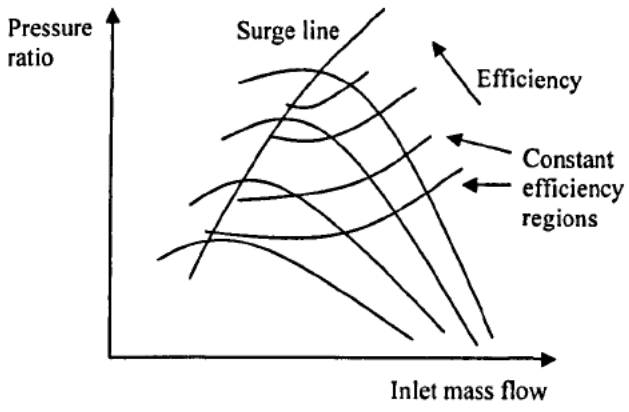

Fig. C.6. Compressor map with efficiency contours.

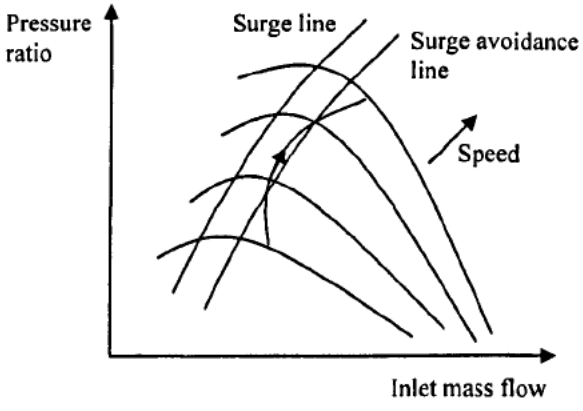

Fig. C.7. Transient trajectory in high pressure compressors while accelerating.

In order to overcome the limitations of the surge/rotating stall avoidance methods, enlarging the region of feasible operating points can be considered. It means that the machine may operate closer to the region of high pressure rise or low specific power consumption, resulting in increasing efficiency and reducing costs. In addition, larger transients are possible. As a result, the machine may react quicker to changing operating condition requirements, leading to increasing effectiveness.

There are several ways to enlarge the region of feasible operating points by preventing or suppressing rotating stall/surge as follows.

- Better matching of compressor and discharge system specifications, resulting in moving closer to the area of peak performance
- Reducing the safety margin, so shifting the surge avoidance line towards the surge line. This is possible by improving flow condition or surge detection, by reducing uncertainty in the location of the surge line in the compressor map, by reducing disturbances in the inlet/outlet flow and pressure fields and by increasing the bandwidth of the surge avoidance system (Harris and Spang III, 1991)
- Shifting the instability region (surge line). This can be done with changes in the compressor design and construction such as the inlet guide vanes (Rodgers, 1991), the vane tip clearance

(Day, 1993), the casing geometry (Botros and Henderson, 1994) or with changes in the equipment into which the compressor discharges

- Active control of rotating stall and surge by modulating the characteristics of the compression system or by modifying the inlet/outlet flow fields of the compressor to suppress instabilities. A compressor with active control has a shifted surge line

Although all the above solutions are appropriate, the last solution seems more promising (Botros and Henderson, 1994) because

1. Surge avoidance techniques are almost a completed field, where only incremental improvements are possible.
2. Surge detection and avoidance methods are limited by the necessary speed of sensors and actuators, where a very large potential of improvements is not expected.
3. Active surge control is a new and active area of research and promises to cause a substantial improvement in both efficiency and effectiveness of the turbomachines.

C.6.2. Surge/rotating stall control

The surge/rotating stall control methodology may be divided into two different classes, passive surge/rotating stall and active surge/rotating stall control. In both active and passive surge/rotating stall control techniques, the characteristic performance map of the compressor is modified and the surge line is shifted to a lower mass flow. By shifting the surge line, the surge avoidance line is also shifted. In other words, some parts of the unstable area in the performance map is being stabilised by this approach. An advantage of this methodology is that the compressor now can operate near peak efficiency and high pressure ratios at lower mass flow rates, without any risk of surge/rotating stall.

In passive surge/rotating stall control, the geometry of the compressor is altered to modify the stall margin. Casing treatments (Bailey and Voit, 1970; Holman and Kidwell, 1975; Lee and Greitzer, 1990; Khalid, 1997) and variable guide vanes (Whitfield, Wallace and Atkey, 1976; Jones, 1970; Pampreen, 1976; Sheridan, 1974) are some different ways of achieving passive surge/rotating stall control. In casing treatments, which have been investigated more in axial compressors, the rotor casing is designed so that the amount of blockage in a flow passage is decreased, leading to suppressing rotating stall.

The use of variable guide vanes is another way of increasing the stall margin and has been used in both axial and centrifugal compressors. In this technique, the incident angle in compressors at lower mass flow rates is reduced and the leading edge separation is prevented. With inlet guide vanes, the direction of the flow at the leading edge is turned so that the angle of attack decreases. Variable inlet guide vanes are also commonly used when starting and accelerating engines to avoid crossing the surge line.

In active rotating stall/surge control, the compressor is equipped with devices such as a bleed valve that can be switched on or off. Generally, this method may be divided into two classes, open-loop and closed-loop. In closed-loop control a feedback law is used to activate the controller, whereas in open-loop control no feedback signal is used. Air injection (Yeung and Murray, 1997), bleeding

(Yeung and Murray, 1997; Fisher, 1988; Pinsley, Guenette, Epstein and Greitzer, 1991), recirculation and a combination of injection and bleeding are examples of active rotating stall/surge control.

Air injection is another way of increasing the stall margin and has been used in both axial and centrifugal compressors. In this method, a small amount of high pressure and high velocity air is injected into the compressor. As a result, the flow is energised and the axial velocity component is increased. This reduces the total angles of attack and thus the leading edge separation is prevented.

One of the oldest and the most investigated approach for increasing the stall/surge margin in both axial and centrifugal compressors is bleeding. Since the early days of building jet engines, bleeding has been the most common approach for avoiding stall/surge during engine acceleration and start-up. Besides the start-up applications, bleeding has also been used to achieve a wide range of operating conditions.

Closed-loop active control was first reported by Epstein, Efowcs and Greitzer (1989). The literature on this approach has become extensive over the last decade. This method promises to be an integral part of the future engines, the so-called smart or intelligent engines. The closed-loop control devices use a sensor for detecting the growth of instabilities when the compressor experiences stall conditions. The stall detection devices are usually located on the circumference of the compressor casing. A feedback law that connects the sensed fluctuations to the rate of bleed is used to stabilise the compressor. The control unit activates a set of actuator devices. Several types of actuators are used for stabilising the compressor system. Bleed valves have been the most commonly used actuators. Other types of actuators include variable inlet guide vanes, recirculation, movable walls and air injections.

C.7. Summary

For many aircraft compromise between performance and safety in turbomachines is the central issue in propulsion. Study of compressor instabilities such as surge and rotating stall has received much attention in recent years. The reason for this interest is that these instabilities limit the performance and effectiveness of jet engines and more importantly, catastrophic damage to the compressor and other components may occur if they are allowed to persist or escalate. In order to improve engine performance and efficiency and to extend the stable operating range of the compressor system, many advanced control strategies have been employed to suppress rotating stall and surge and, therefore, to reduce the surge margin requirements.

This appendix surveys the research literature in this active field to offer an overview of the fundamentals of surge and rotating stall and to summarise the major developments.

Appendix D

Control of the ALSTOM Gasifier

D.1. Introduction

Low emission power generation techniques are being developed around the world to provide environmentally clean and efficient power. To this end, ALSTOM has carried out research on the combustion of pulverised coal using an Integrated Gasification Combined Cycle (IGCC) power plant. The operation of this Pilot Integrated plant (PIP) is based upon the Air Blown Gasification Cycle (ABGC). First, limestone is added to the pulverised coal to minimise sulphur originating from the coal. Then, the mixture is fluidised in a stream of air and steam and conveyed into the gasifier. As a result, a low calorific value fuel gas is produced by the reaction between the air and steam and the carbon and volatiles from the coal. The limestone, ash and unreacted carbon are removed as bed material from the base of the gasifier or elutriated to avoid carrying it out of the top of the gasifier as fines with the product gas.

In order to design a controller for the gasifier, a Benchmark Challenge was issued by ALSTOM to UK Universities (Dixon, Pike and Donne, 1998). In response to this Challenge, nine papers were presented at the ASTOM seminar, but none of the proposed controllers managed to meet all the performance criteria while satisfying the specified constraints.

The best paper in terms of meeting the specified constraints and performance criteria was cited in Dixon (1999) as being a discrete time non-minimal state-space approach, using Proportional-Integral-Plus (PIP) control by Taylor, McCabe, Young and Chotai (1998). Interestingly for this application, none of the so-called robust control design techniques results in a design that is more robust to the changes in the plant than the classical approaches (Dixon, 1999). Further work by Griffin, Schroder, Chipperfield and Fleming (2000) has resulted in improved performance through refinement of the optimisation approach without fully complying with the Challenge specifications.

D.2. System description

The gasifier is a non-linear, multivariable system with six inputs and four outputs as shown in Table D.1. The value of *WLS* must be set to a fixed ratio of *WCOL* of 1:10 and the 6th input is related to the disturbance, therefore, only four inputs are available for the control procedure. The disturbance input represents the pressure upstream of the gas turbine that changes according to the position of the gas turbine fuel value.

Table D.1 Gasifier inputs and outputs

Inputs	Outputs
WCHR-Char extraction flow (kg/s)	*CVGAS*-Calorific value of fuel gas (J/kg)
WAIR-Air mass flow (kg/s)	*MASS*-Bed mass (kg)
WCOL-Coal flow (kg/s)	*PGAS*-Pressure of fuel gas (N/m^2)
WSTM-Steam mass flow (kg/s)	*TGAS*-Temperature of fuel gas (°K)
WLS-Limestone mass flow (kg/s)	
PSINK-Sink pressure (N/m^2)	

Three stable state-space models of 25th order have been derived from the non-linear model of the gasifier by linearization at three important load operating points, namely 100%, 50% and 0% load. It should be noted that the gasifier is usually run at 100% load.

The control aim is to design a controller based on the linear model of the gasifier at 100% to regulate outputs in the event of a disturbance. The test cases used to represent the disturbances are a step of –20000 (N/m^2) applied at t=30s and a sine wave of amplitude 20000 (N/m^2) and of frequency 0.04 Hz applied continuously. Simulation cases are run for 300s. In addition, the system is required to maintain the inputs, outputs and input rates of change within certain bounds in order to represent actuator constraints. Moreover, the controller should also meet the design requirements when applied to the 50% and 0% load operating points.

D.3. Model conditioning

D.3.1. Order reduction

The gasifier is a highly cross-coupled and numerically ill-conditioned system described by:

$$\dot{x}(t) = Ax(t) + Bu(t), \tag{D.1}$$

$$y(t) = Cx(t) + Du(t), \tag{D.2}$$

where

$$x(t) \in R^{25x1},$$
$$u(t) \in R^{6x1},$$
$$y(t) \in R^{4x1}.$$

In order to improve the numerical conditioning, the minimal realizations of the three state-space models are produced. As a result, 8 states that pertain to the uncontrollable and/or unobservable modes are removed. In addition, another mode of the minimal plant was removed using the Hankel norm minimisation approach. The resulting reduced model of 16th order is described by:

$$\dot{x}_r(t) = A_r x_r(t) + B_r u_r(t), \tag{D.3}$$

$$y_r(t) = C_r x_r(t) + D_r u_r(t). \tag{D.4}$$

Table D.2 shows the improvement in numerical conditioning of the original and the reduced systems.

Table D.2 Condition numbers of the state-space model matrices

	Operating points		
	100%	50%	0%
A	5.24e+19	8.4e+19	3.32e+20
A_r	1.76e+5	4.05e+5	1.76e+6
B	1.72e+10	3.28e+9	1.9e+10
B_r	5.34e+4	7.66e+4	4.53e+4
C	6.98e+6	8.68e+6	1.13e+7
C_r	4.71e+3	4.38e+3	4e+3

D.3.2. Scaling

Scaling is a very important step in a number of multivariable control design techniques, as it makes model analysis and controller synthesis much simpler (Skogestad and Postlethwaite, 2001). In general, any matrix $G(s)$, can be scaled by dividing each input and output by its largest expected or desired value. This results in normalised values into [–1, 1] for symmetrical bounds.

The input, output and input rate of change limitations for the main operating point, namely 100% load, are shown in Table D.3.

Table D.3. Input, output and input rate of change bounds for the 100% load operating point

Variable	Min	Max	Peak rate
WCHR (kg/s)	-0.9	2.6	0.2
WAIR (kg/s)	-17.42	2.58	1
WCOL (kg/s)	-8.55	1.45	0.2
WSTM (kg/s)	-2.7	3.3	1
CVGAS (J/kg)	-10000	10000	-
MASS (kg)	-500	500	-
PGAS (N/m^2)	-10000	10000	-
TGAS (°K)	-1	1	-

Considering the given values in Table 5.3, scaling matrices are determined as follows:

$$D_1 = \text{Diag}(0.9, 2.58, 1.45, 2.7),$$
$$D_2 = \text{Diag}(10000, 500, 10000, 1).$$

The condition number of $G(s)$ depends strongly on the scaling of the inputs and outputs. If the condition number is small, then the multivariable effects of uncertainty are not likely to be serious (Skogestad and Postlethwaite, 2001). Hence, minimising the condition number over all possible scaling matrices has been proposed for this uncertain plant. The cost function for optimising the condition number is:

$$\gamma = \min_{D_1, D_2} [cond(D_2 G(s) D_1)], \tag{D.5}$$

and it should be calculated over a specified range of frequencies.

D.4. Design procedure

D.4.1. Control design procedure

The closed-loop control system is shown in Figure D.1, where r, u, d and y refer to the input reference, control signal, disturbance input and output signal, respectively.

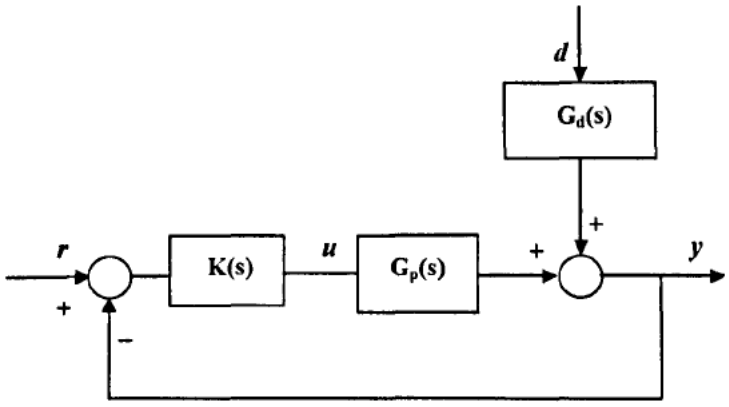

Fig. D.1. Closed-loop control system.

In order to design a controller for the 100% load operating point, a multivariable 4x4 controller, $K(s)$, is used, where the ij^{th} element of $K(s)$ is described by:

$$k_{ij}(s)=a_{ij}\frac{z_{ij}s+1}{p_{ij}s+1}. \tag{D.6}$$

The aim of control is to minimise IAE criterion for all four outputs over the 300s simulation time, whilst retaining the input, output and input rate of change values within the specified bounds. The objective function is given by:

$$f=\sum_{k=1}^{4}\int_{0}^{300}\{|y_{sk}(t)|+|y_{ik}(t)|\}dt, \tag{D.7}$$

where $y_s(t)$ and $y_i(t)$ are output vectors in response to step and sine wave disturbances, respectively. Scaled outputs are used during the design procedure to ensure a similar level of disturbance attention at all outputs.

In order to confine the control signals within their bounds, a saturation function is used. In addition, a rate limiter function is utilised to keep the control signal rates of change within the specified values. Moreover, some appropriate constraints are applied to restrict all closed-loop system poles to lie in the left half s-plane so that their real parts to be far enough from the imaginary axis.

In order to ensure that the resulting controller exhibits robust performance when applied to the other operating points, each candidate solution is also evaluated at the 50% and 0% operating points. Furthermore, the bounds on input and output signals are enforced during these evaluations in an effort to derive control laws that are both robust and realistic over these operating points.

D.4.2. Simulation Results

A 4x4 multivariable controller was designed for the 100% load operating point using a GA to optimise the controller parameters a, z and p as shown in Equation (D.6). Each element of the multivariable controller is a SISO lead/lag controller. In addition, in order to produce better performance, the scaling matrix elements given in Section D.3.2, are also considered as the decision variables. Therefore, the GA is required to optimise 48 parameters related to the controller and 8 parameters of the scaling matrices.

Considering a 4x4 multivariable controller whose elements are lead/lag controllers, the authors' experience shows that only a second order SISO controller along with 3 lead, 2 lag and 10 proportional SISO controllers are sufficient to control the plant appropriately. In light of this configuration, the number of decision variables being reduced from 56 to 36 and the controller being of 7^{th} order. This controller has the lowest order in comparison to the controllers that have been previously designed for the gasifier (Griffin, Schroder, Chipperfield and Fleming, 1998; Griffin, Schroder, Chipperfield and Fleming, 2000; Prempain, Sun and Postlethwaite, 1998; Taylor, McCabe, Young and Chotai, 1998).

The input limitations for the 50% and 0% operating points are shown in Table D.4. The output and input rate of change constraints are the same for all three operating points.

Table D.4. Input limitations for the 50% and 0% load operating points

	Min		Max	
	50%	0%	50%	0%
WCHR	-0.89	-0.5	2.61	3
WAIR	-10.89	-4.34	9.11	15.66
WCOL	-5.34	-2.136	4.66	7.864
WSTM	-1.69	-0.676	4.31	5.324

The dynamic responses to the step and sine wave disturbances for the 100% and 0% load operating points are shown in Figures D.2-D.17.

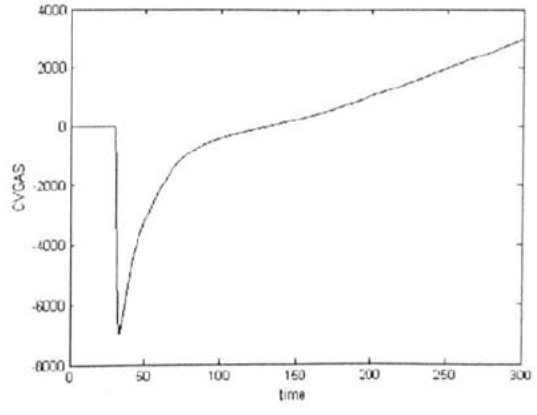

Fig. D.2. CVGAS for step disturbance at 100% load.

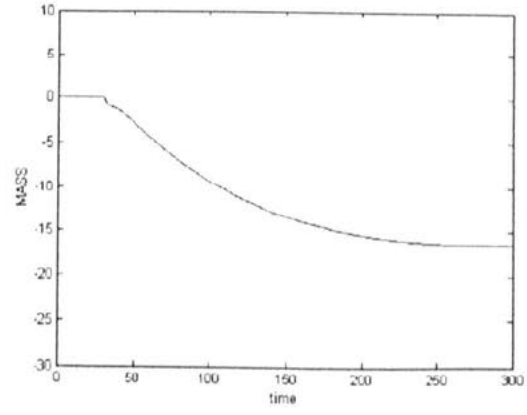

Fig. D.3. MASS for step disturbance at 100% load.

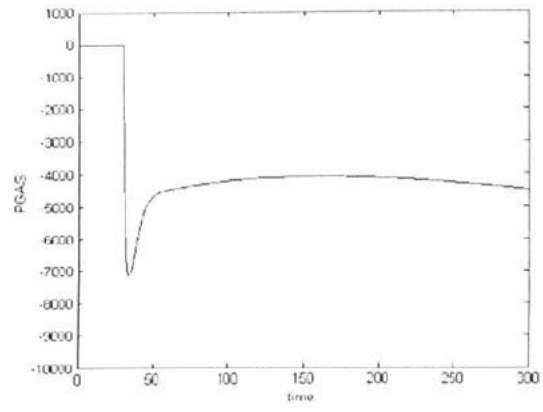

Fig. D.4. PGAS for step disturbance at 100% load.

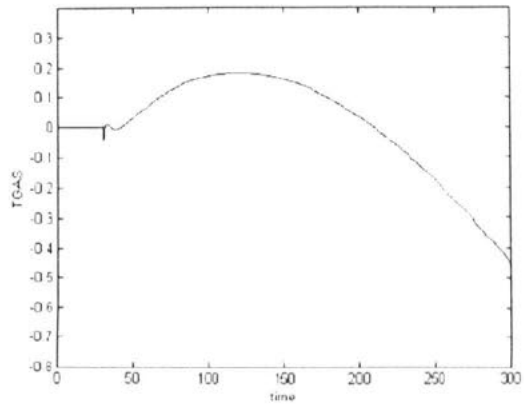

Fig. D.5. TGAS for step disturbance at 100% load.

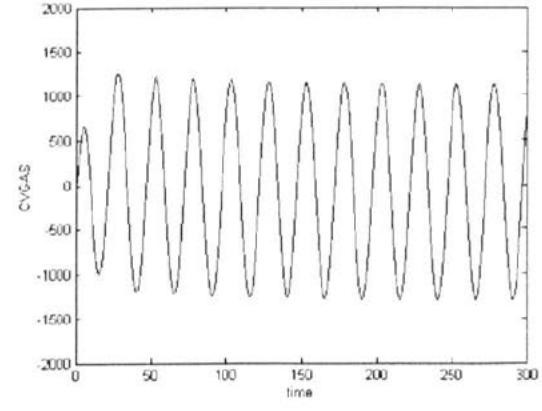

Fig. D.6. CVGASS for sin disturbance at 100% load.

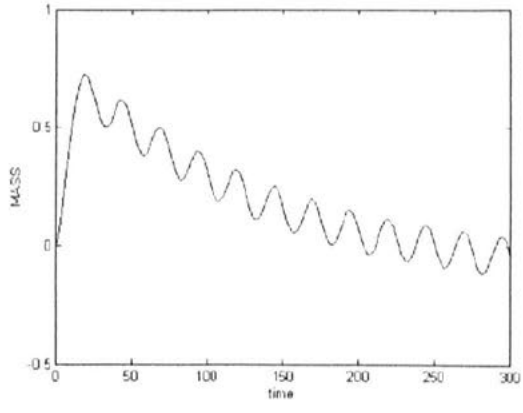

Fig. D.7. MASS for sin disturbance at 100% load.

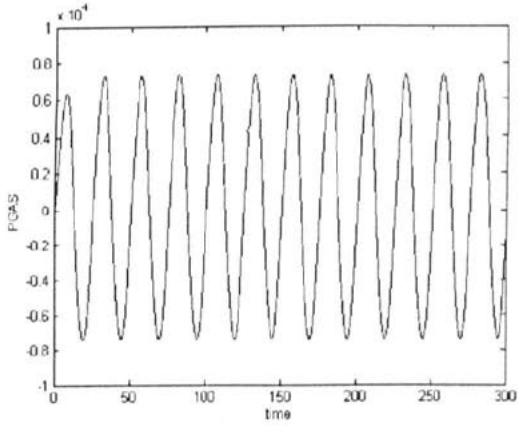

Fig. D.8. PGAS for sin disturbance at 100% load.

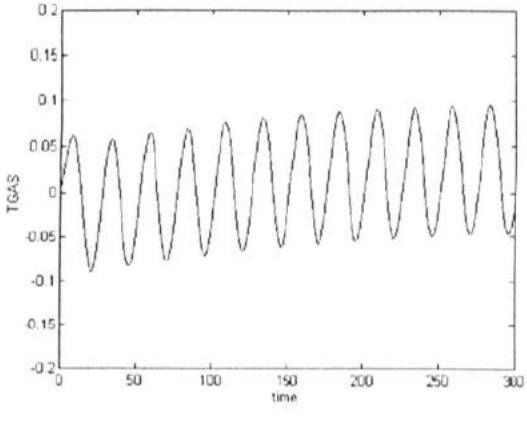

Fig. D.9. TGAS for sin disturbance at 100% load.

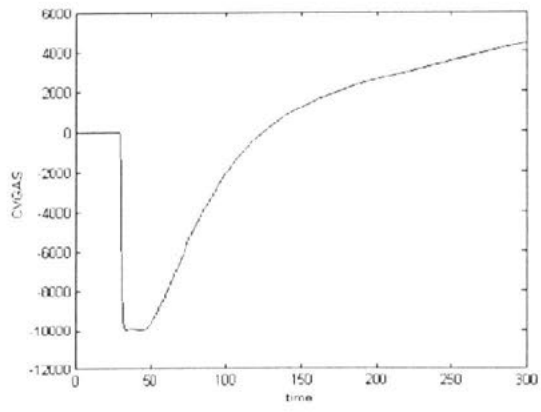

Fig. D.10. CVGAS for step disturbance at 0% load.

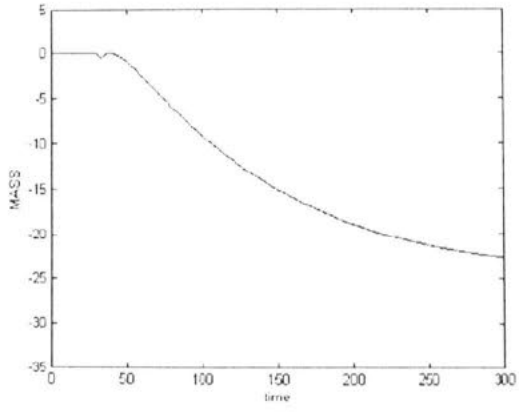

Fig. D.11. MASS for step disturbance at 0% load.

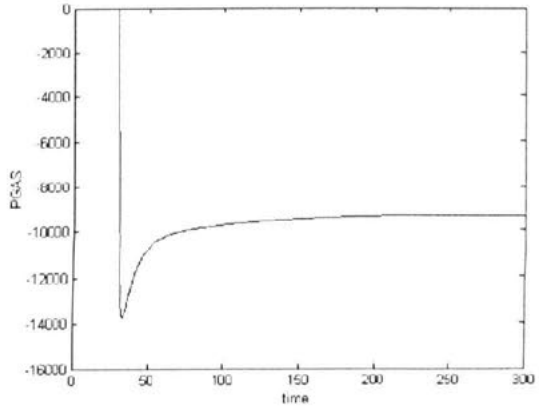

Fig. D.12. PGAS for step disturbance at 0% load.

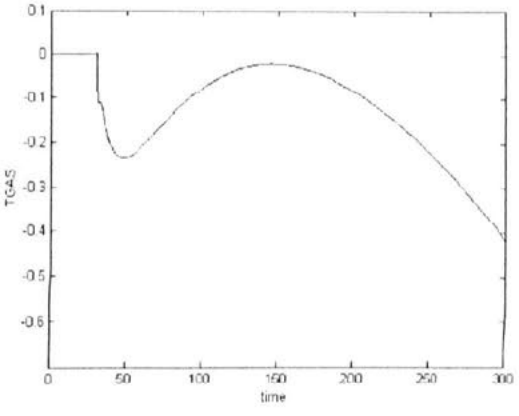

Fig. D.13. TGAS for step disturbance at 0% load.

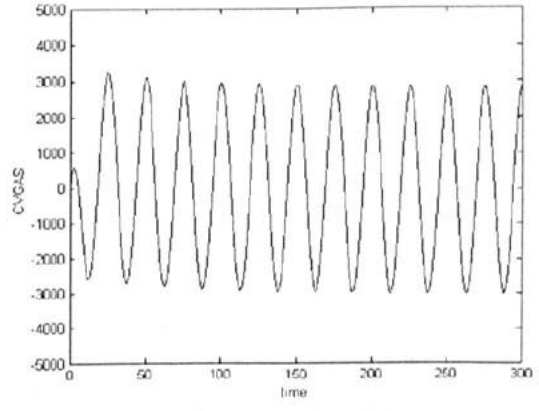

Fig. D.14. CVGAS for sin disturbance at 0% load.

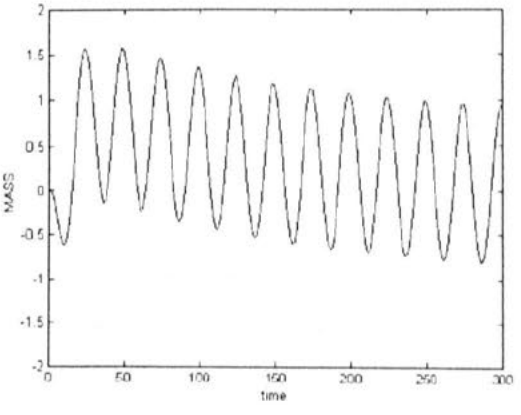

Fig. D.15. MASS for sin disturbance at 0% load.

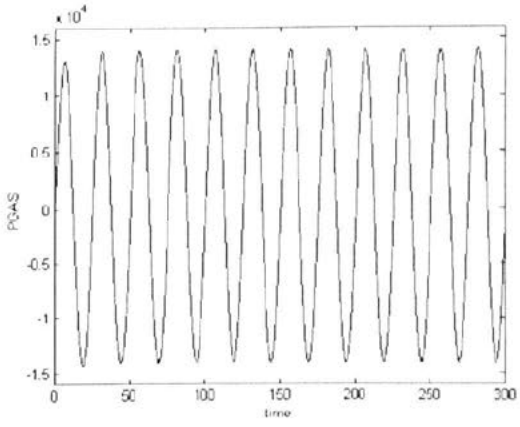

Fig. D.16. PGAS for sin disturbance at 0% load.

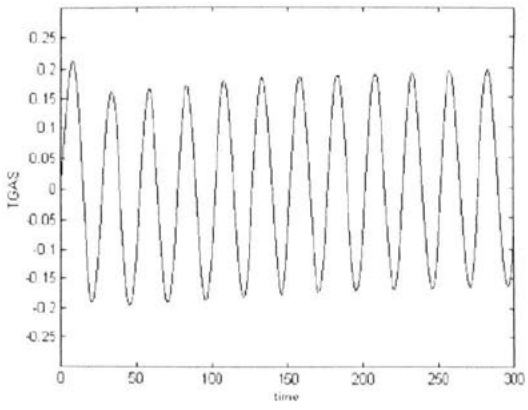

Fig. D.17. TGAS for sin disturbance at 0% load.

The simulation results when using this controller at the three operating points are summarised in Table D.5. It can be seen from Tables D.3-D.5 that all inputs and their rates of change have met the requirements.

D.4.3. Discussion and Comparison

Table D.5 shows that all the design requirements have been successfully satisfied for the both 100% and 50% load operating points. As expected, the performance of the closed-loop system at the main operating point is the best, whilst the poorest responses occurred at the 0% load operating point. For the most difficult case, 0% load, Table D.5 shows that all constraints are satisfied except those relating to *PGAS*, in response to both step and sine wave disturbances.

However, Figures D.12 and D.16 show that, in the worst case, *PGAS* exceeds its specified maximum level by less than 45%, whilst the reported results by Taylor, McCabe, Young and Chotai (1998), selected as the best paper by the ALSTOM review (Dixon, 1999), exhibited a breach of more than 100% for *PGAS* at 0% load operating point.

D.5. Summary

The condition number, which depends strongly on the scaling of the inputs and outputs, has been used as an input-output controllability measure. In particular, it has been postulated that a large condition number indicates sensitivity to uncertainty. This is not true in general, but the reverse holds. In other words, if the condition number is small, the multivariable effects of uncertainty are not likely to be serious.

In this chapter, a condition number minimisation approach is proposed to tackle the ALSTOM gasifier benchmark problem. The resulting 4x4 multivariable controller of 7^{th} order satisfies all of the design requirements at the 100% load operating point. In addition, when applying this controller to the 50% and 0% load models, almost all of the constraints are satisfied. The only deficiency of the resulting controller is that *PGAS* bounds are violated for the most difficult case, 0% load model.

Table D.5. Input, output and input rate of change simulation results for 100%, 50% and 0% load operating points

	Min and max of relative values				Peak rate		IAE	
	Step		Sine		Step	Sine	Step	Sine
	Min	Max	Min	Max				
WCHR 100%	-0.001	0.002	-0.002	0.002	0.002	4.15e-4	-	-
WCHR 50%	-0.001	0.001	-0.002	0.002	0.002	5.37e-4	-	-
WCHR 0%	-0.002	0.002	-0.003	0.003	0.004	7.74e-4	-	-
WAIR 100%	0	0.881	-0.504	0.431	0.465	0.111	-	-
WAIR 50%	0	0.943	-0.513	0.441	0.302	0.114	-	-
WAIR 0%	-0.134	1.416	-0.719	0.589	0.279	0.154	-	-
WCOL 100%	0	0.71	-0.637	0.629	0.2	0.177	-	-
WCOL 50%	0	0.631	-0.573	0.57	0.2	0.175	-	-
WCOL 0%	0	0.692	-0.565	0.559	0.2	0.2	-	-
WSTM 100%	0	0.334	-0.356	0.358	1	0.089	-	-
WSTM 50%	0	0.441	-.475	0.48	1	0.12	-	-
WSTM 0%	0	0.749	-0.677	0.688	1	0.186	-	-
CVGAS 100%	-6965	2983	-1297	1259	3889	306.8	3.95e+5	2.26e+5
CVGAS 50%	-7476	3653	-1907	1906	5268	463.8	5.59e+5	3.41e+5
CVGAS 0%	-9988	4410	-3002	3252	8003	742	9.59e+5	5.47e+5
MASS 100%	-16.4	0	-0.119	0.723	0.347	0.059	-	-
MASS 50%	-14.8	0	-0.404	0.937	0.273	0.106	-	-
MASS 0%	-22.59	0.019	-0.792	1.567	0.236	0.247	-	-
PGAS 100%	-7135	0	-7454	7384	9384	1853	1.17e+6	1.4e+6
PGAS 50%	-9443	0	-9996	9870	11572	2483	1.71e+6	1.87e+6
PGAS 0%	-13718	-0.029	-14327	14072	20540	3548	2.62e+6	2.68e+6
TGAS 100%	-0.446	0.185	-0.09	0.096	1.14	0.018	-	-
TGAS 50%	-0.778	0.001	-0.127	0.143	1.71	0.031	-	-
TGAS 0%	-0.415	0.002	-0.196	0.212	3.78	0.048	-	-

Bibliography

Astrom, K. J., & Hagglund, T. (1984). Automatic tuning of simple regulators with specifications on phase and amplitude margins. *Automatica* **20**, 645-651.

Astrom, K. J., & Hagglund, T. (1995). *PID controllers: theory, design and tuning*. Instrument Society of America. USA.

Astrom, K. J., Panagopoulos, H., & Hagglund, T. (1998). Design of PI controllers based on non-convex optimisation. *Automatica* **34** (5), 585-601.

Astrom, K. J., Albertos, P., & Quevedo, J. (2001). PID control. *Control Engineering Practice* **9**, 1159-1161.

Astrom, K. J., & Hagglund, T. (2001). The future of PID control. *Control Engineering Practice* **9**, 1163-1175.

Astrom, K. J., Johansson, K. H., & Wang, Q. G. (2001). Design of decoupled PID controllers for MIMO systems. *Proc. of the American Control Conference* (pp. 2015-2020).

Athans, M., Kapasouris, P., Kappos, E., & Spang III, H. A. (1986). Linear-quadratic gaussian with loop-transfer recovery methodology for the F100 engine. *Journal of Guidance and Control* **9**.

Atherton, D. P. (1999). PID controller tuning. *Computing & Control Engineering Journal*, 44-50.

Bailey, E. E., & Voit, C. H. (1970). Some observations of effects of porous casing on operating range of a single axial-flow compressor rotor. *NASA TM X 2120*.

Bates, D. G., Gatley, S., Postlethwaite, I., & Berry, A. J. (1999). Integrated flight and propulsion control system design using H_∞ loop shaping technique. *Proc. of the IEEE Conference on Decision and Control* (pp. 1523-1528).

Bennett, S. (1979). *A history of control engineering 1800-1930*. Peter Peregrinus. London, UK.

Bennett, S. (1993). *A history of control engineering 1930-1955*. Peter Peregrinus. London, UK.

Bennett, S. (2000). The past of PID controllers. *Proc. of the IFAC Workshop on Digital Control: past, present and future of PID control* (pp. 1–11).

Bialkowski, W. L. (1993). Dreams versus reality: A view from both sides of the. *Pulp and Paper Canada* **94** (11), 19-27.

Cargill, A. M., & Freeman, C. (1991). High-speed compressor surge with application to active control. *Journal of Turbomachinary* **113**, 303-311.

Chien, I. L., & Fruehauf, P. S. (1990). Consider IMC tuning to improve controller performance. *Chemical Engineering Progress* **86** (10), 33-41.

Cohen, G. H., & Coon, G. A. (1953). Theoretical consideration of related control. *Trans. ASME* **75**, 827-834.

Cominos, P., & Munro, N. (2002). PID controllers: recent tuning methods and design to specification. *IEE Proceedings-Control Theory and applications* **149** (1), 46-53.

Copenhaver, W. W., & Okiishi, T. H. (1993). Rotating stall performance and recoverability of high-speed 10-stage axial flow compressor. *Journal of Propulsion and Power* **9**, 281-292.

Corripio, A. B. (1990). *Tuning of industrial control systems*. Instrument Society of America. USA.

Dadd, G. J., Sutton, A. E., & Greig, A. W. M. (1995). Multivariable control of military engines. *Proc. of AGARD Conference on Advanced Aero-Engine Concepts and Controls* **572** (pp. 1-12).

Day, I. J. (1993). Stall inception in axial flow compressors. *Journal of Turbomachinary* **115**, 1-9.

Day, I. J. (1994). Axial compressor performance during surge. *Journal of Propulsion and Power* **10**, 329-336.

Deb, K. (2001). *Multi-objective optimisation using evolutionary algorithms*. John Wiley & Sons, UK.

DeHoff, R. J., Hall, W. E., Adams, R. J., & Gupta N. K. (1977). F100 multivariable control synthesis program. *AFAPL-TR-77-85* **1-2**.

Desborough, L., & Miller, R. (2001). Increasing customer value of industrial control performance monitoring-Honeywell's experience. *Proc. of 6th International Conference on Chemical Process Control* (pp. 172-192).

Deshpande, P. B. (1989). *Multivariable process control*. ISA, RTP. North Carolina, USA.

Dixon, R., Pike, A. W., & Donne, M. S. (1998). Overview: the MEC benchmark challenge on gasifier control. *Proc. of MEC benchmark challenge on gasifier control*, Control Theory and Applications Centre, Coventry, UK.

Dixon, R. (1999). Advanced gasifier control. *Computing & Control Engineering Journal* **10**, 93-96.

Dodd, N., & Martin, J. (1997). Using neural networks to optimise gas turbine aero engines. *Computing & Control Engineering Journal* **8** (3), 129-135.

Dougherty, D., & Cooper, D. (2003). A practical multiple model adaptive strategy for single-loop MPC. *Control Engineering Practice* **11**, 141-159.

Edmunds, J. M. (1979). Control system design and analysis using closed-loop Nyquist and Bode arrays. *International Journal of Control* **30**.

Epstein, A.H., Efowcs Williams, J. E., & Greitzer, E. M. (1989). Active suppression of aerodynamic instabilities in turbomachines. *Journal of Propulsion* **5**, 204-211.

Fink, D. A., Cumpsty, N. A., & Greitzer, E. M. (1992). Surge dynamics in a free-spool centrifugal compressor system. *Journal of Turbomachinery* **114**, 321-332.

Fisher, F. B. (1988). Application of map width enhancement devices to turbocharger compressor stages. *SAE paper 880794.*

Fleming, P. J., & Purshouse, R. C. (2002). Evolutionary algorithms in control systems engineering: a survey. *Control Engineering Practice* **10**, 1223-1241.

Fonseca, C. M. M. (1995). *Multiobjective genetic algorithms with application to control engineering problem.* PhD Thesis. University of Sheffield, UK.

Frederic, D., Garg, S., & Adibhatla, S. (1996). Turbofan engine control design using robust multivariable control technologies. *Proc. of Joint Propulsion Conference.*

Frederic, D., Garg, S., & Adibhatla, S. (2000). Turbofan engine control design using robust multivariable control technologies. *IEEE Transactions on Control Systems Technology* **11**, 961-970.

Friedland, B. (1996). *Advanced control system design.* Prentice Hall.

Garg, S. (1989). Turbofan engine control system design using the LQG/LTR methodology. *Proc. of the American Control Conference.*

Garg, S. (1993). Robust integrated flight/propulsion control design for a STOVL aircraft using H_∞ control design techniques. *Automatica* **29**, 129-145.

Gawthrop, P. J. (1987). *Continuous-time self-tuning control. 1, design.* Research Studies Press. UK.

Gilbert, A. F., Yousef, A., Natarajan, K., & Deighton, S. (2002). Tuning of PI controllers with one-way decoupling in 2x2 MIMO systems based on finite frequency response date. *Journal of Process Control* **13** (6), 553-567.

Goldberg, D. E. (1989). *Genetic algorithms in search, optimisation and machine learning.* Addison-Wesley.

Goodwin, G. C., Graebe, S. F., & Salgado, M. E. (2001). *Control system design.* Prentice Hall.

Graham, D., & Lathrop, R. C. (1953). The synthesis of "optimum" transient response: Criteria and standard forms. *AIEE Transactions* **72**, *part II: Applications and Industry*, 273-288.

Griffin, I., Schroder, P., Chipperfield, A., & Fleming, P. J. (1998). Multiobjective optimisation approach to gasifier control. *Proc. of MEC benchmark challenge on gasifier control,* Control Theory and Applications Centre, Coventry, UK.

Griffin, I., Schroder, P., Chipperfield, A., & Fleming, P. J. (2000). Multi-objective optimisation approach to the ALSTOM gasifier problem. *Journal of Systems and Control Engineering* **214**, 453-468.

Gysling, D. L., Dugundji, J., & Greitzer, E. M. (1991). Dynamic control of centrifugal compressor surge using tailored structures. *Journal of Turbomachinery* **113**, 710-722.

Haalman, A. (1965). Adjusting controllers for a deadtime process. *Control Engineering* **65**, 71-73.

Hagglund, T. (1996). An industrial dead-time compensating PI controller, *Control Engineering Practice* **4** (6), 749-756.

Hang, C. C., Astrom, K. J., & Ho, W. K. (1991). Refinements of the Ziegler-Nichols tuning formula. *IEE Proceeding-D* **138** (2), 111-117.

Harefors, M. (1997). Application of H_∞ robust control to the RM12 jet engine. *Control Engineering Practice* **5**, 1189-1201.

Harris, L. P., & Spang III, H. A. (1991). Compressor modelling and active control of stall/surge. *Proc. of the American Control Conference* (pp. 2392-2397).

Ho, W. K., Hang, C.C., & Cao, L. S. (1995). Tuning of PID controllers based on gain and phase margin specifications. *Automatica* **31** (3), 497-502.

Ho, W. K., Hang, C.C., & Zhou, J. H. (1995). Performance and gain and phase margins of well-known PI tuning formulae. *IEEE Transactions on Control Systems Technology* **3** (2), 245-248.

Ho, W. K., Gan, O. P., Tay, E. B., & Ang, E. L. (1996). Performance and gain and phase margins of well-known PID tuning formulae. *IEEE Transactions on Control Systems Technology* **4** (4), 473-477.

Ho, W. K., Lim, K.W., & Xu, W. (1998). Optimal gain and phase margin tuning for PID controllers. *Automatica* **34** (8), 1009-1014.

Ho, W. K., Lim, K.W., Hang, C.C., & Ni, L.Y. (1999). Getting more phase margin and performance out of the PID controllers. *Automatica* **35**, 1579-1585.

Ho, W. K., Lee, T.H., Xu, W., Zhou, J.R., & Tay, E.B. (2000). The direct Nyquist array design of PID controllers. *IEEE Transactions on Industrial Electronics* **47** (1), 175-185.

Holman, F.F., & Kidwell, J. R. (1975). Effects of casing treatment on a small transonic axial-flow compressor. *ASME paper 75-WA/GT-5.*

Hughes, E. J. (2003). Multi-objective binary search optimisation. *Proc. of the 2nd International Conference on Evolutionary Multi-criterion Optimization* (pp. 102-117). Faro, Portugal.

Hyde, R. A., Glover, K. (1993). The application of scheduled H_∞ controllers to a VSTOL aircraft. *IEEE Transactions on Automatic Control* **38**, 1021-1039.

Jackson, D. (1988). Investigating of state space architectures for engine models. *Report TDR 9331.*

Jones, B. A. (1970). Single stage experimental evaluation of variable geometry inlet guide vanes and stator blading. *NASA CR-54559.*

Khalid, S. (1997). A practical compressor casing treatment. *ASME paper 97-GT-375.*

Kim, K. H., Fleeter, S. (1994). Compressor unsteady aerodynamic response to rotating stall and surge excitations. *Journal of Propulsion and Power* **10**, 698-708.

Koivo H. N., & Tanttu, J. T. (1991). Tuning of PID controllers: survey of SISO and MIMO techniques. *Proc. of Intelligent Tuning and Adaptive Control* (pp.75-80). Singapore.

Lee, N. K. W., & Greitzer, E. M. (1990). Effects of endwall suction and blowing on compressor stability enhancement. *Journal of Turbomachinery* **112**, 133-144.

Lee, J., & Edgar, T. F. (2002). Improved PI controller with delayed or filtered integral mode. *AIChE Journal* **48** (12), 2844-2850.

Leininger, G. (1979). Multivariable Nyquist array with application to turbofan engine control. *Proc. of Propulsion Control Conference.*

Liu, G. P., & Daley, S. (1999). Optimal-tuning PID controller design in the frequency-domain with application to rotary hydraulic systems. *Control Engineering Practice* **7** (7), 821-830.

Liu, G. P., & Daley, S. (2001). Optimal-tuning PID control for industrial systems. *Control Engineering Practice* **9**, 1185-1194.

Lopez, A. M., Murrill, P. W., & Smith, C. L. (1969). Tuning PI and PID digital controllers. *Instruments and Control Systems* **42**, 89-95.

Luyben, W. L. (1986). Simple method for tuning SISO controllers in multivariable system. *Industrial & Engineering Chemistry Process Design and Development* **25**, 654-660.

Lyantsev, O. D., Breikin, T. V., Kulikov, G. G., & Arkov, V. Y. (2004). Optimal multi-variable control of gas turbine engines. *International Journal of Systems Science* **35** (2), 79-86.

McMillan, G. K. (1983). *Tuning and control loop performance.* Instrument Society of America. USA.

Marlin, T. E. (2000). *Process control.* McGraw Hill.

McFarlane, D. C., & Glover, K. (1990). *Robust controller design using normalized coprime factor plant descriptions.* Lecture notes in Control and Information Sciences **138**. Springer-Verlag.

Morari, M., & Zafiriou, E. (1989). *Robust process control.* Prentice Hall.

Morari, M., & Lee, J. H. (1991). Model predictive control: The good, the bad and the ugly. *Chemical Process Control, CPCIV* (pp.419-442). Padre Island, Texas, USA.

Nisenfeld, A. (1982). *Centrifugal compressors: principles of operation and control,* Instrument Society of America. USA.

Paduano, J. D., Epstein, A. H., Valavani, L., Longley, J. P., Greitzer, E. M., & Guenette, G. R. (1993). Active control of rotating stall in a low-speed axial compressor. *Journal of Turbomachinery* **115**, 48-56.

Palmor, Z. J., Halevi, Y., & Krasney, N. (1993). Automatic tuning of decentralized PID controllers for TITO processes. *Proc. of IFAC World Congress* (pp. 311-314).

Palmor, Z. J., Halevi Y., & Krasney. N. (1995). Automatic tuning of decentralized PID controllers for TITO processes. *Automatica* **31** (7), 1001-1010.

Pampreen, R. C. (1976). The use of variable guide vanes for automotive gas turbine engine augmentation and load control. *SAE paper 760285.*

Panagopoulos, H., Astrom, K. J., & Hagglund, T. (2002). Design of PID controllers based on constrained optimisation. *IEE Proceedings-Control Theory and applications* **149** (1), 32-40.

Pessen, B. W. (1954). How to 'tune in' a three mode controller. *Instrumentation, Second Quarter* (pp. 29-32).

Persson, P. (1992). *Towards autonomous PID control.* PhD Thesis. Lund University, Sweden.

Persson, P., & Astrom, K. J. (1992). Dominant pole design-A unified view of PID controller tuning. *Proc. of 4th IFAC Symposium on Adaptive Systems in Control and Signal Processing* (pp.127-132). Grenoble, France.

Persson, P., & Astrom, K. J. (1993). PID control revisited. *Proc. of IFAC World Congress* (pp. 451-454). Sydney, Australia.

Pinsley, J. E., Guenette, G. R., Epstein, A. H., & Greitzer, E. M. (1991). Active stabilization of centrifugal compressor surge. *Journal of Turbomachinery* **113**, 723-732.

Polly, J. A., Adibhatla, S., & Hoffman, P. J. (1988). Multivariable turbofan engine control for full envelope operation. *Proc. of Gas Turbine and Aeroengine Congress and Exposition.*

Postlethwaite, I., Samar, R., Choi, B. W., & Gu, D. W. (1995). A digital multi-mode H_∞ controller for the Spey turbofan engine. *Proc. of European Control Conference.*

Prempain, E., Sun, X. D., & Postlethwaite, I. (1998). Robust control of the gasifier using a mixed H-infinity approach. *Proc. of MEC benchmark challenge on gasifier control,* Control Theory and Applications Centre, Coventry, UK.

Przybylko, S. J. (1997). Active-control technologies for aircraft engines. *Proc. of Joint Propulsion Conference & Exhibit.* Seattle, USA.

Qin, S. J., & Badgwell, T. A. (2003). A survey of industrial model predictive control technology. *Control Engineering Practice* **11** (7), 733-764.

Rees, D., Mu, J., & Chiras, N. (2003). Optimum gain scheduling PID controllers for gas turbine engines based on NARMAX and neural network models. *GT2003-38667.*

Rivera, D. E., Morari, M., & Skogestad, S. (1986). Internal model control. PID controller design. *Industrial & Engineering Chemistry Process Design and Development* **25**, 252-265.

Rodgers, C. (1991). Centrifugal compressor inlet guide vanes for increased surge margin. *Journal of Turbomachinery* **113**, 696-702.

Rolls-Royce (2005). *The jet engine.* Rolls-Royce Ltd.

Rosenbrock, H. H. (1970). *State-space and multivariable theory.* Nelson. London, UK.

Ruano, A. E., Fleming, P. J., Teixeira, C., Rodriguez-Vazquez, K. , & Fonseca, C. M. (2003). Non-linear identification of aircraft gas-turbine dynamics. *Neurocomputing* **55**, 551-579.

Samar, R. (1995). *Robust multi-mode control of high performance aero-engines.* PhD Thesis. University of Leicester, UK.

Seborg, A. E., Edgar, T. F., & Mellichamp, D. A. (2004). *Process dynamics and control.* John Wiley & Sons.

Semino, D., & Scali, C. (1998). Improved identification and autotuning of PI controllers for MIMO processes by rely techniques. *Journal of Process Control* **8** (3), 219-227.

Shen, S. H., & Yu, C. C. (1994). Use of relay-feedback test or automatic tuning of multivariable systems, *AIChE Journal* **40** (4), 627-646.

Sheridan, D. C., Nordenson, G. E., & Amann, C. A. (1974). Variable compressor geometry in the single-shaft automotive turbine engine. *SAE paper 740166.*

Shinskey, F. G. (1996). *Process control systems: application, design and tuning.* McGraw Hill. New York, USA.

Shinskey, F. G. (1990). How good are our controllers in absolute performance and robustness? *Measurement and Control* **23**, 114-121.

Shinskey, F. G. (1991). Model predictions: The first start controllers. *Instruments and Control Systems*, 75-78.

Silva, V. V. R. (1999). *Multivariable control systems design using evolutionary computing.* PhD Thesis. University of Sheffield, UK.

Silva, V. V. R., Khatib, W., & Fleming, P. J. (2000). Fuel consumption optimization of gas turbine engines using evolutionary computing. *Proc. of the 4th Industry Applications Conference* (pp. 714-717). Porto Alegre, Rio Grande do Sul, Brazil.

Silva, V. V. R., Khatib, W., & Fleming, P. J. (2003). Performance optimisation through evolutionary algorithms. *Proc. of 24th Iberian Latin-American Congress on Computational Methods in Engineering*. Ouro Preto, Minas Gerais, Brazil.

Silva, V. V. R., Khatib, W., & Fleming, P. J. (2005). Performance optimisation of gas turbine engine. *Engineering Applications of Artificial Intelligence* **18**, 575-583.

Simon, J. S., & Valavani, L. (1991). A Lyapunov based nonlinear control scheme for stabilizing a basic compression system using a closed-coupled control valve. *Proc. of the American Control Conference* (pp. 2398-2406).

Skogestad, S., & Pastlethwaite, I. (2001). *Multivariable feedback control analysis and design*. John Wiley & Sons.

Skogestad, S. (2003). Simple analytic rules for model reduction and PID controller tuning. *Journal of Process Control* **13** (4), 291-309.

Smith, C. A., & Corripio, A. B. (1997). *Principles and practice of automatic process control*. John Wiley & Sons.

Soeder, J. F. (1984). F100 multivariable control synthesis program. *NASA Tech. Paper 2231*.

Spang III, H. A., & Brown, H. (1999). Control of Jet engines. *Control Engineering Practice* **7**, 1043-1059.

Staroselsky, N., & Ladin, L. (1979). Improved surge control for centrifugal compressors. *Chemical Engineering*, 175-184.

Tan, K. K., Wang, Q. G., Hang. C. C., & Hagglund, T. J. (1999). *Advances in PID control*. Advances in industrial control. Springer-Verlag.

Tavakoli, S., & Tavakoli, M. (2003). Optimal tuning of PID controllers for first order plus time delay models using dimensional analysis. *Proc. of IEEE 4th International Conference on Control and Automation* (pp. 492-496). Montreal, Canada.

Tavakoli, S., Griffin, I., & Fleming, P. J. (2003). A condition number minimisation approach to the ALSTOM gasifier problem. *Proc. of IFAC International Conference on Intelligent Control Systems and Signal Processing* (pp. 95-100). Faro, Portugal.

Tavakoli, S., & Fleming, P. (2003). Optimal tuning of PI controllers for first order plus dead time/long dead time models using dimensional analysis. *Proc. of European Control Conference*. Cambridge, UK.

Tavakoli, S., Griffin, I., & Fleming, P. J. (2004). An Overview of Compressor Instabilities: Basic Concepts and Control, *Proc. of the 16th IFAC International Symposium on Automatic Control in Aerospace*. Saint Petersburg, Russia.

Tavakoli, S., Griffin, I., & Fleming, P. J. (2005a). Tuning of decentralised PI (PID) controllers for TITO processes. *Control Engineering Practice* (in press).

Tavakoli, S., Griffin, I., & Fleming, P. J. (2005b). Analytically derived PI tuning formulae for optimal load disturbance rejection with constraints on gain and phase margins. *Journal of Process Control* (submitted).

Tavakoli, S., Griffin, I., & Fleming, P. J. (2005c). Robust PI controller for load disturbance rejection and setpoint regulation, *Proc. of IEEE International Conference on Control Applications*. Toronto, Canada.

Tavakoli, S., Griffin, I., & Fleming, P. J. (2005d). Decentralised PI control of a Rolls-Royce jet engine, *Proc. of IEEE International Conference on Control Applications*. Toronto, Canada.

Tavakoli, S., Griffin, I., & Fleming, P. J. (2005e). Optimal PID tuning for second order plus dead time processes, *14th Iranian Conference on Electrical Engineering* (submitted).

Tavakoli, S., Griffin, I., & Fleming, P. J. (2005f). PI control tuning using multi-objective optimisation techniques, *14th Iranian Conference on Electrical Engineering* (submitted).

Taylor, E. S. (1974). *Dimensional analysis for engineers*. Clarendon Press. Oxford, UK.

Taylor, J., McCabe, A., Young, P., & Chotai, A. (1998). Proportional-integral-plus (PIP) control of the GEC ALSTOM gasifier benchmark challenge. *Proc. of MEC benchmark challenge on gasifier control*, Control Theory and Applications Centre, Coventry, UK.

Toscano, R. (2005). A simple robust PI/PID controller design via numerical optimization approach. *Journal of Process Control* **15**, 81-88.

Tyreus, B. D., & Luyben, W. L. (1992). Tuning PI controllers for integrator/dead time processes. *Industrial & Engineering Chemistry Research*, 2628-2631.

Ucer, A. S., Show, P., & Hirsch, C. (1985). *Thermodynamics and Fluid Mechanics of Turbomachinery* **1-2**. Kluwer Academic Print.

Vachtsevanos, G., Kang, H., Cheng, J., & Kim, I. (1992). Detection and identification of axial flow compressor instabilities. *Journal of Guidance, Control and Dynamics* **15**, 1216-1223.

Walsh, P. P., & Fletcher, P. (1998). *Gas turbine performance*. Blackwell Science.

Wang, Q. G., Zou, B., Lee, T. H., & Bi, Q. (1997). Auto-tuning of multi-variable PID controllers from decentralized relay feedback. *Automatica* **33** (3), 319-330.

Wang, Q. G., Lee, T. H., Fung, H. W., Bi Q., & Zhang, Y. (1999). PID tuning for improved performance. *IEEE Transactions on Control Systems Technology* **7** (4), 457-465.

Wang, Q. G., Fung, H. W., & Zhang Y. (1999). PID tuning with exact gain and phase margins. *ISA Transactions* **38**, 243-249.

Wang, Q. G., Huang, B., & Guo, X. (2000). Auto-tuning of TITO decoupling controllers from step tests. *ISA Transactions* **39**, 407-418.

Watts, S. R., & Garg, S. (1995). A comparison of multivariable control design techniques for a turbofan engine control. *Proc. of ASME 40th Gas Turbine and Aeroengine Congress And Exposition.*

Whitfield, A., Wallace, F. J., & Atkey, R. C. (1976). The effect of variable geometry on the operating range and surge margin of a centrifugal compressor. *ASME paper 76-GT-98.*

Wo. A. M., & Bons, J. P. (1994). Flow physics leading to system instability in a centrifugal pump. *Journal of Turbomachinery* **116**, 612-620.

Wood, R. K., & Berry, M. W. (1973). Terminal composition control of a binary distillation column. *Chemical Engineering Science* **28**, 1707-1717.

Yeung, S., & Murray, R. M. (1997). Reduction of bleed valve requirements for control of rotating stall using continuous air injection. *Proc. of the IEEE International Conference on Control Application* (pp. 683-690).

Ziegler, J. G., & Nichols, N. B. (1942). Optimum settings for automatic controllers. *Trans. ASME* ***64***, 759-768.

Zlokarnik, M. (1991). *Dimensional analysis and scale-up in chemical engineering.* Springer-Verlag, Berlin, Germany.